

Study on Chromium Chalcogenide Cluster Complexes

Study on Chromium Chalcogenide Cluster Complexes
(クロムカルコゲニドクラスター錯体の研究)

上口 賢

①

学位論文

Study on Chromium Chalcogenide
Cluster Complexes

クロムカルコゲニドクラスター錯体の研究

平成 10 年 12 月博士（理学）申請

東京大学大学院理学系研究科

化学専攻

上口 賢

**Study on Chromium Chalcogenide
Cluster Complexes**

Dissertation for a Degree of Doctor (Science)

Submitted in December 1998

Department of Chemistry
Graduate School of Science
The University of Tokyo

Satoshi Kamiguchi

Study on chromium chalcogenide cluster complexes

CONTENTS

General Introduction	2
Chapter 1 Chemistry of Chromium Chalcogenido Hexanuclear Cluster Complexes	11
1-1. Introduction / 11	
1-2. Experimental Section / 12	
1-3. Results and Discussion / 32	
1-3-1. Syntheses of Hexanuclear Chromium Cluster Complexes / 32	
1-3-2. Molecular Orbital Calculation / 34	
1-3-3. FAB Mass Spectra / 36	
1-3-4. X-ray Structure Analyses / 39	
1-3-5. Powder Neutron Diffraction Analysis / 43	
1-3-6. The Reactivity of the Hydride / 52	
1-3-7. Magnetic Properties / 53	
1-3-8. Conclusion / 68	
1-4. References / 69	
Chapter 2 Chemistry of Chromium Sulfido Dodecanuclear Cluster Complexes	74
2-1. Introduction / 74	
2-2. Experimental Section / 77	
2-3. Results and Discussion / 85	
2-3-1. Synthesis of Dodecanuclear Cluster Complex $[\text{Cr}_{12}\text{S}_{16}(\text{H})_2(\text{PEt}_3)_{10}]$ / 85	
2-3-2. FAB Mass Spectrum / 86	
2-3-3. X-ray Structure Analysis / 86	
2-3-4. Electrochemistry / 94	
2-3-5. Magnetic Property / 96	
2-3-6. Conclusion / 99	
2-4. References / 100	
General Conclusion	102
Acknowledgement	110

General Introduction

A metal-chalcogenido cluster complex contains more than three metal atoms held together by direct metal-metal bonds. The bondings between metal atoms are reinforced by bridging chalcogenido ligands.¹ Owing to the progress of synthetic methods and the improvement of characterizations such as X-ray structure determination, a large number of cluster complexes are being prepared. In the early stage of the development, the diversity of their structures attracted much attention,² but the recent interest has also been concentrated on the various properties based on the multinuclear nature and metal-metal bonding interaction.

Magnetochemistry of Cluster Complexes

The metal-metal bonds in 3d-metal cluster complexes are weaker than those in 4d- or 5d-metal ones because 3d orbital is less expanding. Thus 3d-metal clusters display much different properties from those of 4d- or 5d-metal cluster complexes. This difference is apparent in magnetic properties. Since 3d-metal cluster complexes have weak metal-metal bonds, the energy gaps between the ground and excited states are small. Therefore, some 3d-metal cluster complexes do not obey the Curie law but display significant thermal variation of the number of unpaired electrons (temperature-dependent paramagnetism).³⁻⁷ In these complexes, the spin-spin interaction takes place through metal-metal bonds and bridging ligands synergically.

In spite of such interesting magnetic behaviors in 3d-metal cluster complexes, there have been only a few reports on their magnetism,⁴⁻¹³ and the relation between structures and magnetic properties have remained unclear. The temperature-dependent paramagnetism has also been observed for many polynuclear complexes without metal-metal bonds, and their magnetic behaviors have been investigated theoretically by using the calculation with the Heisenberg-Dirac-Van Vleck (HDVV) Hamiltonian.¹⁴ Recently, this calculation has been applied to some iron-sulfide tetranuclear⁷ and hexanuclear-cluster complexes.^{5, 6} By

introducing this theoretical calculation to the cluster complexes, the magneto-structural correlation in 3d-metal cluster complexes will be clarified more significantly.

Cr₆E₈ Octahedral Cores

The author has been interested mainly in the magneto-structural correlation in 3d-metal cluster complexes. As the target system, the author selected chromium-chalcogenide complexes with Cr₆E₈ (E = S, Se) octahedral cluster cores (Figure 1). This cluster unit has a very highly symmetrical structure. When the symmetry of this cluster is assumed to be *O_h*, there is only one type of distinct metal-metal bonds, which leads to easy analyses of the magnetostructure in the cluster core.

Our laboratory previously reported "[Cr₆S₈(PEt₃)₆]" and "[Cr₆Se₈(PEt₃)₆]" with a Cr₆E₈ octahedral cluster unit.¹⁵ As shown in Figure 2, these complexes exhibit the decrease of the effective magnetic moments (μ_{eff}) on lowering the temperature, and the μ_{eff} values at 4.5 K are 1.8 μ_B for the sulfide and 1.6 μ_B for the selenide, which are very close to the value (1.73 μ_B) of spin-only magnetic moment for one unpaired electron. However, this odd number could not be explained by the molecular formula "[Cr₆E₈(PEt₃)₆]", because it gives an even number of metal cluster electrons (MCE) (20 e). This inconsistency may be attributed to the existence of an extra hydrogen atom which could not be detected by the previous single-crystal X-ray structure analyses. If the chromium cluster complexes contain an extra hydrogen atom, the resulting molecular formula "[Cr₆E₈(H)(PEt₃)₆]" affords 21 MCE. Whereas a large number of [M₆E₈L₆] type molecular clusters of zirconium,¹⁶ vanadium,¹⁶ chromium,^{12, 15, 17} molybdenum,¹⁸⁻²³ tungsten,²⁴⁻³⁰ rhenium,³¹⁻³⁸ iron,^{13, 39-42} and cobalt⁴³⁻⁵² have been prepared, there have been only two complexes ([Re₆S₇(SH)Br₆]³⁻ and [Re₆Se₇(SeH)]₆³⁻) containing extra hydrogen atoms associated with the M₆E₈ cluster unit.³² These rhenium complexes have a chalcogen-bonded hydrogen. There have been no precedent examples of [M₆E₈L₆] type clusters with an interstitial hydride, in contrast to some reports on the interstitial hydride in the octahedral halide⁵³⁻⁶⁰ or carbonyl-clusters.⁶¹⁻⁶⁵ Therefore, the investigation of "[Cr₆E₈(PEt₃)₆]" may give the first examples of chalcogenido clusters with an interstitial hydride as well as clarify the magneto-structural correlation in 3d-metal cluster complexes.

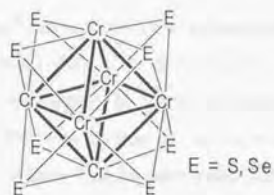


Figure 1. Cr_6E_8 (E = S, Se) octahedral cluster core.

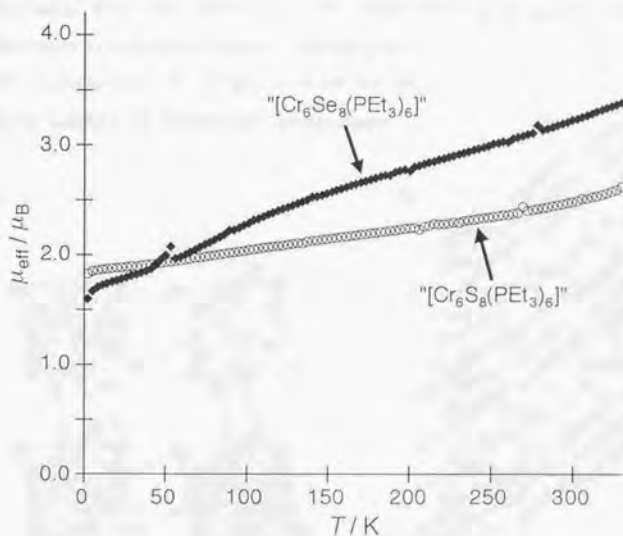
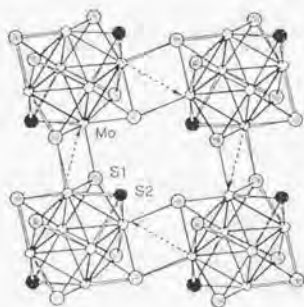


Figure 2. Temperature dependence of the magnetic susceptibilities of $[\text{Cr}_6\text{S}_8(\text{PEt}_3)_6]$ and $[\text{Cr}_6\text{Se}_8(\text{PEt}_3)_6]$ in the form of μ_{eff} vs. T .

The study on "[Cr₆E₈(PEt₃)₆]" also concerns the superconducting Chevrel phases M_xMo₆E₈ (M = Cu, Sn, Pb, La, etc.; x = 0 - 4; E = S, Se, Te).⁶⁶ In Chevrel phases, the Mo₆E₈ octahedral cluster cores are connected in a three-dimensional arrangement (Figure 3). The superconductivity has been related to the interaction between the cluster units.⁶⁷ In contrast to the extensive studies on these molybdenum compounds, no chromium analogue is known. Steigerwald *et al.* have attempted to prepare a chromium Chevrel compound by the condensation of a molecular cluster complex [Cr₆Te₈(PEt₃)₆], but the trial has been unsuccessful.¹² The establishment of condensation method of the Cr₆E₈ cluster core may give an approach to the synthesis of still unknown "chromium Chevrels." In addition, the preparation on the Cr₆E₈ cluster oligomers may lead to the investigation of interaction between M₆E₈ type octahedral cluster units. The study on intercluster interaction has been attracting much attention not only in relation to non-molecular cluster compounds but also in the field of molecular clusters.⁶⁸⁻⁷⁰ The present thesis describes the preparation of a chromium sulfide dodecanuclear cluster complex by dimerization of a Cr₆E₈ cluster core as the first step for the synthesis of "chromium Chevrel phases."

a)



b)

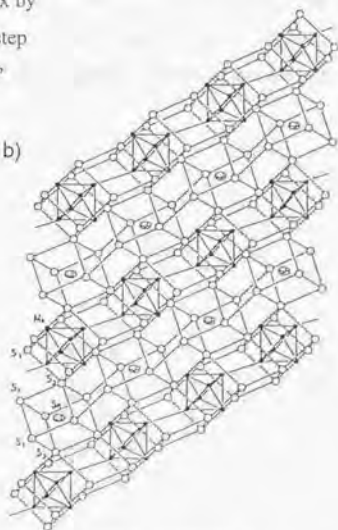


Figure 3. (a) The bridging mode of four cluster units in Mo₆S₈. (From ref. 1.)

(b) Structure of SnMo₆S₈. (From ref. 66.)

Scope of the Present Thesis

The present thesis has been concentrated on the following purposes, namely,

- (i) The clarification of the relation between the structure and magnetism in 3d-metal chalcogenido cluster complexes.
- (ii) The preparation of metal-chalcogenido hydrido clusters.
- (iii) The elucidation of intercluster electronic and magnetic interaction.

Chapter 1 concerns the study on the hexanuclear chromium chalcogenido cluster complexes with one Cr_6E_8 ($\text{E} = \text{S}, \text{Se}$) cluster unit. The investigation of the previously reported " $[\text{Cr}_6\text{E}_8(\text{PEt}_3)_6]$ " gave three novel cluster compounds $[\text{Cr}_6\text{Se}_8(\text{PEt}_3)_6](\mathbf{1})$, $[\text{Cr}_6\text{Se}_8(\text{H})(\text{PEt}_3)_6](\mathbf{2})$, and $[\text{Cr}_6\text{S}_8(\text{H})(\text{PEt}_3)_6](\mathbf{3})$. Complexes $\mathbf{2}$ and $\mathbf{3}$ are the first examples of metal-chalcogenido clusters with an interstitial hydride so far. In addition, the magneto-structural correlation in $\mathbf{1-3}$ was studied by using the HDVV Hamiltonian. Chapter 2 describes the synthesis of the dodecanuclear chromium sulfide cluster complexes $[\text{Cr}_{12}\text{S}_{16}(\text{H})_2(\text{PEt}_3)_{10}](\mathbf{6})$ by the condensation of $\mathbf{3}$. Complex $\mathbf{6}$ has two Cr_6S_8 cluster cores per molecule, and the cores are connected in a similar linking mode to those in the molybdenum Chevrel phases. The electronic and magnetic interaction between the Cr_6S_8 cluster units was investigated.

References

1. Saito, T. In *Early Transition Metal Clusters with π -Donor Ligands*; Chisholm, M. H., Ed.; VCH: New York, 1995, pp 63-164.
2. Vahrenkamp, H. *Struct. Bonding* **1977**, *32*, 1.
3. Bottomley, F.; Chen, J.; MacIntosh, S. M.; Thompson, R. C. *Organometallics* **1991**, *10*, 906.
4. Bencini, A.; Midollini, S.; Zanchini, C. *Inorg. Chem.* **1992**, *31*, 2132.
5. Bencini, A.; Uytterhoeven, M. G.; Zanchini, C. *Int. J. Quantum. Chem.* **1994**, *52*, 903.
6. Bencini, A.; Ghilardi, C. A.; Midollini, S.; Orlandini, A.; Russo, U.; Uytterhoeven, M. G.; Zanchini, C. *J. Chem. Soc. Dalton Trans.* **1995**, 963.
7. Yoo, S. J.; Hu, Z.; Goh, C.; Bominaar, E. L.; Holm, R. H.; Münck, E. *J. Am. Chem. Soc.* **1997**, *119*, 8732.
8. Noodleman, L. *Inorg. Chem.* **1988**, *27*, 3677.
9. Noodleman, L. *Inorg. Chem.* **1991**, *30*, 246.
10. Noodleman, L. *Inorg. Chem.* **1991**, *30*, 256.
11. Bencini, A.; Ghilardi, C. A.; Orlandini, A.; Midollini, S.; Zanchini, C. *J. Am. Chem. Soc.* **1992**, *114*, 9898.
12. Hessen, B.; Siegrist, T.; Palstra, T.; Tanzler, S. M.; Steigerwald, M. L. *Inorg. Chem.* **1993**, *32*, 5165.
13. Goddard, C. A.; Long, J. R.; Holm, R. H. *Inorg. Chem.* **1996**, *35*, 4347.
14. Bencini, A.; Gatteschi, D. In *Electron Paramagnetic Resonance of Exchange Coupled Systems*; Springer, Berlin, 1990.
15. Tsuge, K.; Imoto, H.; Saito, T. *Bull. Chem. Soc. Jpn.* **1996**, *69*, 627.
16. Fenske, D.; Grissinger, A.; Loos, M.; Magull, J. *Z. Anorg. Allg. Chem.* **1991**, *598/599*, 121.
17. Kamiguchi, S.; Imoto, H.; Saito, T. *Chem. Lett.* **1996**, 555.
18. Saito, T.; Yamamoto, N.; Nagase, T.; Tsuboi, T.; Kobayashi, K.; Yamagata, T.; Imoto, H.; Unoura, K. *Inorg. Chem.* **1990**, *29*, 764.
19. Hilsenbeck, S. J.; Young, V. G.; McCarley, R. E. *Inorg. Chem.* **1994**, *33*, 1822.

20. Hilsenbeck, S. J.; McCarley, R. E. *Chem. Mater.* **1995**, *7*, 499.
21. McCarley, R. E.; Hilsenbeck, S. J.; Xie, X. *J. Solid State Chem.* **1995**, *117*, 269.
22. Amari, S.; Imoto, H.; Saito, T. *Chem. Lett.* **1997**, 967.
23. Mizutani, J.; Amari, S.; Imoto, H.; Saito, T. *J. Chem. Soc. Dalton Trans.* **1998**, 819.
24. Saito, T.; Yoshikawa, A.; Yamagata, T.; Imoto, H.; Unoura, K. *Inorg. Chem.* **1989**, *28*, 3588.
25. Zhang, X.; McCarley, R. E. *Inorg. Chem.* **1995**, *34*, 2678.
26. Ehrlich, G. M.; Warren, C. J.; Vennos, D. A.; Ho, D. M.; Haushalter, R. C.; DiSalvo, F. J. *Inorg. Chem.* **1995**, *34*, 4454.
27. Xie, X.; McCarley, R. E. *Inorg. Chem.* **1995**, *34*, 6124.
28. Xie, X.; McCarley, R. E. *Inorg. Chem.* **1996**, *35*, 2713.
29. Xie, X.; McCarley, R. E. *Inorg. Chem.* **1997**, *36*, 4011.
30. Xie, X.; McCarley, R. E. *Inorg. Chem.* **1997**, *36*, 4665.
31. Uriel, S.; Boubekeur, K.; Batail, P.; Orduna, J.; Canadell, E. *Inorg. Chem.* **1995**, *34*, 5307.
32. Long, J. R.; McCarty, L. S.; Holm, R. H. *J. Am. Chem. Soc.* **1996**, *118*, 4603.
33. Mironov, Y. V.; Pell, M. A.; Ibers, J. A. *Inorg. Chem.* **1996**, *35*, 2709.
34. Mironov, Y. V.; Cody, J. A.; Albrecht-Schmitt, T. E.; Ibers, J. A. *J. Am. Chem. Soc.* **1997**, *119*, 493.
35. Zheng, Z.; Long, J. R.; Holm, R. H. *J. Am. Chem. Soc.* **1997**, *119*, 2163.
36. Fedin, V. P.; Fedorov, V. E.; Imoto, H.; Saito, T. *Polyhedron* **1997**, *16*, 1615.
37. Zheng, Z.; Holm, R. H. *Inorg. Chem.* **1997**, *36*, 5173.
38. Willer, M. W.; Long, J. R.; McLauchlan, C. C.; Holm, R. H. *Inorg. Chem.* **1998**, *37*, 328.
39. Cecconi, F.; Ghilardi, C. A.; Midollini, S. *J. Chem. Soc. Chem. Commun.* **1981**, 640.
40. Agresti, A.; Bacci, M.; Cecconi, F.; Ghilardi, C. A.; Midollini, S. *Inorg. Chem.* **1985**, *24*, 689.
41. Cecconi, F.; Ghilardi, C. A.; Midollini, S.; Orlandini, A.; Zanello, P. *J. Chem. Soc. Dalton Trans.* **1987**, 831.
42. Steigerwald, M. L.; Siegrist, T.; Gyorgy, E. M.; Hessen, B.; Kwon, Y. -U.; Tanzler, S. M. *Inorg. Chem.* **1994**, *33*, 3389.

43. Cecconi, F.; Ghilardi, C. A.; Midollini, S.; Orlandini, A. *Inorg. Chim. Acta* **1981**, *64*, L47.
44. Fenske, D.; Hachgenei, J.; Ohmer, J. *Angew. Chem. Int. Ed. Engl.* **1985**, *24*, 706.
45. Fenske, D.; Ohmer, J.; Hachgenei, J. *Angew. Chem. Int. Ed. Engl.* **1985**, *24*, 993.
46. Diana, E.; Gervasio, G.; Rossetti, R.; Valdemarin, F.; Bor, G.; Stanghellini, P. L. *Inorg. Chem.* **1991**, *30*, 294.
47. Steigerwald, M. L.; Siegrist, T.; Stuczynski, S. M. *Inorg. Chem.* **1991**, *30*, 2256.
48. Hong, M.; Huang, Z.; Lei, X.; Wei, G.; Kang, B.; Liu, H. *Polyhedron* **1991**, *10*, 927.
49. Cecconi, F.; Ghilardi, C. A.; Midollini, S.; Orlandini, A. *Inorg. Chim. Acta* **1993**, *214*, 13.
50. Cecconi, F.; Ghilardi, C. A.; Midollini, S.; Orlandini, A.; Zanello, P.; Cinquantini, A.; Bencini, A.; Uytterhoeven, M. G.; Giorgi, G. *J. Chem. Soc. Dalton Trans.* **1995**, 3881.
51. Cecconi, F.; Ghilardi, C. A.; Midollini, S.; Orlandini, A.; Zanello, P. *Polyhedron* **1996**, *5*, 2021.
52. Cecconi, F.; Ghilardi, C. A.; Midollini, S.; Orlandini, A.; Bencini, A. *J. Chem. Soc. Dalton Trans.* **1996**, 3991.
53. Simon, V. A. *Z. Anorg. Allg. Chem.* **1967**, *355*, 311.
54. Imoto, H.; Corbett, J. D. *Inorg. Chem.* **1980**, *19*, 1241.
55. Imoto, H.; Simon, A. *Inorg. Chem.* **1982**, *21*, 308.
56. Fitch, A. N.; Barrett, S. A.; Fender, B. E. F. *J. Chem. Soc. Dalton Trans.* **1984**, 501.
57. Simon, A.; Stollmaier, F.; Gregson, D.; Fuess, H. *J. Chem. Soc. Dalton Trans.* **1987**, 431.
58. Chu, P. J.; Ziebarth, R. P.; Corbett, J. D.; Gerstein, B. C. *J. Am. Chem. Soc.* **1988**, *110*, 5324.
59. Meyer, H. -J.; Corbett, J. D. *Inorg. Chem.* **1991**, *30*, 963.
60. Gade, L. H.; Johnson, F. G.; Lewis, J. *Croat. Chem. Acta* **1995**, *68*, 693.
61. Eady, C. R.; Johnson, B. F. G.; Lewis, J.; Malatesta, M. C. *J. Chem. Soc. Chem. Commun.* **1976**, 945.
62. Hart, D. W.; Teller, R. G.; Wei, C. -Y.; Bau, R.; Longoni, G.; Campanella, S.; Chimi, P.; Koetzle, T. F. *Angew. Chem. Int. Ed. Engl.* **1979**, *18*, 80.
63. Eady, C. R.; Jackson, P. F.; Johnson, B. F. G.; Lewis, J.; Malatesta, M. C. *J. Chem. Soc. Dalton Trans.* **1980**, 383.

64. Jackson, P. F.; Johnson, B. F. G.; Lewis, J.; Raithby, P. R.; McPartlin, M.; Nelson, W. J. H.; Rouse, K. D.; Allibon, J.; Mason, S. A. *J. Chem. Soc. Chem. Commun.* **1980**, 295.
65. Hart, D. W.; Teller, R. G.; Wei, C. -Y.; Bau, R.; Campanella, S.; Chini, P.; Koetzle, T. F. *J. Am. Chem. Soc.* **1981**, *103*, 1458.
66. Chevrel, R.; Sergent, M. In *Superconductivity in Ternary Compounds I*; Springer, Berlin, 1982, pp 25-86.
67. Nohl, H.; Klose, W.; Anderson, O. K. In *Superconductivity in Ternary Compounds I*; Springer, Berlin, 1982, pp 165-221.
68. Wilson, S. T.; Bondurant, R. F.; Meyer, T. J.; Salmon, D. J. *J. Am. Chem. Soc.* **1975**, *97*, 2285.
69. Baumann, J. A.; Salmon, D. J.; Wilson, S. T.; Meyer, T. J. *Inorg. Chem.* **1979**, *18*, 2472.
70. Baumann, J. A.; Wilson, S. T.; Salmon, D. J.; Hood, P. L.; Meyer, T. J. *J. Am. Chem. Soc.* **1979**, *101*, 2916.

Chapter 1

Chemistry of Chromium Chalcogenido Hexanuclear Cluster Complexes

1-1 Introduction

The chemistry of metal-chalcogenide cluster compounds with the M_6E_8 ($E = S, Se, Te$) cluster unit consisting of a M_6 octahedron and eight face-capping E atoms has made a remarkable progress in the last decade.¹⁻⁵ The $[M_6E_8L_6]$ type molecular complexes of zirconium,⁶ vanadium,⁶ chromium,⁷⁻⁹ molybdenum,¹⁰⁻¹⁵ tungsten,¹⁶⁻²² rhenium,²³⁻³⁰ iron,³¹⁻³⁵ and cobalt³⁶⁻⁴⁵ have been prepared.

As mentioned in the General Introduction, our laboratory previously reported the syntheses and structures of the hexanuclear chromium cluster complexes " $[Cr_6Se_8(PEt_3)_6]$ " and " $[Cr_6S_8(PEt_3)_6]$."⁸ However, the magnetic measurements suggested that these complexes should contain an extra hydrogen atom which could not be detected by the previous single-crystal X-ray structure analyses. In the course of the further studies on the redox properties of the selenide cluster " $[Cr_6Se_8(PEt_3)_6]$," the cyclic voltammetry indicated that it was actually a mixture of two compounds. In the present study, they have been separated. The measurements of FAB (fast-atom-bombardment) mass spectra have indicated that one of them is $[Cr_6Se_8(PEt_3)_6]$ and the other is $[Cr_6Se_8(H)(PEt_3)_6]$ having an extra hydrogen atom associated with the cluster unit. The measurements have also suggested that the sulfide cluster " $[Cr_6S_8(PEt_3)_6]$ " should be reformulated as $[Cr_6S_8(H)(PEt_3)_6]$ containing an extra hydrogen atom. This chapter describes the syntheses, FAB mass spectra, and structures of these complexes. The probable position of the extra hydrogen atom is also discussed. All these chromium cluster complexes display temperature-dependent paramagnetic behaviors. These magnetic properties have been analyzed by the Heisenberg-Dirac-Van Vleck (HDVV) Hamiltonian, and the relation between the structure and magnetism has been clarified.

1-2 Experimental Section

1-2-1. Syntheses

All of the manipulations were carried out under nitrogen or argon using conventional Schlenk techniques unless stated otherwise. Solvents were dried and distilled under argon from appropriate drying agents (sodium metal wire for benzene and toluene, magnesium for methanol and ethanol, calcium sulfate for acetone, and sodium/benzophenone for tetrahydrofuran (THF)). Phosphorus trichloride and phosphorus tribromide were distilled under argon without any drying agents. Sodium hydrogen sulfide (NaSH) was prepared by a reaction of sodium ethoxide and hydrogen sulfide. Deuterated sodium hydrogen sulfide (NaSD) was prepared by the dissolution of NaSH in MeOD, followed by the removal of the solvent *in vacuo*. Sodium polyselenide (Na_2Se_x ; $x = 1.33$) was prepared by a supersonic reaction of sodium metal and selenium powder in THF with a catalytic amount of naphthalene.⁴⁶ Triethylphosphine (Kanto Kagaku) and the other reagents (Aldrich) were used as received.

Synthesis of $[\text{Cr}_6\text{Se}_8(\text{PEt}_3)_6]$ (1).

A methanol solution (20 cm^3) of Na_2Se_x ($x = 1.33$; 0.52 g, 3.5 mmol) was added dropwise to a suspension of anhydrous chromium dichloride (CrCl_2) (0.43 g, 3.5 mmol) in methanol (10 cm^3) at $-78 \text{ }^\circ\text{C}$. A mixture of a brown solution and a brown precipitate was formed. Subsequently, PEt_3 (20% w/w toluene; 4.9 cm^3 , 7.1 mmol) was added to the mixture, which was stirred and allowed to warm slowly (*ca.* 8 h) to room temperature. The resulting suspension was refluxed for 8 h. The solvent was removed *in vacuo* and the black material was extracted with hot benzene (30 cm^3). After benzene was removed *in vacuo*, the resulting solid was washed with acetone ($3 \times 30 \text{ cm}^3$) and dried *in vacuo* to give a black mixture of 1 and 2. These complexes were separated by a selective oxidation of 2. To a suspension of this mixture in toluene (90 cm^3) was added an acetone solution (10 cm^3) of ferrocenium hexafluorophosphate (0.030 g, 0.091 mmol). The amount of ferrocenium cation was controlled so that only complex 2 was oxidized. The solution was stirred at room temperature for 5 h, and the solvent was removed *in vacuo*. In order to remove 2', the residue was washed with acetone (100 cm^3 and $2 \times 10 \text{ cm}^3$), dried *in vacuo*, and extracted

with toluene (20 cm³). Ethanol (85 cm³) was added to the extract and the solution was allowed to stand at -20 °C for 4 d to form **1** (0.044 g, 4 %) as black crystals. **1**: ¹H NMR (C₆D₆): δ = 1.67 (54H, PCH₂CH₃), -4.05 (36H, PCH₂). Found: C, 26.30; H, 5.25%. Calcd for C₃₆H₉₀Cr₆P₆Se₈: C, 26.16; H, 5.49%.

Synthesis of [Cr₆Se₈(H)(PEt₃)₆]**·**2THF (**2·**2THF).

The mixture of **1** and **2** obtained by the reaction of CrCl₂, Na₂Se₈, and PEt₃ was suspended in toluene (90 cm³) as described for the synthesis of **1**. After an acetone solution (10 cm³) of ferrocenium hexafluorophosphate (0.022 g, 0.066 mmol) was added, the resulting mixture was stirred at room temperature for 5 h, and the solvent was removed *in vacuo*. By extracting the residue with acetone (100 cm³), only acetone-soluble **2**⁺ was extracted. In order to reduce **2**⁺ to the neutral cluster **2**, an acetone solution (10 cm³) of cobaltocene (0.017 g, 0.09 mmol) was added to the extract. The resulting mixture was stirred at room temperature for 1 h to give a yellow solution and a black precipitate. After the solution was filtered off, the precipitate was washed with acetone (2 × 10 cm³), dried *in vacuo*, and extracted with hot THF (75 cm³). The THF extract was allowed to stand at -20 °C for 5 d to yield **2·**2THF (0.081 g, 8 %) as black crystals. **2·**2THF: ¹H NMR (C₆D₆): δ = 3.68 (8H, OCH₂), 1.63 (54H, PCH₂CH₃), 1.53 (8H, OCH₂CH₂), -0.26 (36H, PCH₂). The signal due to the hydride associated with the cluster unit could not be detected. Found: C, 29.28; H, 5.88%. Calcd for C₄₄H₁₀₇O₂Cr₆P₆Se₈: C, 29.40; H, 6.00%.

Synthesis of [Cr₆S₈(H)(PEt₃)₆]**·**2C₆H₆ (**3·**2C₆H₆).

Complex **3** was prepared following the procedure previously reported for "[Cr₆S₈(PEt₃)₆]"⁸. A solution of NaS_xH (x = 1.33) prepared from NaSH (0.23 g, 4.1 mmol) and S₈ (0.043 g, 0.17 mmol) in methanol (20 cm³) was added to a suspension of CrCl₂ (0.50 g, 4.1 mmol) in methanol (10 cm³) at -78 °C. A mixture of a brown solution and a brown precipitate formed. PEt₃ (1.2 cm³, 8.2 mmol) was added to the mixture, which was stirred and allowed to warm slowly (*ca.* 8 h) to room temperature. The solvent was removed *in vacuo*, and the resulting solid was extracted with hot benzene (30 cm³). The benzene extract was allowed to stand at room temperature to yield **3·**2C₆H₆ (0.20 g, 21 %) as black crystals. **3·**2C₆H₆:

$^1\text{H NMR}$ (C_6D_6): $\delta = 7.27$ (12H, C_6H_6), 1.80 (54H, PCH_2CH_3), 0.04 (36H, PCH_2). The signal due to the hydride associated with the cluster unit could not be detected. Found: C, 39.45; H, 7.06; S, 17.62%. Calcd for $\text{C}_{48}\text{H}_{103}\text{Cr}_6\text{P}_6\text{S}_8$: C, 40.18; H, 7.24; S, 17.88%.

Synthesis of $[\text{Cr}_6\text{S}_8(\text{D})_{0.8}(\text{H})_{0.2}(\text{PEt}_3)_6]\cdot 2\text{C}_6\text{H}_6$ ($4\cdot 2\text{C}_6\text{H}_6$).

The procedure for $3\cdot 2\text{C}_6\text{H}_6$ was followed, except for using MeOD as solvent. Yield 0.20 g (21%). The IR spectrum and $^1\text{H NMR}$ spectrum are identical with those of $3\cdot 2\text{C}_6\text{H}_6$. $4\cdot 2\text{C}_6\text{H}_6$: Found: C, 39.38; H, 6.87; S, 17.39%. Calcd for $\text{C}_{48}\text{H}_{103}\text{Cr}_6\text{P}_6\text{S}_8$: C, 40.18; H, 7.24; S, 17.88%.

Synthesis of $[\text{Cr}_6\text{S}_8(\text{D})(\text{PEt}_3-d_{15})_6]\cdot 2\text{C}_6\text{D}_6$ ($5\cdot 2\text{C}_6\text{D}_6$).

1. Preparation of Bromoethane- d_5 .

The procedure for the preparation of bromoethane- d_5 was nearly similar to that for 1-bromo-2-methylpropane.⁴⁷ Phosphorus tribromide (195 g, 0.70 mol) was added dropwise to ethanol- d_6 (99 g, 1.9 mol) at -20°C . The crude bromoethane- d_5 was distilled from the reaction mixture at $38 - 40^\circ\text{C}$. The distillate was opened to the air, and diluted with *o*-xylene (150 cm^3) for the prevention of the volatilization of bromoethane- d_5 . The *o*-xylene solution was washed with an aqueous solution of sodium hydroxide (*ca.* 0.01 M) until the odor of hydrobromic acid disappeared. The solution was dried with anhydrous sodium sulfate (Na_2SO_4) (100 g) and distilled under argon. The fraction boiling between $38 - 40^\circ\text{C}$ was collected. Yield 114 g (53%).

2. Preparation of PEt_3-d_{15} .

A 2000 cm^3 three-necked round-bottomed flask was fitted with a mechanical stirrer and a reflux condenser. Magnesium (27 g, 1.1 mol) and diethyl ether (Et_2O) (430 cm^3) were placed in the flask, to which a mixture of bromoethane- d_5 (80 cm^3 , 1.1 mol) and Et_2O (130 cm^3) was added dropwise during 80 min. The resulting suspension was refluxed for 1 h, and cooled to -78°C . A mixture of phosphorus trichloride (26 cm^3 , 0.30 mol) and Et_2O (54 cm^3) was added dropwise to the suspension, which was allowed to warm to room temperature, stirred for 2 h, and cooled again to -20°C . The unreacted reagents were

hydrolyzed with an aqueous solution (60 g) of ammonium chloride (500 cm³). The organic layer was extracted. The residual mixture was washed with Et₂O (4 × 100 cm³), and the washings were added to the extract. The resulting Et₂O solution was dried with Na₂SO₄ (100 g) and distilled. The fraction boiling between 128 - 130 °C was collected. Yield 14.1 g (42%).

3. Preparation of the Deuterated Cluster 5-2C₆D₆.

Complex 5-2C₆D₆ was prepared following the procedure for 3-2C₆H₆ except for the use of deuterated compounds. A solution of NaS_xD ($x = 1.33$) prepared from NaSD (1.85 g, 32.8 mmol) and S₈ (0.34 g, 1.4 mmol) in MeOD (160 cm³) was added to a suspension of CrCl₂ (4.03 g, 32.8 mmol) in MeOD (80 cm³) at -78 °C. A mixture of a brown solution and a brown precipitate formed. PEt₃-d₁₅ (9.5 cm³, 65.6 mmol) was added to the mixture, which was stirred, allowed to warm slowly (ca. 8 h) to room temperature, and stirred additionally for 24 h. The solvent was removed *in vacuo*, and the resulting solid was extracted with hot benzene (230 cm³). The benzene extract was allowed to stand at room temperature to yield 5-2C₆D₆ (1.43 g, 17 %) as black crystals. The perfect deuterium substitution in 5 was confirmed by FAB mass spectrum (Figure 14 under **Results and Discussion**).

1-2-2. Molecular Orbital Calculation

The molecular orbitals of model clusters [Cr₆Se₈(PH₃)₆] and [Cr₆Se₈(H)(PH₃)₆] were calculated by the DV-X α method with the self-consistent charge approximation.⁴⁸⁻⁵³ All calculations were performed on a GATEWAY2000 computer. The exchange parameter α was taken to be 0.70 in all calculations. Numerical atomic orbitals from atomic Hartree-Fock-Slater calculations were used as basis functions. The radial functions of the AOs were calculated at the points of the distance $r = r_n \exp(-k/32)$ ($k = 0.299$) from the nucleus, where r_n was 30 au for non-hydrogen atoms, and 20 au for hydrogen atoms (1 au = 0.52918 Å for length). For the calculation of higher AOs, additional well potentials were added,⁴⁹ which were constant for $r < r_w$ and proportional to $1/r$ for $r > r_w$, where the potential depth is -0.05 au for Cr, -0.5 au for P, and -0.8 au for Se (1 au = 4.3597 × 10⁻¹⁸ J for energy). All the orbitals through 4d were included for Se, through 4p for Cr, through 3d for S and P, and only

1s was used for H. The sampling points for the numerical integration of the matrix elements were distributed according to the literature.⁴⁹ The number of the sampling points was 50 000. The coulomb potential was approximated by using the sum of the spherical atomic potentials. After the molecular orbitals were obtained as the solution of secular equations, the electron population on each atomic orbitals was calculated and the values were used for the next calculation of the atomic orbitals. The process was cycled until the transfer of the electron by the Löwdin population analysis^{54, 55} was less than 0.0001 for all atomic orbitals.

The symmetries of the model compounds were assumed as O_h . The geometric parameters were taken from the averaged values obtained by the X-ray structure analyses. In the PH_3 ligands, the P-H distances were set to 1.40 Å and the Cr-P-H angles to 115°. Hydrogen atoms which lower the symmetries of the whole structures were treated according to the literature.⁵⁶ For all the complexes, spin-unrestricted calculations were performed.

1-2-3. FAB Mass Spectra

FAB mass spectra were obtained with a JEOL JMS-HX 110A double-focusing mass spectrometer equipped with an XMS data system. A fast-atom xenon beam was generated from Xe^+ ions, which were accelerated to 1 kV with a FAB gun emission current of 1 mA. The crystalline samples (~1 µg) were placed on the stainless-steel tip of the probe, mixed with *m*-nitrobenzyl alcohol (Aldrich) as a matrix, and exposed to the xenon beam for the desorption.

1-2-4. Cyclic Voltammetry

Cyclic voltammetry (CV) was performed on a BAS CV-50W cyclic voltammograph. Three electrodes consisting of a platinum working electrode, a platinum wire counter electrode, and a Ag/Ag^+ (AgNO_3 (0.01 N) in CH_3CN) reference electrode were used for the measurements. The compounds were dissolved in THF together with 0.1 M tetrabutylammonium perchlorate as a supporting electrolyte, and scanning rate was 100 mV/s.

1-2-5. X-ray Structure Determination

A single crystal of 1 suitable for X-ray analysis was obtained by allowing a toluene-ethanol

solution to stand at room temperature and that of **2** by recrystallization from THF. The crystals were sealed in glass capillaries for the X-ray measurements. Because the crystal of **2** contained THF molecules escaping from the crystal, the solvent was also sealed for **2**. The X-ray measurements of the crystals were performed on a Rigaku AFC-7R diffractometer with graphite-monochromated Mo K α radiation at 226 K for **1** and at 293 K for **2**. Intensity data were collected with 2θ - ω scans in the range $5^\circ < 2\theta < 55^\circ$ for **1** and $7^\circ < 2\theta < 55^\circ$ for **2**. Three standard reflections were monitored every 150 reflections. Neither of the crystals showed significant decay over the period of data collections. All calculations were performed using the TEXSAN crystallographic package.⁵⁷ The data were corrected for the Lp factor and empirically for the absorption using the ψ -scan method. The positions of the chromium and selenium atoms were determined by the direct method (SHELXS86),⁵⁸ and the other non-hydrogen atoms were located using Fourier techniques (DIRDIF94).⁵⁹ The THF molecules in the crystal of **2** are orientationally disordered around the 3-fold axis. The four carbon atoms and one oxygen atom of the THF molecule were positionally disordered. Thus each of the mixed carbon-oxygen sites of the THF molecule was refined as a carbon atom with a site-occupancy factor of $4/15$ and an oxygen atom with that of $1/15$, and their positional and thermal parameters were constrained to move together. The atoms of the THF molecules in the crystal of **2** were refined isotropically, and all the other non-hydrogen atoms in the crystals of **1** and **2** were refined anisotropically. The hydrogen atoms of the triethylphosphine ligands were located on calculated positions. At the final stage of the refinements, an empirical extinction correction proportional to the observed intensities was included. The final cycle of full-matrix least-squares refinement was based on 9491 observed reflections ($|F_o| > 3\sigma(F_o)$) for **1** and on 2087 observed reflections ($|F_o| > 4\sigma(F_o)$) for **2**. The crystallographic data are given in Table 1. The final atomic parameters of **1** and **2** are listed in Tables 2 and 3.

Table 1. Crystal Parameters and X-ray Diffraction Data for 1 and 2·2THF

	1	2·2THF
Formula	C ₃₆ H ₉₀ Cr ₆ P ₆ Se ₈	C ₄₄ H ₁₀₇ O ₂ Cr ₆ P ₆ Se ₈
Fw	1652.61	1797.83
Crystal size, mm	0.3 × 0.3 × 0.1	0.6 × 0.6 × 0.5
Space group	<i>P</i> $\bar{1}$ (No.2)	<i>R</i> $\bar{3}$ (No.148)
<i>a</i> , Å	12.887(2)	17.384(4)
<i>b</i> , Å	25.332(7)	
<i>c</i> , Å	12.061(3)	19.768(4)
α , deg.	111.23(2)	
β , deg.	108.25(2)	
γ , deg.	109.86(2)	
<i>V</i> , Å ³	2994(2)	5173(2)
λ , Å	0.7107	0.7107
<i>T</i> , K	226	293
<i>Z</i>	2	3
μ , cm ⁻¹	60.99	53.04
$\rho_{\text{calcd.}}$, g/cm ³	1.833	1.731
<i>R</i> ^a , <i>R</i> _w ^b	0.045, 0.037	0.038, 0.032

^a $R = \sum ||F_o| - |F_c|| / \sum |F_o|$. ^b $R_w = \{ \sum [w(|F_o| - |F_c|)^2] / \sum [w|F_o|^2] \}^{1/2}$; $w = 1 / \{ \sigma^2(F_o) + p^2|F_o|^2/4 \}$; $p = 0.0115$ for 1 and 0.0033 for 2·2THF.

Table 2. Atomic Coordinates and Temperature Parameters for $[\text{Cr}_6\text{Se}_8(\text{PEt}_3)_6]$ (1)

atom	x/a	y/b	z/c	U_{iso}^a
Se1	0.08480(6)	0.01817(3)	0.27983(7)	0.0223(2)
Se2	0.04498(6)	0.13014(3)	0.19643(7)	0.0229(2)
Se3	-0.20219(6)	-0.11023(3)	-0.01374(7)	0.0232(2)
Se4	0.24415(6)	-0.00176(3)	0.09592(7)	0.0225(2)
Se5	0.25737(6)	0.51395(3)	0.62445(7)	0.0260(2)
Se6	0.05168(6)	0.49493(3)	0.75509(7)	0.0258(2)
Se7	0.00505(6)	0.38978(3)	0.29813(7)	0.0269(2)
Se8	0.20181(6)	-0.36982(3)	-0.42823(7)	0.0252(2)
Cr1	-0.09073(9)	0.01146(5)	0.1046(1)	0.0204(3)
Cr2	0.16394(9)	0.07281(5)	0.1673(1)	0.0202(3)
Cr3	0.02403(9)	-0.06409(5)	0.0477(1)	0.0205(3)
Cr4	0.03148(10)	0.43435(5)	0.5301(1)	0.0232(3)
Cr5	0.14519(10)	0.57159(5)	0.6871(1)	0.0239(3)
Cr6	0.11827(10)	0.51122(5)	0.4251(1)	0.0233(3)
P1	-0.2065(2)	0.02450(9)	0.2255(2)	0.0274(5)
P2	0.3612(2)	0.15708(8)	0.3770(2)	0.0279(5)
P3	0.0520(2)	-0.14038(8)	0.1109(2)	0.0281(5)
P4	0.0707(2)	0.35685(9)	0.5790(2)	0.0303(5)
P5	0.3227(2)	0.66039(9)	0.9103(2)	0.0346(5)
P6	0.2574(2)	0.52231(9)	0.3299(2)	0.0316(5)
C1	-0.1921(7)	0.1056(3)	0.3001(8)	0.043(2)
C2	-0.2467(8)	0.1232(4)	0.1970(8)	0.049(3)
C3	-0.1591(6)	0.0166(4)	0.3741(7)	0.038(2)
C4	-0.1854(8)	-0.0521(4)	0.3438(8)	0.050(3)
C5	-0.3788(7)	-0.0334(4)	0.1215(8)	0.040(2)
C6	-0.4566(7)	-0.0286(4)	0.1938(9)	0.060(3)
C7	0.3537(7)	0.2208(3)	0.5051(7)	0.040(2)
C8	0.2720(8)	0.1960(4)	0.5610(8)	0.050(3)
C9	0.4331(7)	0.1252(3)	0.4719(7)	0.036(2)
C10	0.5583(8)	0.1759(4)	0.6075(9)	0.065(3)
C11	0.4885(7)	0.2081(3)	0.3613(8)	0.041(2)
C12	0.5410(7)	0.1729(4)	0.2848(9)	0.055(3)
C13	-0.0046(7)	-0.1467(3)	0.2283(7)	0.036(2)
C14	0.0147(9)	-0.1914(4)	0.2797(9)	0.066(3)
C15	0.2164(7)	-0.1218(4)	0.1963(8)	0.043(2)
C16	0.3018(7)	-0.0605(4)	0.3378(8)	0.051(3)
C17	-0.0270(7)	-0.2264(3)	-0.0296(8)	0.043(2)
C18	-0.1676(9)	-0.2633(4)	-0.1015(10)	0.069(3)
C19	0.2028(7)	0.3960(3)	0.7511(8)	0.041(2)
C20	0.2374(9)	0.3526(4)	0.7938(10)	0.073(3)

C21	-0.0628(7)	0.2917(3)	0.5636(7)	0.036(2)
C22	-0.1039(8)	0.3156(4)	0.6693(9)	0.051(3)
C23	0.1091(8)	0.3057(4)	0.4652(9)	0.048(3)
C24	0.2303(9)	0.3418(4)	0.4709(10)	0.063(4)
C25	0.3049(8)	0.7303(4)	0.9946(8)	0.057(3)
C26	0.2995(9)	0.7696(4)	0.9236(9)	0.061(3)
C27	0.3609(7)	0.6407(4)	1.0422(8)	0.051(3)
C28	0.4046(8)	0.5903(4)	1.0172(9)	0.065(3)
C29	0.4719(7)	0.6978(4)	0.9111(8)	0.047(2)
C30	0.5895(8)	0.7543(4)	1.0510(9)	0.071(3)
C31	0.4017(7)	0.6043(3)	0.4248(8)	0.042(2)
C32	0.4916(7)	0.6257(4)	0.5687(9)	0.051(3)
C33	0.1893(8)	0.5095(4)	0.1591(8)	0.049(3)
C34	0.0821(9)	0.4396(5)	0.0455(9)	0.070(3)
C35	0.3194(7)	0.4662(3)	0.3152(8)	0.044(2)
C36	0.4042(8)	0.4690(4)	0.2505(10)	0.063(3)

$${}^a U_{\text{iso}} = (1/3) \sum_i \sum_j U_{ij} a_i^* a_j^* \mathbf{a}_i \cdot \mathbf{a}_j$$

$(U_{ij}) (\times 100)$

atom	U_{11}	U_{22}	U_{33}	U_{12}	U_{13}	U_{23}
Se1	2.47(4)	2.51(3)	1.89(3)	1.43(3)	1.06(3)	1.18(3)
Se2	2.58(4)	2.06(3)	2.21(4)	1.45(3)	1.13(3)	0.88(3)
Se3	2.24(3)	2.17(3)	2.51(4)	1.02(3)	1.20(3)	1.27(3)
Se4	2.00(3)	2.49(3)	2.30(4)	1.40(3)	0.98(3)	1.14(3)
Se5	2.11(3)	2.76(4)	3.01(4)	1.40(3)	1.22(3)	1.48(3)
Se6	2.61(4)	2.70(4)	2.53(4)	1.42(3)	1.30(3)	1.39(3)
Se7	2.88(4)	2.26(3)	2.83(4)	1.48(3)	1.57(3)	0.97(3)
Se8	2.27(4)	2.04(3)	2.84(4)	0.98(3)	1.19(3)	1.11(3)
Cr1	2.05(5)	2.11(5)	1.99(6)	1.22(4)	0.99(5)	0.97(4)
Cr2	2.06(5)	2.02(5)	2.04(6)	1.21(5)	1.00(5)	0.99(5)
Cr3	2.17(5)	2.08(5)	1.98(6)	1.24(4)	1.00(5)	1.01(4)
Cr4	2.14(5)	2.16(5)	2.60(6)	1.18(5)	1.22(5)	1.09(5)
Cr5	2.30(6)	2.17(5)	2.52(6)	1.17(5)	1.17(5)	1.05(5)
Cr6	2.22(6)	2.16(5)	2.49(6)	1.19(5)	1.13(5)	1.06(5)
P1	2.39(9)	3.16(10)	2.54(10)	1.57(8)	1.33(8)	1.14(8)
P2	2.64(10)	2.27(9)	2.45(10)	1.25(8)	0.76(8)	0.76(8)
P3	3.2(1)	2.43(9)	2.8(1)	1.65(8)	1.26(9)	1.38(8)
P4	3.1(1)	2.78(10)	3.6(1)	1.76(9)	1.76(9)	1.76(9)
P5	3.3(1)	3.1(1)	2.4(1)	0.96(9)	1.11(9)	1.00(9)
P6	3.1(1)	3.1(1)	3.7(1)	1.84(9)	2.09(10)	1.72(9)
C1	4.6(5)	3.7(4)	4.5(5)	2.5(4)	2.8(4)	1.2(4)

C2	6.0(6)	5.2(5)	4.6(5)	4.2(5)	2.9(5)	2.3(4)
C3	2.8(4)	5.3(5)	3.2(4)	2.0(4)	1.7(4)	2.1(4)
C4	5.2(5)	6.2(6)	4.5(5)	2.8(5)	2.7(5)	3.5(5)
C5	3.1(4)	4.4(4)	3.7(5)	1.9(4)	1.6(4)	1.5(4)
C6	3.6(5)	7.5(6)	6.8(7)	2.9(5)	3.4(5)	2.9(5)
C7	4.5(5)	3.2(4)	2.9(4)	2.4(4)	1.1(4)	0.6(3)
C8	6.8(6)	5.1(5)	3.3(5)	4.0(5)	2.6(5)	1.4(4)
C9	3.5(4)	3.2(4)	2.9(4)	1.7(3)	0.9(4)	1.1(3)
C10	5.3(6)	5.3(6)	4.5(6)	2.5(5)	-0.8(5)	1.5(5)
C11	3.5(4)	2.6(4)	4.8(5)	1.0(3)	1.8(4)	1.5(4)
C12	3.7(5)	4.6(5)	6.1(6)	1.2(4)	2.7(5)	1.6(5)
C13	4.1(4)	3.1(4)	3.2(4)	1.7(4)	1.4(4)	2.0(3)
C14	8.6(7)	6.2(6)	6.8(7)	4.1(6)	3.4(6)	4.9(6)
C15	4.7(5)	4.6(5)	5.1(5)	3.5(4)	2.3(4)	2.9(4)
C16	3.8(5)	5.0(5)	4.8(5)	2.4(4)	0.7(4)	2.2(4)
C17	4.5(5)	2.9(4)	4.0(5)	1.7(4)	1.5(4)	1.1(4)
C18	6.8(7)	2.7(5)	6.6(7)	1.5(5)	1.4(6)	0.9(5)
C19	3.1(4)	3.5(4)	4.4(5)	1.8(4)	0.8(4)	1.9(4)
C20	6.5(7)	6.4(6)	6.3(7)	3.3(5)	0.2(5)	3.5(6)
C21	3.6(4)	2.8(4)	4.0(5)	1.5(3)	1.5(4)	1.8(4)
C22	5.0(5)	4.2(5)	5.5(6)	1.1(4)	3.1(5)	2.6(4)
C23	6.2(6)	3.6(4)	6.5(6)	3.3(4)	4.2(5)	2.6(4)
C24	8.3(7)	7.3(6)	9.4(8)	6.4(6)	6.7(7)	5.6(6)
C25	6.3(6)	4.6(5)	3.7(5)	2.1(5)	2.4(5)	0.5(4)
C26	9.3(7)	3.3(5)	6.0(6)	3.5(5)	4.1(6)	2.2(4)
C27	4.2(5)	4.8(5)	4.1(5)	0.8(4)	1.5(4)	2.2(4)
C28	5.2(6)	7.5(7)	5.4(6)	2.5(5)	1.0(5)	4.0(5)
C29	2.9(4)	3.9(5)	4.0(5)	0.4(4)	0.8(4)	1.1(4)
C30	4.7(6)	6.2(6)	4.5(6)	-0.3(5)	1.1(5)	1.3(5)
C31	4.4(5)	3.8(4)	5.1(5)	2.3(4)	2.9(4)	2.3(4)
C32	3.3(5)	4.3(5)	5.8(6)	1.3(4)	2.0(4)	1.6(4)
C33	5.1(5)	7.5(6)	4.7(5)	3.9(5)	3.6(5)	3.8(5)
C34	6.3(6)	9.3(8)	3.7(5)	4.6(6)	2.1(5)	1.7(5)
C35	3.8(5)	3.7(4)	6.5(6)	2.5(4)	3.3(5)	2.2(4)
C36	5.6(6)	7.1(6)	8.4(7)	4.6(5)	4.7(6)	3.7(6)

Table 3. Atomic Coordinates and Thermal Parameters for $[\text{Cr}_6\text{Se}_8(\text{H})(\text{PEt}_3)_6]\cdot 2\text{THF}(2\cdot 2\text{THF})$

atom	x/a	y/b	z/c	U_{iso}^a
Se1	0.0000	0.0000	0.15221(5)	0.0311(1)
Se2	-0.11894(3)	0.06583(3)	0.05077(3)	0.0305(2)
Cr	0.03613(5)	0.10054(5)	0.05482(4)	0.0261(2)
P	0.08799(10)	0.23125(10)	0.12360(8)	0.0369(4)
C1	0.1610(4)	0.2401(4)	0.1936(3)	0.048(2)
C2	0.1962(5)	0.3210(5)	0.2390(4)	0.078(3)
C3	0.0036(4)	0.2488(4)	0.1639(3)	0.056(2)
C4	-0.0511(5)	0.1807(5)	0.2184(4)	0.074(3)
C5	0.1515(4)	0.3389(4)	0.0804(3)	0.053(2)
C6	0.2393(4)	0.3574(4)	0.0490(4)	0.069(2)
OC11	-0.076(2)	-0.023(3)	0.368(2)	0.11(1)
OC12	-0.046(3)	0.030(3)	0.423(2)	0.13(1)
OC13	0.046(3)	0.088(2)	0.410(2)	0.13(1)
OC14	0.081(2)	0.014(3)	0.386(2)	0.102(9)
OC15	-0.023(4)	-0.053(2)	0.348(1)	0.13(1)

$$^a U_{\text{iso}} = \frac{1}{3} \sum_i \sum_j U_{ij} a_i^* a_j^* \cdot \mathbf{a}_i \cdot \mathbf{a}_j$$

$(U_{ij}) (\times 100)$

atom	U_{11}	U_{22}	U_{33}	U_{12}	U_{13}	U_{23}
Se1	3.37(3)	3.37	2.58(5)	1.69	0.00	0.00
Se2	2.99(3)	3.12(3)	3.44(3)	1.81(3)	0.25(3)	-0.07(3)
Cr	2.55(4)	2.58(5)	2.72(4)	1.29(4)	0.05(4)	-0.03(4)
P	3.95(9)	3.43(9)	3.94(9)	2.03(8)	-0.18(8)	-0.72(7)
C1	5.2(4)	4.6(4)	4.4(4)	2.4(3)	-0.7(3)	-1.3(3)
C2	8.8(6)	8.4(6)	6.3(5)	4.4(5)	-2.8(4)	-3.8(4)
C3	6.3(5)	5.0(4)	6.7(5)	3.7(4)	-0.9(4)	-2.4(4)
C4	8.0(6)	9.6(6)	6.4(5)	5.7(5)	1.3(4)	-1.5(5)
C5	6.4(5)	3.1(3)	6.0(4)	2.1(3)	-0.6(4)	-0.8(3)
C6	5.5(4)	4.1(4)	8.8(6)	0.7(4)	-0.3(4)	0.7(4)

1-2-6. Powder Neutron Diffraction Analysis

Neutron diffraction data of $5\cdot 2C_6D_6$ were collected on the time-of-flight (TOF) powder diffractometer VEGA⁶⁰ installed at the pulsed spallation cold neutron source in the National Laboratory for High-Energy Physics (KEK) in Tsukuba, Japan. The sample crystals (1.43 g) were crushed into fine powder and contained in a vacuum-tight cylindrical holder made of vanadium (10 mm in diameter, 50 mm in height, and 0.2 mm in thickness) under argon atmosphere. Its intensity data were recorded with the back scattering bank of detectors in the TOF, t , region 12 484 - 46 000 μ s, corresponding to the d -spacing range 1.25 - 4.6 \AA ($d = 1/9979.69$). The structural analyses were carried out with the Rietveld refinement program RIETAN-96T⁶¹ on a GATEWAY2000 computer. The values of coherent scattering lengths in fm used for the analysis were 3.635 for Cr, 2.847 for S, 5.130 for P, 6.646 for C, and 6.671 for D.⁶² The intensity data in the t region 30 866 - 31 250, 33 400 - 33 750, 34 200 - 34 600, 38 600 - 39 400, 42 500 - 43 000, 45 000 - 45 500 μ s were excluded in the refinement, where peaks unassignable to **5** were observed. The peak profiles and baseline were fitted with pseudo-Voigt functions (the linear combination of Gaussian and Lorentzian functions) and Legendre polynomials, respectively. The space group, lattice constants, and atomic coordinates were taken from those obtained by the single-crystal X-ray structure analysis for **3**.⁸ For D atoms, the positions were calculated as follows. In the triethylphosphine ligands, the C-D distances were set to 1.10 \AA , the P-C-D and C-C-D angles to 109°, and the orientation of the methyl group to be staggered relative to the neighboring methylene group. In the benzene molecule, the C-D distances and the C-C-D angles were set to 1.10 \AA and 120°, respectively. All the atoms were refined isotropically. Preferred orientation was not corrected.

1-2-7. Magnetic Measurement and Calculation

Magnetic susceptibilities of **1-3** were measured in the temperature ranges 2 - 330, 2 - 330, and 4.5 - 330 K, respectively, with a Quantum Design MPMS SQUID. The absence of ferromagnetic impurities was checked by the magnetization measurements at 300 K. The magnetic field of the measurements was 100 G over the whole measured temperature range

for **1** and 5 kG in the temperature range 4.5 - 30 K and 10 kG in the range 30 - 330 K for **2** and **3**, where the magnetization versus magnetic field curves were linear. The crystalline samples (*ca.* 30 mg for **1**, *ca.* 90 mg for **2**-2THF, and *ca.* 100 mg for **3**-2C₆H₆) were filled in cellophane sample holders under nitrogen atmosphere. The magnetic susceptibilities of the holders were determined separately. Diamagnetic corrections were estimated from Pascal's constants. All calculations were performed on a GATEWAY2000 computer. The programs for calculating the energy levels of the spin states and for the non-linear least-squares fittings were made with the turbo-pascal soft and the Maple V release 4 soft, respectively.

1-2-8. Other Physical Measurements

The FT-IR spectra for **1** (Figure 1), **2**-2THF (Figure 2), and **3**-2C₆H₆ (Figure 3) were measured (4000 - 400 cm⁻¹) with a JASCO FT/IR-300E spectrometer using KBr disks. The electronic spectra of hexane solution for **1** (Figure 4), **2**-2THF (Figure 5), and **3**-2C₆H₆ (Figure 6) were measured (210 - 1680 nm) with a HITACHI U-3500 spectrometer. The ¹H NMR (500 MHz) spectra were measured in C₆D₆ with a JEOL A500 spectrometer using C₆H₆ as the internal standard (illustrated in Figure 7).

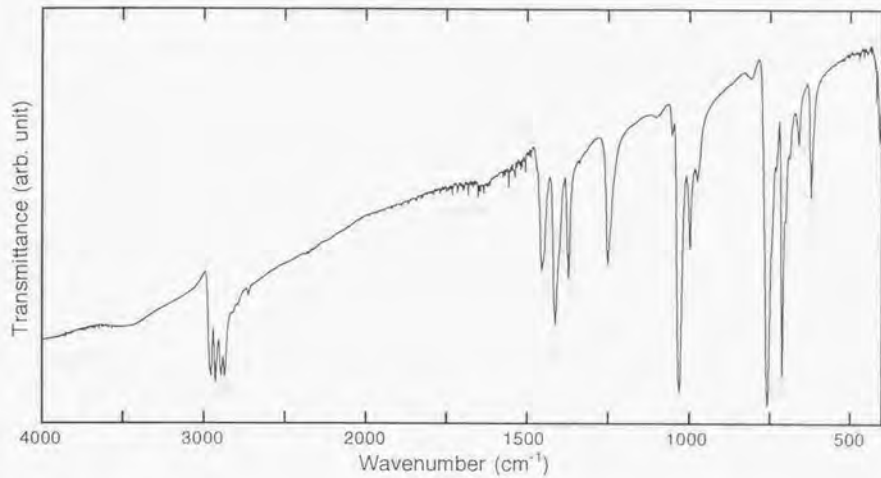


Figure 1. FT-IR spectrum of $[\text{Cr}_6\text{Se}_8(\text{PEt}_3)_6]$ (**1**). All the peaks are due to triethylphosphine ligands.⁶³

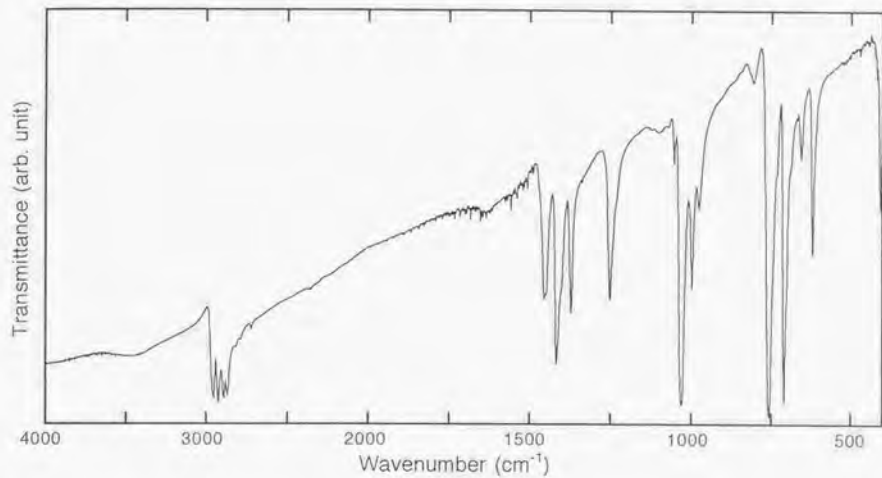


Figure 2. FT-IR spectrum of $[\text{Cr}_6\text{Se}_8(\text{H})(\text{PEt}_3)_6] \cdot 2\text{THF}$ (**2·2THF**). All the peaks are due to triethylphosphine ligands.⁶³

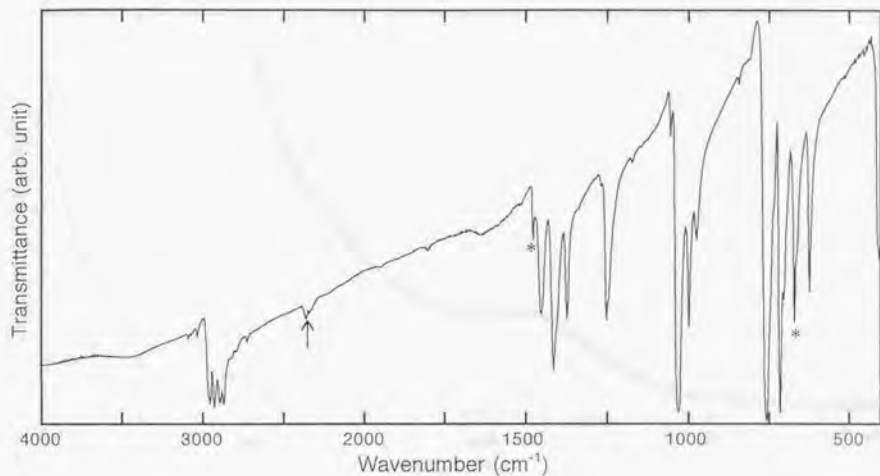


Figure 3. FT-IR spectrum of $[\text{Cr}_6\text{S}_8(\text{H})(\text{PEt}_3)_6] \cdot 2\text{C}_6\text{H}_6$ ($3 \cdot 2\text{C}_6\text{H}_6$). Asterisks and an arrow indicate the peaks due to solvent benzene molecules and CO_2 in the air, respectively. All the other absorptions are assignable to those for triethylphosphine ligands.⁶³

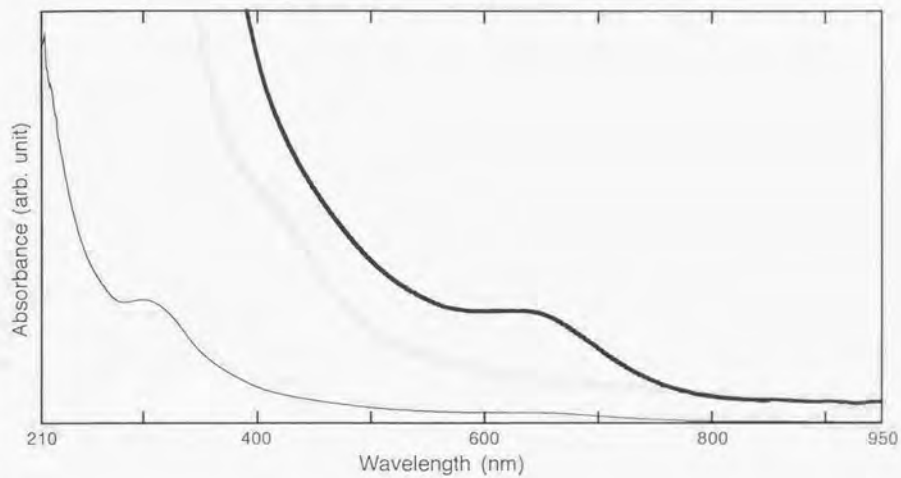


Figure 4. Electronic spectrum of $[\text{Cr}_6\text{Se}_8(\text{PEt}_3)_6]$ (1) in hexane. No absorption peak was observed between 950 and 1680 nm.

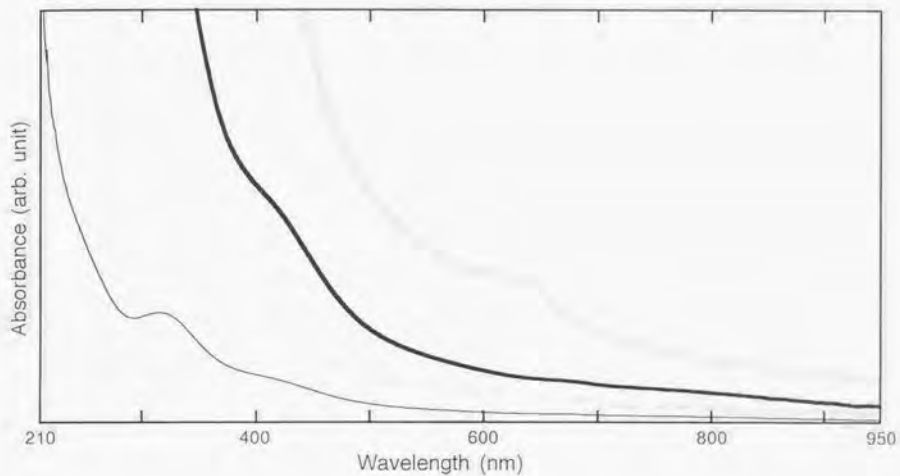


Figure 5. Electronic spectrum of $[\text{Cr}_6\text{Se}_8(\text{H})(\text{PEt}_3)_6] \cdot 2\text{THF}$ (2·2THF) in hexane. No absorption peak was observed between 950 and 1680 nm.

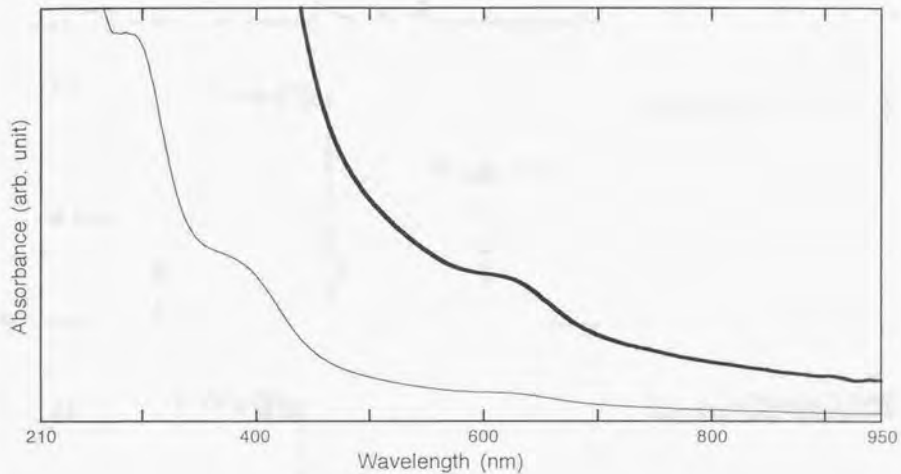


Figure 6. Electronic spectrum of $[\text{Cr}_6\text{S}_8(\text{H})(\text{PEt}_3)_6] \cdot 2\text{C}_6\text{H}_6$ ($3 \cdot 2\text{C}_6\text{H}_6$) in hexane. No absorption peak was observed between 950 and 1680 nm.

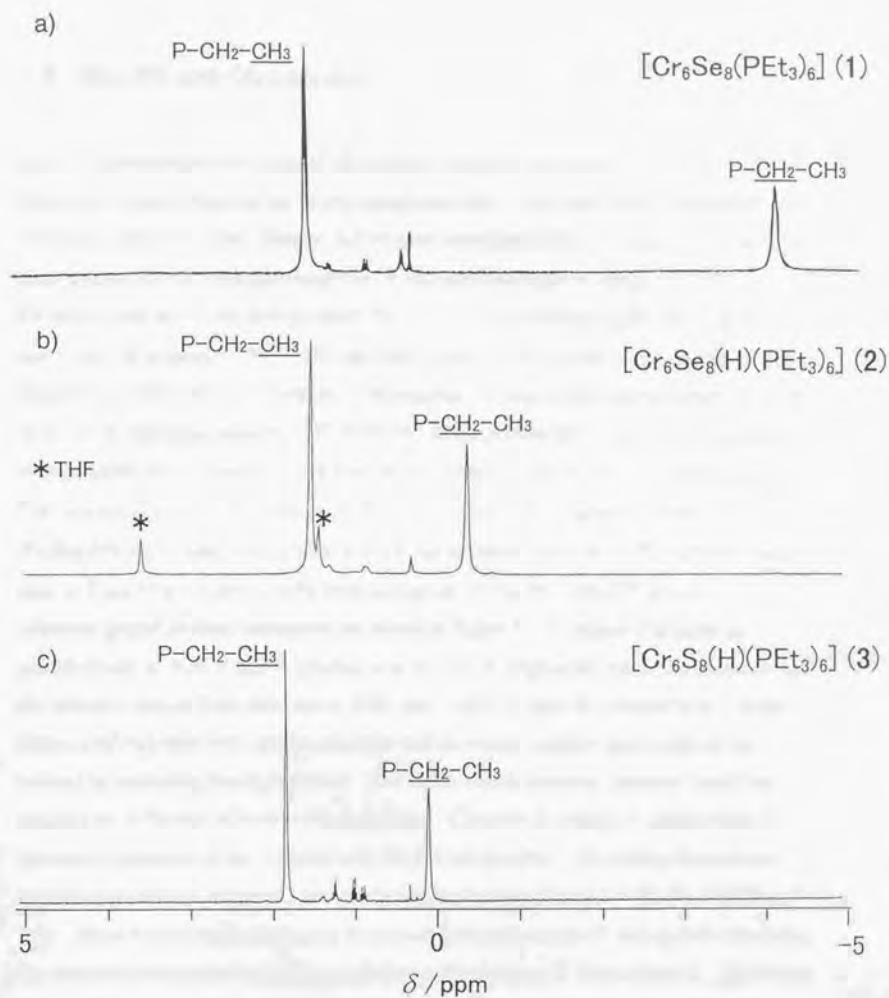


Figure 7. ^1H NMR spectra of (a) $[\text{Cr}_6\text{Se}_8(\text{PET}_3)_6]$ (1), (b) $[\text{Cr}_6\text{Se}_8(\text{H})(\text{PET}_3)_6] \cdot 2\text{THF}$ (2·2THF), and (c) $[\text{Cr}_6\text{S}_8(\text{H})(\text{PET}_3)_6] \cdot 2\text{C}_6\text{H}_6$ (3·2C₆H₆). Asterisks in the spectrum of 2 indicate the signals due to solvent THF molecules.

1-3 Results and Discussion

1-3-1. Syntheses of Hexanuclear Chromium Cluster Complexes

Metal chalcogenide hexanuclear cluster complexes with a M_6E_8 unit have been synthesized by various methods. Molybdenum and tungsten complexes have been prepared by reductive condensation of two trinuclear complexes or halogen-chalcogen exchange.^{11, 17-20, 22} Rhenium complexes have been prepared by cutting out a molecular cluster skeleton from non-molecular clusters.^{24, 26, 28} On the other hand, iron and cobalt complexes have been obtained by "self-assembly" methods, in which cluster cores are formed spontaneously from mono- or di-nuclear complexes.^{31-35, 37-41, 44} In the present study, the chromium clusters were prepared by self-assembly reactions of non-molecular $CrCl_2$ with chalcogen sources. The reaction of $CrCl_2$ with Na_2Se_x and PEt_3 in MeOH at $-78^\circ C$ gave a mixture of $[Cr_6Se_8(PEt_3)_6]$ (**1**) and $[Cr_6Se_8(H)(PEt_3)_6]$ (**2**) (in a ratio of *ca.* 4 : 5). The extra hydrogen atom in **2** must have come from the hydroxyl group of MeOH. The CV (cyclic voltammograms) of these complexes are shown in Figure 8. Complex **1** exhibits an oxidation step at -0.50 V and a reduction step at -1.75 V (Figure 8a), while the oxidation and the reduction step of **2** are observed at -0.81 and -1.48 V (Figure 8b), respectively. Since these complexes have very similar solubility and molecular weights, they could not be isolated by exploiting these properties. The author could, however, separate **1** and **2** by utilizing the difference of their redox properties. Complex **2** is easier to oxidize than **1** because the potential of the oxidation step for **2** is less positive. By adding ferrocenium hexafluorophosphate, complex **2** was oxidized selectively and turned to $[Cr_6Se_8(H)(PEt_3)_6]^+$ (**2⁺**). Since this oxidized cluster was acetone-soluble and complex **1** was acetone-insoluble, the extraction with acetone could separate the oxidized cluster **2⁺** from cluster **1**. Reduction of the oxidized cluster **2⁺** by cobaltocene returned it to the neutral cluster **2**. When the reaction of $CrCl_2$ with Na_2Se_x and PEt_3 was carried out in the presence of *p*-toluenesulfonic acid, the ratio of **1** to **2** decreased. The reaction using $NaSe_4H^{64}$ instead of Na_2Se_x also lowered the ratio. The proportion of **1** and **2** may be dependent on the pH in MeOH solution.

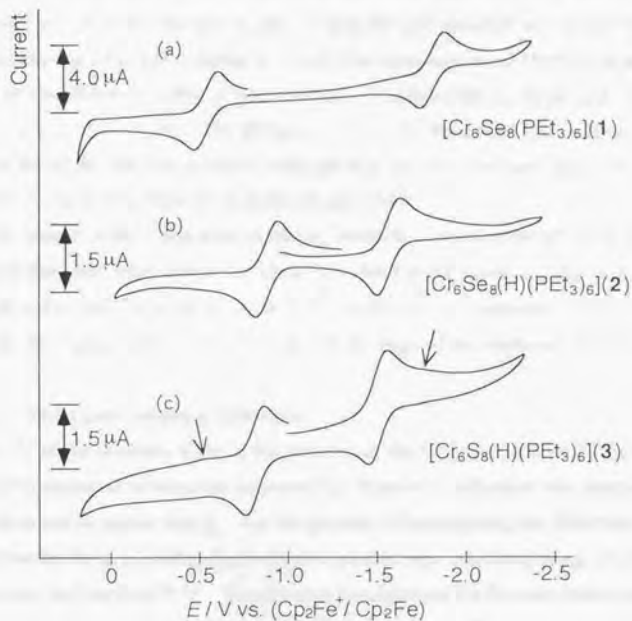


Figure 8. Cyclic voltammograms of (a) $[\text{Cr}_6\text{Se}_8(\text{PEt}_3)_6]$ (1), (b) $[\text{Cr}_6\text{Se}_8(\text{H})(\text{PEt}_3)_6] \cdot 2\text{THF}$ (2·2THF), and (c) $[\text{Cr}_6\text{S}_8(\text{H})(\text{PEt}_3)_6] \cdot 2\text{C}_6\text{H}_6$ (3·2C₆H₆). The very weak peaks marked by arrows in the CV of 3 suggest the existence of non-hydride cluster $[\text{Cr}_6\text{S}_8(\text{PEt}_3)_6]$.

The reaction of CrCl_2 with NaS_2H and PEt_3 in MeOH at -78°C gave $[\text{Cr}_6\text{S}_8(\text{H})(\text{PEt}_3)_6]$ (**3**). In this reaction, only very little amount of the non-hydride $[\text{Cr}_6\text{S}_8(\text{PEt}_3)_6]$ formed as indicated by the CV (Figure 8c). The FAB mass spectra and the magnetic measurements have shown that complex **3** has an extra hydrogen atom associated with the Cr_6S_8 cluster unit (*vide infra*). Thus the cluster complex " $[\text{Cr}_6\text{S}_8(\text{PEt}_3)_6]$ " reported previously⁸ has been reformulated as a hydride complex **3**. A similar procedure using MeOD in place of MeOH gave the deuterated derivative $[\text{Cr}_6\text{S}_8(\text{D})(\text{PEt}_3)_6]$ together with a little amount of undeuterated one (in a ratio of *ca.* 4 : 1). The formation of both the deuterated and undeuterated derivatives by the reaction in MeOD indicates that the extra hydrogen atom for **3** and **4** has come from the hydroxyl group of methanol and NaSH .

In contrast to the preparation of the two selenide cluster complexes using sodium polyselenide, only intractable materials were yielded in the reaction using Na_2S_x instead of NaS_2H , and neither **3** nor the non-hydride $[\text{Cr}_6\text{S}_8(\text{PEt}_3)_6]$ was obtained. This may be because the Cr_6S_8 cluster core did not form at the stage of the treatment of CrCl_2 with Na_2S_x .

1-3-2. Molecular Orbital Calculation

In the CV of the selenides **1** and **2**, the potential of the oxidation step for **2** is less positive and that of the reduction process less negative than those of **1**, indicating that complex **2** is easier to oxidize and to reduce than **1**. For the purpose of investigating the difference of redox properties for these selenides, the molecular orbitals were calculated using DV- $X\alpha$ (discrete-variational $X\alpha$) method.⁴⁸⁻⁵³ The structural models used for the calculations were $[\text{Cr}_6\text{Se}_8(\text{PH}_3)_6]$ and $[\text{Cr}_6\text{Se}_8(\text{H})(\text{PH}_3)_6]$ in the O_h symmetry, whose geometric parameters were taken from the averaged values obtained by the X-ray structure analyses for **1** and **2**, respectively. Substitutions of PEt_3 for PH_3 in the models were for the saving of the calculation time. The substitution has been used for the calculation of other compounds, and it is demonstrated that the substitution caused little differences in the results of the calculations.⁵⁶

The calculated orbitals near Fermi level for two model complexes are shown in Figure 9. The result for $[\text{Cr}_6\text{Se}_8(\text{PH}_3)_6]$ (Figure 9a) shows that $28t_{1u}$ is a fully occupied HOMO and $16e_g$ is LUMO, while HOMO of $[\text{Cr}_6\text{Se}_8(\text{H})(\text{PH}_3)_6]$ (Figure 9b) is upspin-state $16e_g$ orbital, whose energy level is between HOMO and LUMO of $[\text{Cr}_6\text{Se}_8(\text{PH}_3)_6]$. The oxidation step eliminates an electron of HOMO. Since HOMO of **2** (-2.336 eV) has higher energy level

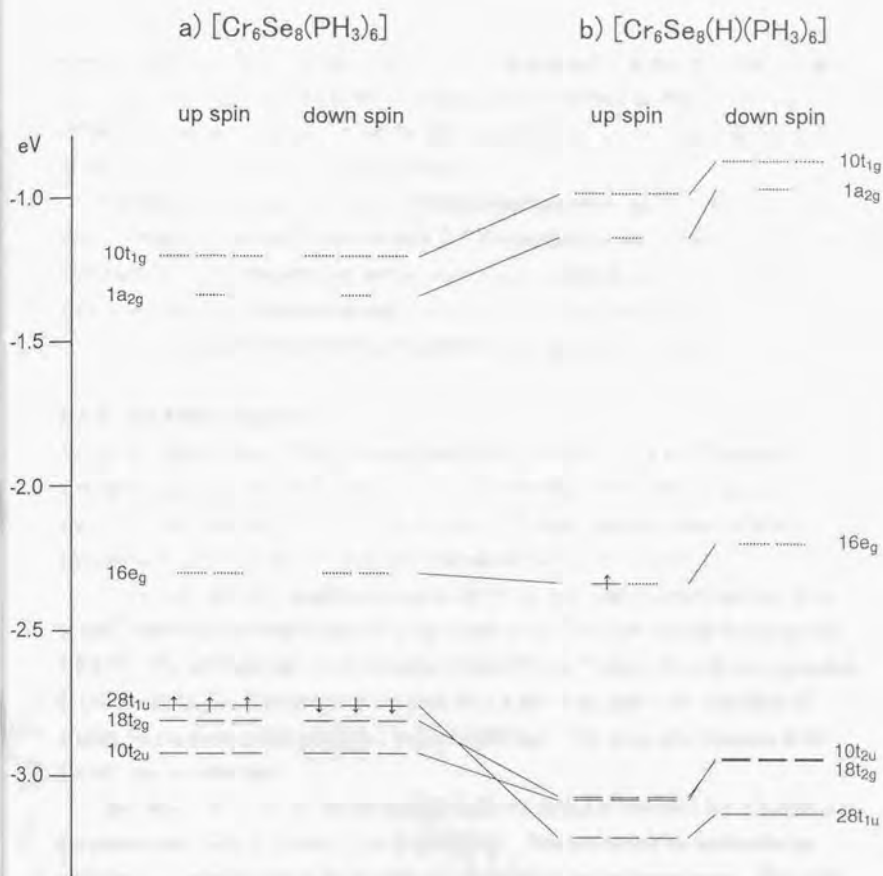


Figure 9. Electronic levels near Fermi level for $[\text{Cr}_6\text{Se}_8(\text{PH}_3)_6]$ and $[\text{Cr}_6\text{Se}_8(\text{H})(\text{PH}_3)_6]$ modeled after the crystallographic structures of **1** and **2**. Solid and broken lines show occupied and unoccupied levels, respectively. Related orbitals between the models are connected by lines.

than that of **1** (-2.757 eV), complex **2** is easier to oxidize than **1**. In the reduction step, an electron enters $16e_g$ LUMO for **1**, while complex **2** accommodates an electron on $16e_g$ HOMO. Because the energy level of the latter orbital (-2.336 eV) is lower than that of the former (-2.301 eV), **2** is easier to reduce than **1**.

Complexes **1** and **2** display the temperature-dependent paramagnetic behaviors (*vide infra*). However, the results of the present DV-X α calculations may not give a quantitative explanation for these magnetic properties, since this calculation method cannot afford each electronic level value accurately enough to account for the small energy gaps (the order of $10 \sim 10^2 \text{ cm}^{-1}$) which cause the temperature-dependent paramagnetism of **1** and **2**.

1-3-3. FAB Mass Spectra

To confirm the existence of the extra hydrogen atoms, the positive-ion FAB (fast-atom-bombardment) mass spectra of **1-4** were measured with NBA (*m*-nitrobenzyl alcohol) as a matrix. The comparisons of the isotope patterns of the molecular ion peaks of these complexes with the calculated patterns are summarized in Figures 10 and 11.

It is known that some neutral compounds show the molecular ion peaks corresponding to $[M]^+$ rather than protonated $[M-H]^+$ in the positive-ion FAB mass spectra measured with NBA.⁶⁵ The molybdenum cluster complex $[Mo_6S_8(PEt_3)_6]^{10}$ shows the peak corresponding to $[Mo_6S_8(PEt_3)_6]^+$. The molecular ion peak for **1** is also assignable to $[Cr_6Se_8(PEt_3)_6]^+$ (Figure 10a) indicating that complex **1** is $[Cr_6Se_8(PEt_3)_6]$. The peak corresponding to the $[M-H]^+$ was not observed.

The pattern of the molecular ion peak for **2** is very similar to that for **1** but it is shifted in the positive direction by one mass unit (Figure 10b). This shows that the molecular ion peak for **2** is assignable to $[Cr_6Se_8(H)(PEt_3)_6]^+$, having an extra hydrogen atom. This peak cannot be ascribable to $[M-H]^+$ because $[Cr_6Se_8(PEt_3)_6]$ (**1**) exhibited only the molecular ion corresponding to $[M]^+$ as described above.

The molecular ion peak for **3** is due to $[Cr_6S_8(H)(PEt_3)_6]^+$ (Figure 11a) suggesting that complex **3** has an extra hydrogen. This is also supported by the molecular ion peak for **4** obtained by the reaction in MeOD. The peak for **4** corresponds to $[Cr_6S_8(D)_{0.8}(H)_{0.2}(PEt_3)_6]^+$ (Figure 11b) in which the deuterated and the undeuterated derivative are mixed in a ratio of *ca.* 4 : 1.

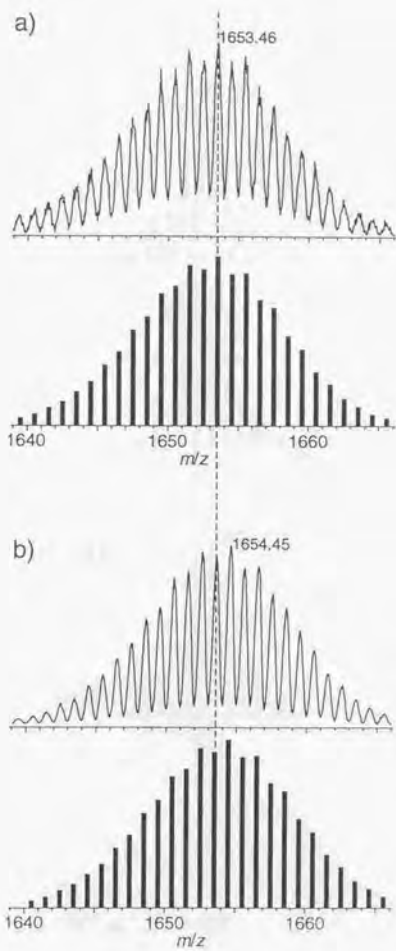


Figure 10. Measured and calculated isotope patterns for the molecular ions of (a) $[\text{Cr}_6\text{Se}_8(\text{PEt}_3)_6]$ (1) and (b) $[\text{Cr}_6\text{Se}_8(\text{H})(\text{PEt}_3)_6]$ (2).

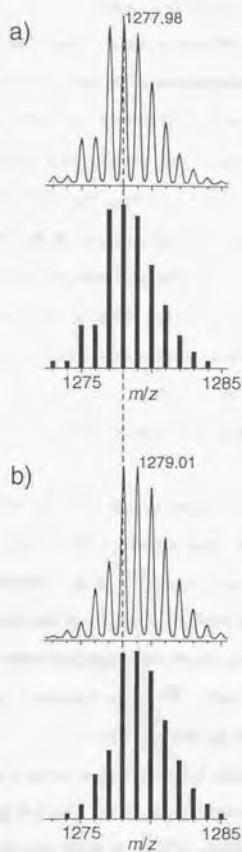


Figure 11. Measured and calculated isotope patterns for the molecular ions of (a) $[\text{Cr}_6\text{S}_8(\text{H})(\text{PEt}_3)_6]$ (3) and (b) $[\text{Cr}_6\text{S}_8(\text{D})_{0.8}(\text{H})_{0.2}(\text{PEt}_3)_6]$ (4).

1-3-4. X-ray Structure Analyses

The structures of the selenide complexes **1** and **2** were determined with the single-crystal X-ray structure analyses. Molecular structural drawings of these selenides are shown in Figures 12 and 13. Ranges and mean values of selected interatomic distances and angles are listed in Table 4. Table 4 also contains the corresponding geometric parameters for the sulfide complex **3** which was reported previously.⁸ The space group of the crystal of **1** is $P\bar{1}$, and two crystallographically independent molecules are found in a unit cell. Since their structures are not meaningfully different from each other, Figure 12 shows the drawing of only one of them. Complex **2** crystallizes in the space group $R\bar{3}$ with three crystallographically equivalent molecules in a unit cell, and is isotypic with the sulfide **3** except that the solvent molecule contained in the crystal is THF for **2** in place of benzene for **3**. Complexes **1-3** comprise a Cr_6 regular octahedron and eight face-capping chalcogen atoms. One triethylphosphine ligand coordinates to each chromium atom. All the chromium atoms have a distorted square-pyramidal coordination environment if the Cr-Cr bonds are neglected.

Complexes **2** and **3** have an extra hydrogen atom as indicated by the FAB mass spectra. There are three possible positions of the hydrogen atom in **2** and **3**: (1) interstitial, (2) bridging, or (3) chalcogen-bonded. In the first case, the hydrogen atom is inside the octahedron, while in the second and third cases, the hydrogen atom is outside the octahedron. An absorption due to a chromium-hydrogen or a chalcogen-hydrogen stretch was not observed in the FT-IR spectra (Figures 2 and 3).⁶⁶ The 1H NMR spectra did not show any hydride protons probably because of the paramagnetism of the cluster complexes (Figure 7). However, the final difference-Fourier map of **2** and **3** showed a peak at the center of the Cr_6 octahedron ($1.2 e/\text{\AA}^3$ for **2** and $0.4 e/\text{\AA}^3$ for **3**), while that of **1** exhibited no peak. The existence of an interstitial hydrogen atom in the Cr_6 octahedron was supported also by its reactivity and powder neutron diffraction analysis (*vide infra*). If the hydrogen atom is at the interstitial position, the Cr-H bond distance is 1.88 Å of **2** and 1.84 Å of **3**. These lengths are slightly longer than those of $[Cr_2(CO)_{10}(\mu-H)]^-$ (mean 1.73 Å)^{67a} and $[Cp^*_4Cr_4(\mu-H)_5(\mu_6-H)_2]$ (where $Cp^* = \eta^5$ -tetramethyl-ethyl-cyclopentadienyl) (mean 1.79 Å).^{67b}

Whereas several interstitial hydride in the octahedral metal clusters are known,⁶⁸⁻⁸⁰ metal-chalcogenide octahedral cluster complexes with an interstitial hydride have not been reported yet.

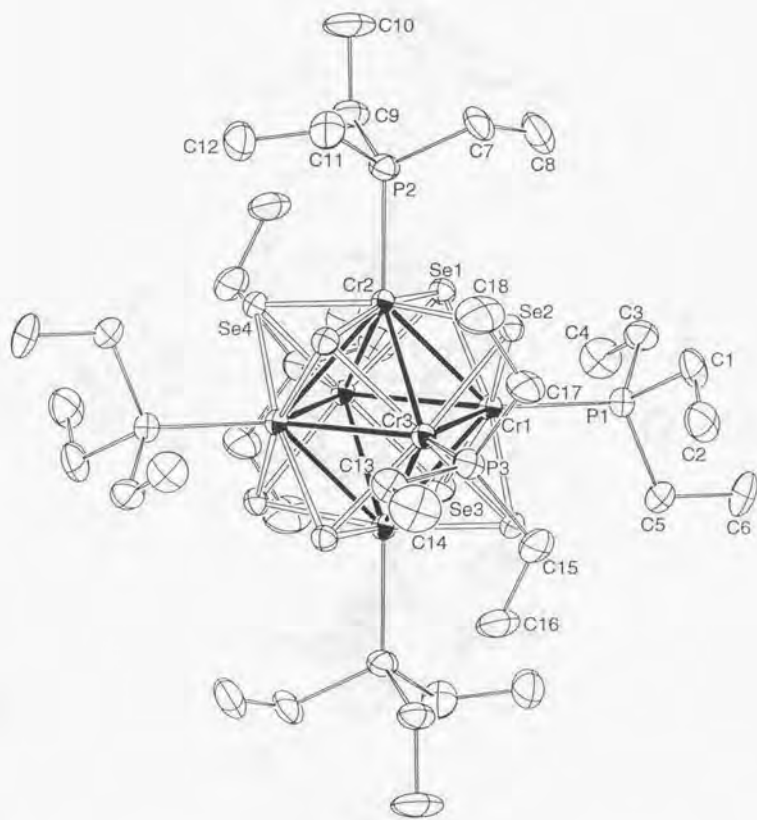


Figure 12. ORTEP drawing of $[\text{Cr}_6\text{Se}_8(\text{PEt}_3)_6]$ (1) with 50% probability ellipsoids. Hydrogen atoms are omitted for clarity. One of two crystallographically independent molecules is shown. The Cr_6Se_8 cluster unit is centered on a $\bar{1}$ position.

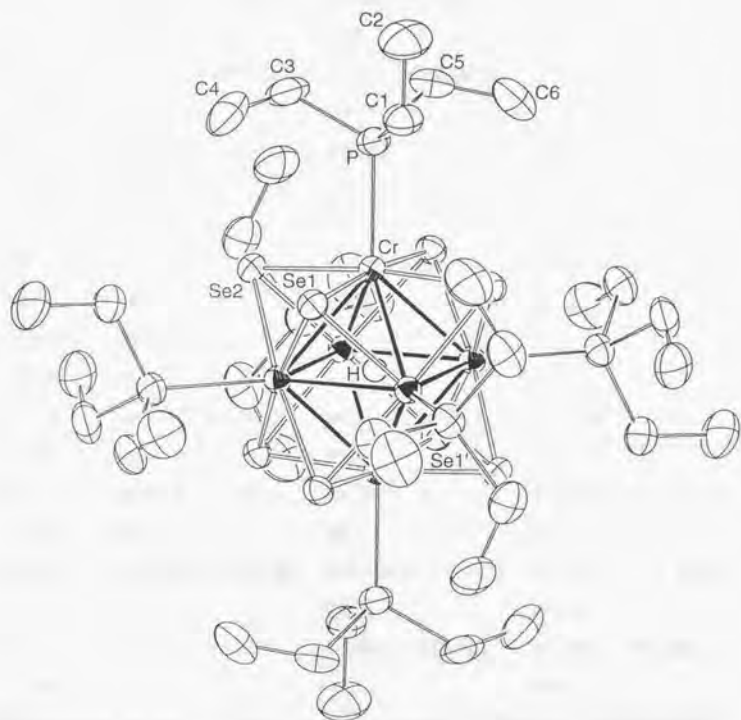


Figure 13. ORTEP drawing of $[\text{Cr}_6\text{Se}_8(\text{H})(\text{PEt}_3)_6]$ (**2**) with 50% probability ellipsoids. The proposed location of the interstitial hydride is shown in this drawing. The other hydrogen atoms are omitted for clarity. The Cr_6Se_8 cluster unit is centered on a $\bar{3}$ position. The 3-fold axis runs through Se1, H, and Se1' atoms.

Table 4. Ranges and Mean Values of Selected Interatomic Distances (Å) and Angles (deg) for 1-3

	1	2	3
Cr-Cr	2.796(2) - 2.816(1)	2.655(1) - 2.656(1)	2.592(1) - 2.596(1)
mean	2.81	2.66	2.59
Cr-E	2.458(1) - 2.477(1)	2.441(1) - 2.461(1)	2.327(1) - 2.342(2)
mean	2.47	2.45	2.34
Cr-P	2.405(2) - 2.411(2)	2.403(2)	2.395(1)
mean	2.41		
Cr-Cr-Cr ^a	59.58(3) - 60.67(4)	59.98(2) - 60.03(4)	59.94(1) - 60.12(3)
mean	60.0	60.0	60.0
Cr-Cr-Cr ^b	89.23(4) - 90.77(4)	90.0	90.0
mean	90.0		
Cr-E-Cr	68.97(4) - 69.90(4)	65.31(4) - 65.76(4)	67.32(5) - 67.66(4)
mean	69.3	65.5	67.5
E-Cr-E ^c	88.76(4) - 89.95(4)	89.78(3) - 90.05(3)	89.26(4) - 90.00(4)
mean	89.4	89.9	89.6
E-Cr-E ^d	167.98(5) - 169.41(5)	173.10(4) - 173.10(4)	170.65(5) - 170.89(5)
mean	168.4	173.1	170.8
E-Cr-P	92.28(6) - 99.05(6)	91.29(5) - 95.61(5)	92.23(4) - 96.87(4)
mean	95.7	93.5	94.6

^a Within triangular faces. ^b Within equatorial squares. ^c Between *cis*-chalcogenides.

^d Between *trans*-chalcogenides.

Though Cr-Se and Cr-P bond distances of **2** are almost the same as those of **1**, the 12 Cr-Cr bond distances (mean 2.66 Å) of **2** are shorter by 0.13-0.16 Å than those of **1** (mean 2.81 Å). The interstitial hydrogen atom is considered to have bonding interaction with the six chromium atoms in **2**. Therefore, the Cr-H bonding probably attracts the chromium atoms toward the center of the Cr₆ octahedron, and the Cr-Cr bond distances of **2** become shorter than those of **1**. The 12 Cr-Cr bond distances in the structure of "[Cr₆Se₈(PEt₃)₆]" previously reported were 2.71±0.01 Å.⁸ These values are between those of **1** and **2**, indicating that the crystals in the previous paper are mixed crystals of **1** and **2**.

The chromium-chalcogen bond lengths of **2** are longer by 0.10-0.14 Å than those of the sulfide complex **3** (mean 2.34 Å),⁸ as expected from the difference in the covalent radii of S (1.04 Å) and Se (1.17 Å).⁸¹ The 12 Cr-Cr bond distances of **2** are longer by 0.07 Å than those of **3** (mean 2.59 Å).⁸

1-3-5. Powder Neutron Diffraction Analysis

It is difficult to detect a hydrogen atom in metal cluster compounds by X-ray structure analyses owing to its much smaller scattering cross section for X-ray in comparison with heavier metal atoms. On the other hand, neutron diffraction analysis is advantageous for characterizing a hydrido-ligand because its coherent scattering length (corresponding to the scattering cross section for X-ray) is of the same order of magnitude as those of the transition metals,⁸² and the analyses have been applied to the structure determinations for some hydrido-coordinated cluster complexes.^{70, 73, 83, 84} In the present study, the existence of the interstitial hydride in the chromium sulfide cluster complex was investigated by powder neutron diffraction analysis. The result of the refinement including the interstitial hydrogen atom was compared with that when the hydride was excluded. Since a D atom absorbs much less amount of neutron flux and gives better structure determination than a H atom,⁸² the completely deuterated compound [Cr₆S₈(D)(PEt₃-d₁₅)₆]·2C₆D₆ (5·2C₆D₆) was prepared for measurement. The complete deuterium substitution in **5** was revealed by FAB mass spectrum (Figure 14).

The intensity data were collected by the TOF (time-of-flight) method. In this technique, a wavelength dispersion method is employed, and pulsed white neutron beam is

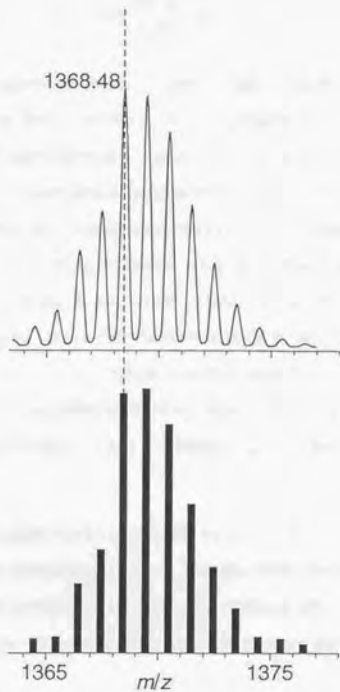


Figure 14. Measured and calculated isotope patterns for the molecular ion of $[\text{Cr}_6\text{S}_8(\text{D})(\text{PEt}_3-d_{15})_6]$ (5).

used. The wavelengths of neutron are determined by measuring the time of its flight from the neutron source to the detector (t). The d -spacing values are given by the following equation.

$$d = \frac{1}{2} \cdot \left(\frac{h}{m} \right) \cdot (L_i + L_s)^{-1} \cdot \left\{ \sin \left(\frac{2\theta}{2} \right) \right\}^{-1} \cdot t$$

where h , m , 2θ , L_i , and L_s represent Planck constant, mass of neutron, scattering angle, flight path of incident neutron, and that of scattered neutron, respectively.

The analysis of the obtained data of **5** was performed by using the Rietveld refinement.⁶¹ Since the intensity data exhibited some peaks not assignable to the chromium complex **5**, the d regions near these peaks were excluded in the refinement. The space group, lattice constants, and atomic coordinates of Cr, S, P, and C atoms were initially set to those obtained by the single-crystal X-ray structure analysis for the undeuterated derivative **3**.⁸ The D atoms were placed on the calculated positions as described under **Experimental**. When all the structure parameters were refined, several isotropic thermal parameters converged to negative values, and almost all of the atoms shifted significantly, which lead to unreasonable interatomic distances. Thus the following restriction was added in the refinement:

- (i) All the atomic coordinates were fixed at the initial values.
- (ii) The isotropic thermal parameters of D, C, and the other atoms (Cr, S, and P) in the cluster molecule were constrained to be equal, respectively. The D and C atoms in the benzene solvent molecule were also assumed to have the same isotropic thermal parameter values.

Tables 5 and 6 summarize the obtained structure parameters for the models including and excluding the interstitial D atom, respectively. Figures 15 and 16 illustrate the profile fits and difference patterns for the two models. When the interstitial hydride was included, the obtained R factors were $R_p = 2.64\%$, $R_{wp} = 3.46\%$, $R_l = 8.27\%$, and $R_f = 4.09\%$, and the S was obtained as 1.3713. (The meanings of these values are presented below Table 5.) All of these values are better than those for the model excluding the interstitial D atom ($R_p = 2.66\%$, $R_{wp} = 3.50\%$, $R_l = 8.46\%$, $R_f = 4.16\%$, and $S = 1.3856$), which suggests the existence of the interstitial D in the chromium cluster **5**.

Table 5. Structure Parameters for $[\text{Cr}_6\text{S}_8(\text{D})(\text{PEt}_3-d_{15})_6] \cdot 2\text{C}_6\text{D}_6 (5 \cdot 2\text{C}_6\text{D}_6)$ for the model including the interstitial D atoms.

Lattice Constants^a: $a = 17.3093(5) \text{ \AA}$, $c = 19.7569(7) \text{ \AA}$
 $R_p^b = 2.64\%$, $R_{wp}^b = 3.46\%$, $R_1^b = 8.27\%$, and $R_F^b = 4.09\%$, $S^b = 1.3713$

atom	occupancy	x/a	y/b	z/c	B_{150}^c
Cr	1.0000	0.06414	-0.03442	0.05355	0.8(5)
S1	0.3333	0.00000	0.00000	0.14472	0.8(5)
S2	1.0000	0.11531	-0.06106	-0.04859	0.8(5)
P	1.0000	0.14439	-0.08566	0.12137	0.8(5)
C1	1.0000	0.18689	-0.14911	0.07671	5.1(4)
C2	1.0000	0.11567	-0.23735	0.04518	5.1(4)
C3	1.0000	0.24753	0.00053	0.16122	5.1(4)
C4	1.0000	0.23577	0.05583	0.21472	5.1(4)
C5	1.0000	0.07927	-0.15766	0.19176	5.1(4)
C6	1.0000	0.12539	-0.19359	0.23744	5.1(4)
C01	0.3333	-0.02659	-0.03241	0.33355	8.7(8)
C02	0.3333	-0.09952	-0.06390	0.37742	8.7(8)
C03	0.3333	-0.09603	-0.01310	0.43358	8.7(8)
C04	0.3333	-0.01959	0.06920	0.44585	8.7(8)
C05	0.3333	0.05334	0.10069	0.40198	8.7(8)
C06	0.3333	0.04984	0.04988	0.34583	8.7(8)
D1	1.0000	0.22575	-0.16434	0.11294	7.5(2)
D2	1.0000	0.23092	-0.10685	0.03580	7.5(2)
D3	1.0000	0.29048	0.04594	0.12119	7.5(2)
D4	1.0000	0.28086	-0.03266	0.18478	7.5(2)
D5	1.0000	0.01985	-0.21538	0.17013	7.5(2)
D6	1.0000	0.05856	-0.11920	0.22383	7.5(2)
D7	1.0000	0.14803	-0.27199	0.02243	7.5(2)
D8	1.0000	0.06875	-0.27973	0.08470	7.5(2)
D9	1.0000	0.07917	-0.22357	0.00581	7.5(2)
D10	1.0000	0.30011	0.09886	0.23981	7.5(2)
D11	1.0000	0.21182	0.09753	0.19102	7.5(2)
D12	1.0000	0.18679	0.01151	0.25241	7.5(2)
D13	1.0000	0.07650	-0.24253	0.27304	7.5(2)
D14	1.0000	0.15375	-0.22598	0.20620	7.5(2)
D15	1.0000	0.17914	-0.13815	0.26598	7.5(2)
D16	0.3333	-0.02971	-0.07741	0.30097	36(2)

D17	0.3333	0.13152	-0.10363	0.36605	36(2)
D18	0.3333	0.13476	-0.01179	0.47819	36(2)
D19	0.3333	-0.02819	0.07214	0.48103	36(2)
D20	0.3333	0.09190	0.17400	0.39953	36(2)
D21	0.3333	0.07311	0.09083	0.29964	36(2)
D	0.1667	0.00000	0.00000	0.00000	7.5(2)

^a These constants are very similar to those ($a = 17.301(3) \text{ \AA}$, $c = 19.740(2) \text{ \AA}$)

obtained by the previous X-ray analysis.⁸

^b R factors and S were calculated as follows:

$$R_p = \sum w |Y_o - Y_c| / \sum w Y_o$$

$$R_{wp} = \{ \sum w (Y_o - Y_c)^2 / \sum w Y_o^2 \}^{1/2}$$

$$R_I = \{ \sum (I_o)^{1/2} - (I_c)^{1/2} / \sum (I_o)^{1/2} \}$$

$$R_1 = \sum |I_o - I_c| / \sum I_o$$

$$S = [R_{wp} / \{ (N-M) / \sum w Y_o^2 \}^{1/2}]$$

where Y_o and Y_c are the observed and calculated intensities, respectively, I_o and I_c mean the observed and calculated integrated intensities, respectively, w is represented as $1 / Y_o$. N and M denote the number of the points and the parameters used for least-squares fittings, respectively.

^c Isotropic thermal parameters.

Table 6. Structure Parameters for $[\text{Cr}_6\text{S}_8(\text{D})(\text{PEt}_3-d_{15})_6] \cdot 2\text{C}_6\text{D}_6$ ($5 \cdot 2\text{C}_6\text{D}_6$) for the model excluding the interstitial D atoms.

Lattice Constants^a: $a = 17.3093(5) \text{ \AA}$, $c = 19.7569(8) \text{ \AA}$
 $R_p^b = 2.66\%$, $R_{wp}^b = 3.50\%$, $R_I^b = 8.46\%$, and $R_F^b = 4.16\%$, $S^b = 1.3856$

atom	occupancy	x/a	y/b	z/c	B_{iso}^c
Cr	1.0000	0.06414	-0.03442	0.05355	0.8(5)
S1	0.3333	0.00000	0.00000	0.14472	0.8(5)
S2	1.0000	0.11531	-0.06106	-0.04859	0.8(5)
P	1.0000	0.14439	-0.08566	0.12137	0.8(5)
C1	1.0000	0.18689	-0.14911	0.07671	5.2(4)
C2	1.0000	0.11567	-0.23735	0.04518	5.2(4)
C3	1.0000	0.24753	0.00053	0.16122	5.2(4)
C4	1.0000	0.23577	0.05583	0.21472	5.2(4)
C5	1.0000	0.07927	-0.15766	0.19176	5.2(4)
C6	1.0000	0.12539	-0.19359	0.23744	5.2(4)
C01	0.3333	-0.02659	-0.03241	0.33355	7.7(8)
C02	0.3333	-0.09952	-0.06390	0.37742	7.7(8)
C03	0.3333	-0.09603	-0.01310	0.43358	7.7(8)
C04	0.3333	-0.01959	0.06920	0.44585	7.7(8)
C05	0.3333	0.05334	0.10069	0.40198	7.7(8)
C06	0.3333	0.04984	0.04988	0.34583	7.7(8)
D1	1.0000	0.22575	-0.16434	0.11294	7.6(2)
D2	1.0000	0.23092	-0.10685	0.03580	7.6(2)
D3	1.0000	0.29048	0.04594	0.12119	7.6(2)
D4	1.0000	0.28086	-0.03266	0.18478	7.6(2)
D5	1.0000	0.01985	-0.21538	0.17013	7.6(2)
D6	1.0000	0.05856	-0.11920	0.22383	7.6(2)
D7	1.0000	0.14803	-0.27199	0.02243	7.6(2)
D8	1.0000	0.06875	-0.27973	0.08470	7.6(2)
D9	1.0000	0.07917	-0.22357	0.00581	7.6(2)
D10	1.0000	0.30011	0.09886	0.23981	7.6(2)
D11	1.0000	0.21182	0.09753	0.19102	7.6(2)
D12	1.0000	0.18679	0.01151	0.25241	7.6(2)
D13	1.0000	0.07650	-0.24253	0.27304	7.6(2)
D14	1.0000	0.15375	-0.22598	0.20620	7.6(2)
D15	1.0000	0.17914	-0.13815	0.26598	7.6(2)
D16	0.3333	-0.02971	-0.07741	0.30097	37(2)

D17	0.3333	0.13152	-0.10363	0.36605	37(2)
D18	0.3333	0.13476	-0.01179	0.47819	37(2)
D19	0.3333	-0.02819	0.07214	0.48103	37(2)
D20	0.3333	0.09190	0.17400	0.39953	37(2)
D21	0.3333	0.07311	0.09083	0.29964	37(2)

^a These constants are very similar to those ($a = 17.301(3) \text{ \AA}$, $c = 19.740(2) \text{ \AA}$) obtained by the previous X-ray analysis.⁸

^b R factors and S were calculated as follows:

$$R_P = \Sigma w|Y_o - Y_c| / \Sigma w Y_o$$

$$R_{WP} = \{\Sigma w(Y_o - Y_c)^2 / \Sigma w Y_o^2\}^{1/2}$$

$$R_F = \Sigma (I_o)^{1/2} - (I_c)^{1/2} / \Sigma (I_o)^{1/2}$$

$$R_I = \Sigma |I_o - I_c| / \Sigma I_o$$

$$S = [R_{WP} / \{(N-M) / \Sigma w Y_o^2\}^{1/2}]$$

where Y_o and Y_c are the observed and calculated intensities, respectively, I_o and I_c mean the observed and calculated integrated intensities, respectively, w is represented as $1 / Y_o$. N and M denote the number of the points and the parameters used for least-squares fittings, respectively.

^c Isotropic thermal parameters.

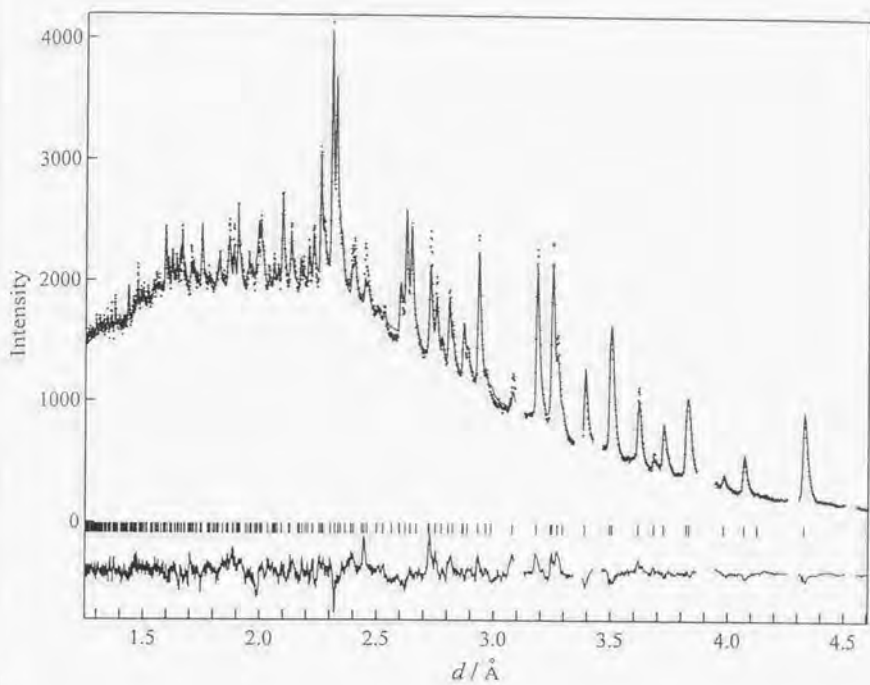


Figure 15. The result of the Rietveld refinement of $5 \cdot 2C_6D_6$ when the interstitial D atom was included. The cross marks and solid line at the top represent the observed and calculated intensities, respectively. The stick marks show the calculated peak positions. The solid line of the bottom indicates the difference between the observed and calculated intensities.

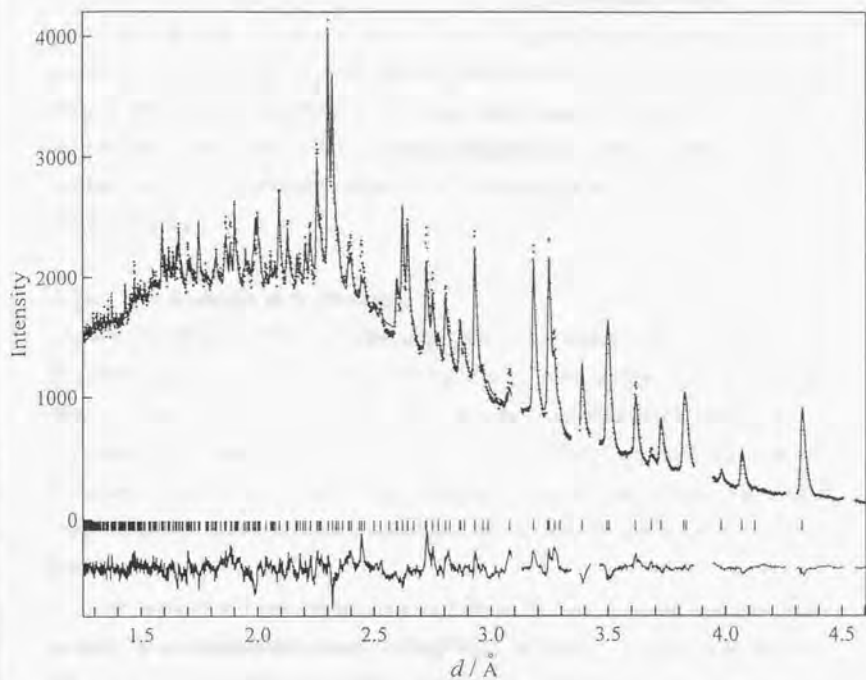


Figure 16. The result of the Rietveld refinement of $5\cdot 2C_6D_6$ when the interstitial D atom was excluded. The cross marks and solid line at the top represent the observed and calculated intensities, respectively. The stick marks show the calculated peak positions. The solid line of the bottom indicates the difference between the observed and calculated intensities.

However, it is conceivable that this result does not give sufficient evidence for the definitive position of the hydride. The calculated intensities for even the hydride-included model are not correspondent so well with the observed data. The discrepancy may have resulted from (i) high background probably due to the disorder of solvent benzene molecules, (ii) overlaps of many peaks, and (iii) presence of impurities. Further conclusive evidence for the existence of the interstitial hydride may be obtained by the single-crystal neutron diffraction analysis.

1-3-6. The Reactivity of the Hydride

The reactivity of the hydrides in cluster compounds are sometimes related to their positions. It has been reported that the reaction of $[\text{Re}_7\text{H}_2\text{C}(\text{CO})_{21}]^-$ with methanol, acetone, and THF removes the edge-bridging hydrides as protons and the cluster framework decomposes.⁸⁵ The chalcogen-bonded hydrogen atom in $[\text{Re}_6\text{S}_7(\text{SH})\text{Br}_6]^{3-}$ and $[\text{Re}_6\text{Se}_7(\text{SeH})\text{I}_6]^{3-}$ is also eliminated by primary amines at room temperature.²⁴ On the other hand, the interstitial hydride in $[\text{HRu}_6(\text{CO})_{18}]^-$ is stable in a methanol solution of KOH and in a THF solution of KH.⁷¹

The reactivity of **2** with ethanol, acetone, THF, or $^t\text{BuNH}_2$ in toluene solutions has been studied. If the deprotonated cluster $[\text{Cr}_6\text{Se}_8(\text{PEt}_3)_6]^-$ (**1**) forms, it should exhibit the same CV as that of **1** except the rest potential. However, the CV of the products of the reactions did not change, which indicated that the hydride in **2** was not removed by these reagents. Also the hydride in **3** was not eliminated. These results suggest that the hydrogen atoms in **2** and **3** are inert because of the steric protection by the Cr_6 octahedral skeleton and also because of the Cr-H bondings.

1-3-7. Magnetic Properties

Correlation between μ_{eff} Values and Metal Cluster Electrons

The measured thermal variations of the molar magnetic susceptibilities (χ_M) and the effective magnetic moments ($\mu_{\text{eff}} = 2.828(\chi_M T)^{1/2} \mu_B$) of 1-3 are shown as plots in Figures 17-19, respectively. Additionally, the experimental μ_{eff} vs. T curves of 1-3 are summarized as plots in Figure 20. All these chromium complexes are paramagnetic over the whole temperature range measured. The magnetic moments of these complexes do not obey the Curie law and the μ_{eff} values decrease as the temperature is lowered, indicating that complexes 1-3 exhibit temperature-dependent paramagnetism. The excited spin states become less populated in lower temperatures, and the magnetic susceptibility at very low temperatures represents the ground state of each chromium complex. These results contrast with the diamagnetism of the molybdenum cluster complexes $[\text{Mo}_6\text{S}_8(\text{PEt}_3)_6]$ and $[\text{Mo}_6\text{Se}_8(\text{PEt}_3)_6]$.¹⁰

The μ_{eff} value for 1 at 2 K is 0.2 μ_B . The number of unpaired spins approaches zero at very low temperatures due to antiferromagnetic interactions, and $S = 0$ should be the ground state. This magnetic property is compatible with the even number of MCE (metal cluster electrons) (20 e). On the other hand, the μ_{eff} value for 2 at 2 K is 2.0 μ_B , and that for 3 at 4.5 K is 1.7 μ_B ; these values are close to the value (1.73 μ_B) of the spin-only magnetic moment for the $S = 1/2$ state. Therefore, complexes 2 and 3 have one unpaired spin in the ground state and have an odd number of MCE (21 e), consistent with the presence of an extra hydrogen atom. These results accord with the FAB mass spectra demonstrating that complexes 2 and 3 are hydrides (*vide supra*).

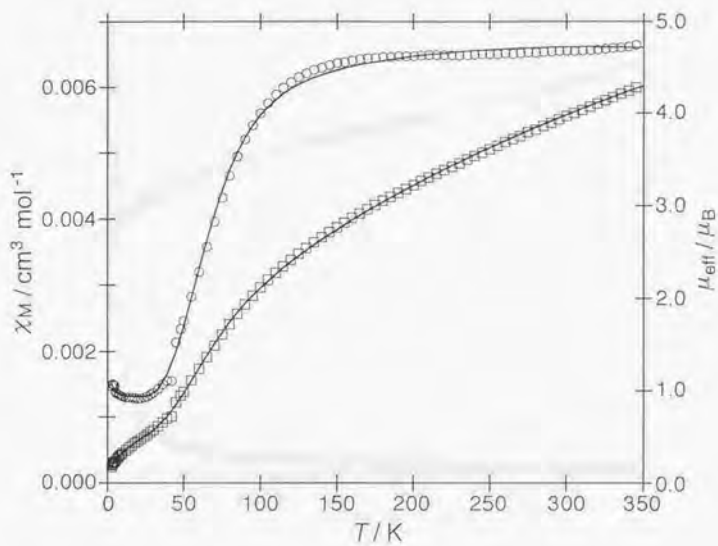


Figure 17. Thermal variations of experimental molar magnetic susceptibility (○) and effective magnetic moment (□) for 1. The solid lines are the calculated values using the best-fit parameters given in Table 7.

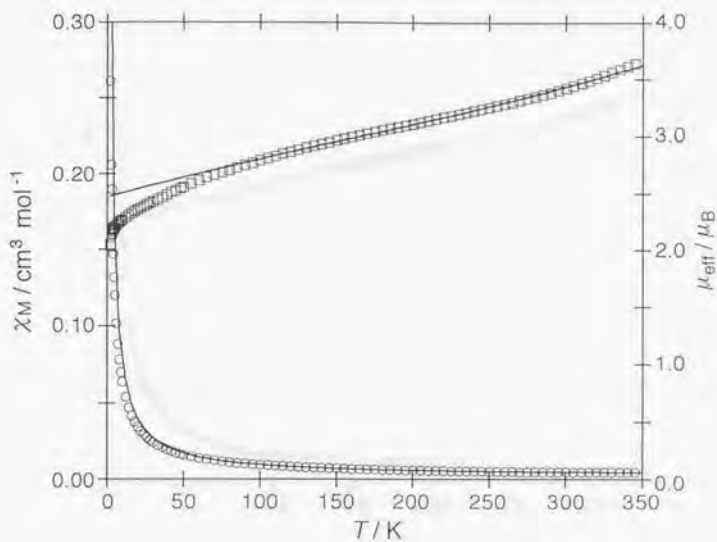


Figure 18. Thermal variations of experimental molar magnetic susceptibility (○) and effective magnetic moment (□) for 2. The solid lines are the calculated values using the best-fit parameters given in Table 7.

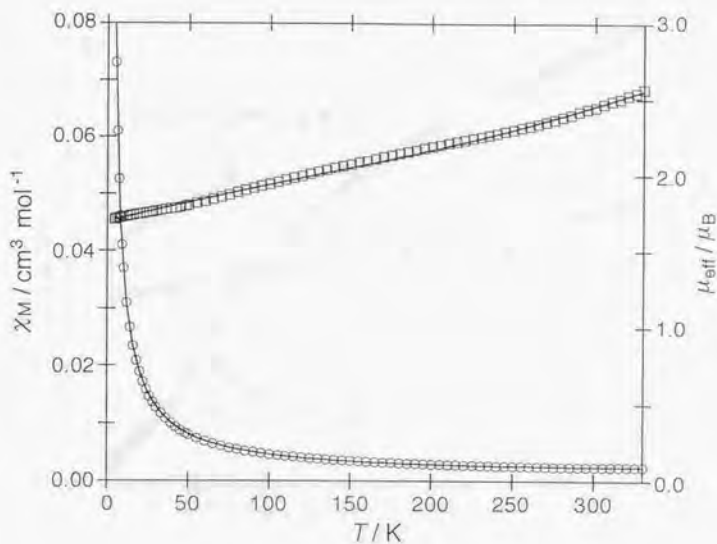


Figure 19. Thermal variations of experimental molar magnetic susceptibility (○) and effective magnetic moment (□) for **3**. The solid lines are the calculated values using the best-fit parameters given in Table 7.

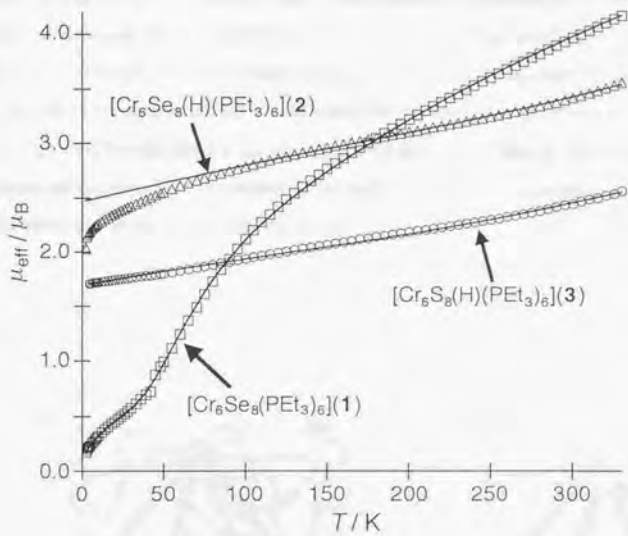


Figure 20. Temperature dependence of the magnetic susceptibilities of $[\text{Cr}_6\text{Se}_8(\text{PEt}_3)_6]$ (1), $[\text{Cr}_6\text{Se}_8(\text{H})(\text{PEt}_3)_6]$ (2), and $[\text{Cr}_6\text{S}_8(\text{H})(\text{PEt}_3)_6]$ (3) in the form of μ_{eff} vs. T .

Fitting Calculation

For the purpose of investigating the magneto-structural correlation in the Cr_6E_8 cluster unit, the temperature-dependent paramagnetic data of **1-3** were analyzed by the Heisenberg-Dirac-Van Vleck (HDVV) Hamiltonian. Because the Cr_6 octahedra are almost regular as indicated by the X-ray structure determinations (*vide supra*), these complexes have only two topologically distinct types of exchange interactions: (1) between *trans*-chromium atoms (the *trans*-interaction) and (2) between *cis*-chromium atoms (the *cis*-interaction) (Figure 21b). The *trans*-interaction is very weak because it is mediated by no atom in **1** and by only one interstitial hydrogen atom in **2** and **3**, while the *cis*-interaction is effectively transmitted through Cr-Cr bonds and Cr-(μ_3 -chalcogen)-Cr bridges. Thus the *trans*-interaction has been neglected and only the *cis*-interaction has been taken into consideration. Then the spin Hamiltonian can be formulated as follows:

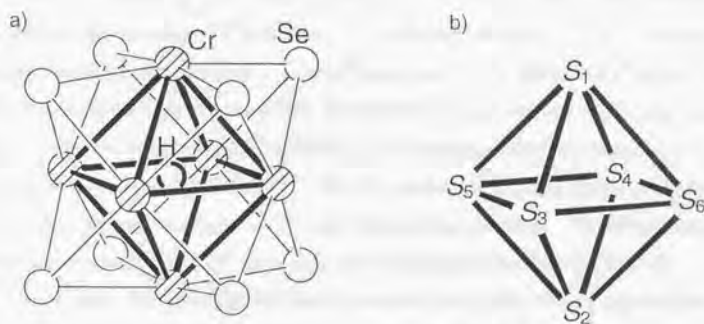


Figure 21. (a) The structure of the $\text{Cr}_6\text{Se}_8(\text{H})$ cluster unit in **2**. (b) Schematic view of the spin-spin magnetic interaction in complexes **1**, **2**, and **3**. Bold lines represent *cis*-interaction with $2J$ value.

$$H = -2J(S_1 \cdot S_3 + S_3 \cdot S_2 + S_2 \cdot S_4 + S_4 \cdot S_1 + S_1 \cdot S_6 + S_6 \cdot S_2 + S_2 \cdot S_5 + S_5 \cdot S_1 + S_3 \cdot S_6 + S_6 \cdot S_4 + S_4 \cdot S_5 + S_5 \cdot S_3) \quad (1)$$

where $2J$ corresponds to the interaction between *cis*-chromium atoms. The equation (1) can be simplified with the following vector coupling method.⁸⁶ By defining $S_{12} = S_1 + S_2$, $S_{34} = S_3 + S_4$, $S_{56} = S_5 + S_6$, $S^* = S_{12} + S_{34}$, and $S_T = S^* + S_{56}$, the Hamiltonian (1) is rewritten as (2).

$$H = -J(S_T^2 - S_{12}^2 - S_{34}^2 - S_{56}^2) \quad (2)$$

Since the eigenvalues of S_j^2 , S^{*2} , and S_T^2 are $S_j(S_j + 1)$, $S^*(S^* + 1)$, and $S_T(S_T + 1)$, respectively, the energy levels E are given by the equation (3).

$$E(S_T, S_{12}, S_{34}, S_{56}) = -J[S_T(S_T + 1) - S_{12}(S_{12} + 1) - S_{34}(S_{34} + 1) - S_{56}(S_{56} + 1)] \quad (3)$$

(S_j varies from $|S_i + S_j|$ to $|S_i - S_j|$, S^* from $|S_{12} + S_{34}|$ to $|S_{12} - S_{34}|$, and S_T from $|S^* + S_{56}|$ to $|S^* - S_{56}|$ in integer increments.)

All the compounds are in a mixed-valence state. Complex **1** has two Cr^{II} and four Cr^{III} ions, whereas there are three Cr^{II} and three Cr^{III} centers for **2** and **3** when the interstitial hydrogen atoms are regarded as H^+ . The Cr^{III} ions have $S = 3/2$, while the Cr^{II} centers are assumed to be in the high-spin $S = 2$ state because the low-spin chromium (II) complexes are rare and limited to those with such ligands as 2,2'-bipyridine, 1,10-phenanthroline, or CN⁻ which exert very strong ligand fields.⁸⁷ The Cr_6 octahedron of **1-3** is almost perfectly regular, and six chromium atoms lie in equal chemical environments. Therefore, there is no distinction between Cr^{II} and Cr^{III} sites, indicative of the spin-delocalization over six chromium atoms. It is demonstrated that the magnetic properties of such spin-delocalized complexes cannot be explained strictly by using only the HDVV Hamiltonian, and the double-exchange spin Hamiltonian has been used instead for several di-, tri-, and tetra-nuclear complexes assuming the correction for the effect of spin-delocalization.^{88, 89} This Hamiltonian, however, is inconvenient to apply to the chromium cluster complexes **1-3** because too many parameters are necessary. Thus Cr^{II} and Cr^{III} sites are assumed to be

localized and the experimental data have been analyzed by using the HDVV Hamiltonian alone. There are two possible isomers for each complex in this localized model. For complex 1, they are a *cis*- and a *trans*-isomer in which two Cr^{II} sites are placed on the *cis*- and the *trans*-positions, respectively. In complexes 2 and 3, the Cr^{II} centers can be placed on the facial position to give a *fac*-isomer or on the meridional position to give a *mer*-isomer. Thus the fitting calculations have been performed for these isomers, separately. For complex 1, the S_{ij} , S^* , and S_T values of the *cis*-isomer can be obtained by setting $S_1 = S_3 = 2$ and $S_2 = S_4 = S_5 = S_6 = 3/2$, and those of the *trans*-isomer by setting $S_1 = S_2 = 2$ and $S_3 = S_4 = S_5 = S_6 = 3/2$. On the other hand, the S_{ij} , S^* , and S_T values of complexes 2 and 3 are given by setting $S_1 = S_3 = S_5 = 2$ and $S_2 = S_4 = S_6 = 3/2$ for the *fac*-isomer and $S_1 = S_2 = S_3 = 2$ and $S_4 = S_5 = S_6 = 3/2$ for the *mer*-isomer, respectively. After substituting S_{ij} , S^* , and S_T values to the equation (3), the obtained energy levels $E(S_T, S_{12}, S_{34}, S_{56})$ are inserted into the Van Vleck formula including the contribution of temperature-independent paramagnetism (TIP). Since complex 1 exhibits increase of the χ_M values at lower temperatures, the presence of impurity obeying the Curie law ($S = 1/2$) has also been taken into consideration in the analysis for 1. Thus the theoretical magnetic susceptibility is as follows:

$$\chi_M = \frac{N\mu_B^2 g^2}{3kT} \frac{\sum_{S_T} S_T(S_T + 1)(2S_T + 1)e^{-E(S_T, S_{12}, S_{34}, S_{56})/kT}}{\sum_{S_T} (2S_T + 1)e^{-E(S_T, S_{12}, S_{34}, S_{56})/kT}} (1 - \rho) + \frac{N\mu_B^2 g^2 \rho}{4kT} + N\alpha \quad (4)$$

where N , μ_B , g , k , T , and $N\alpha$ are Avogadro constant, Bohr magneton, g -factor, Boltzmann constant, temperature, and the temperature-independent paramagnetism, respectively. The fraction of paramagnetic impurity present are represented by ρ , which was fixed at 0 for 2 and 3. Non-linear least-squares fittings of the theoretical expression to the experimental data for 1-3 have been made by varying g , $2J$, ρ (only for 1), and $N\alpha$ by minimizing the residual $R = [\sum(\chi_{\text{obs}} - \chi_{\text{calc}})^2 / \sum(\chi_{\text{obs}})^2]$.

Complex 1 showed satisfactory least-squares fits. The best-fit parameters are as follows: $g = 1.973(6)$, $2J = -174.7(10) \text{ cm}^{-1}$, $\rho = 0.0016(5)$, and $N\alpha = 0.00128(3) \text{ cm}^3 \text{ mol}^{-1}$ for the *cis*-isomer; $g = 1.993(2)$, $2J = -176.7(8) \text{ cm}^{-1}$, $\rho = 0.0014(4)$, and $N\alpha = 0.00129(2) \text{ cm}^3 \text{ mol}^{-1}$ for the *trans*-isomer. These two isomers exhibit very similar parameter values.

The theoretical fits of χ_M and μ_{eff} vs. T for the *cis*-isomer are shown in Figure 17 as solid lines. The theoretical curves for the *trans*-isomer are also very similar to those for the *cis*-isomer. (The difference of the calculated χ_M values for the two isomers is smaller than $6.0 \times 10^{-6} \text{ cm}^3 \text{ mol}^{-1}$ over the whole measured temperature range.) Complex 3 also gave the best-fit parameters as $g = 1.9566(8)$, $2J = -612(16) \text{ cm}^{-1}$, and $N\alpha = 0.00110(1) \text{ cm}^3 \text{ mol}^{-1}$ for both *fac*- and *mer*-isomers. The calculated thermal dependence of χ_M and μ_{eff} for the *fac*-isomer are shown in Figure 19 as solid lines. The theoretical fits are very similar between the *fac*-isomer and the *mer*-isomer. (The difference of the theoretical χ_M values for the two isomers is smaller than $1.0 \times 10^{-6} \text{ cm}^3 \text{ mol}^{-1}$ over the whole measured temperature range.) On the other hand, no satisfactory fits were obtained for either isomers of 2 by using the equation (4). This is because complex 2 displays sharper decrease of the experimental μ_{eff} values with decreasing the temperature from 100 K, while the analysis with the HDVV Hamiltonian never reproduces such a magnetic curve. The magnetic anomaly at lower temperatures is probably due to the spin-orbital coupling at each chromium site (*vide infra*). Therefore, the calculation was applied to the data only above 100 K at the next stage. This approach gave satisfactory fits. The best-fit parameters are $g = 2.847(10)$, $2J = -748(14) \text{ cm}^{-1}$, and $N\alpha = 0.00219(3) \text{ cm}^3 \text{ mol}^{-1}$ for both *fac*- and *mer*-isomers. The theoretical fits of χ_M and μ_{eff} vs. T for the *fac*-isomer are shown in Figure 18 as solid lines. The theoretical curves for the *mer*-isomer are also very similar to those for the *fac*-isomer. (The difference of the calculated χ_M values for the two isomers is smaller than $1.0 \times 10^{-6} \text{ cm}^3 \text{ mol}^{-1}$ over the whole measured temperature range.)

Table 7. Parameters Resulting from Fitting of the Magnetic Data

compd	g	$2J / \text{cm}^{-1}$	$N\alpha / \text{cm}^3 \text{ mol}^{-1}$	ρ
1 (<i>cis</i> -isomer)	1.973(6)	-174.7(10)	0.00128(3)	0.0016(5)
(<i>trans</i> -isomer)	1.993(6)	-176.7(8)	0.00129(2)	0.0014(4)
2	2.847(10)	-748(14)	0.00219(3)	
3	1.9566(8)	-612(16)	0.00110(1)	

The calculated parameters are summarized in Table 7. Complexes 1-3 showed negative $2J$ values, indicative of antiferromagnetic interaction between six chromium atoms. The coupling constants $|2J|$ decrease in the order $2 (748 \text{ cm}^{-1}) > 3 (612 \text{ cm}^{-1}) > 1 (174.7 \text{ and } 176.7 \text{ cm}^{-1} \text{ for } \textit{cis}\text{- and } \textit{trans}\text{-isomers, respectively})$. The antiferromagnetic couplings in these complexes are transmitted through Cr-Cr bonds and Cr-(μ_3 -chalcogen)-Cr bridges, and the magnitude of the interaction depends on the Cr-Cr bond lengths and the difference of the chalcogen atoms. In the comparison of the two selenide clusters, the antiferromagnetic couplings between chromium atoms in 2 are stronger than those in 1. Since the Cr-Se bond lengths (2.47 Å vs. 2.45 Å) and Cr-Se-Cr angles (69.3° vs. 65.5°) in 1 and 2 are not very different, the interaction through the Cr-(μ_3 -Se)-Cr pathways should be similar in these two complexes. Therefore, the difference of exchange couplings between chromium atoms is mainly due to the interaction through the Cr-Cr bonds. The Cr-Cr bond distances of 2 (2.66 Å (average)) being shorter by *ca.* 0.15 Å than those of 1 (2.81 Å (average)), the interaction through Cr-Cr bonds is stronger and chromium atoms are more strongly coupled than those in 1. In the comparison of the sulfide 3 with the selenide 2, however, the Cr-Cr bond distances in 3 (2.59 Å (average)) are shorter than those in the selenide 2 by *ca.* 0.07 Å, and the interaction through the Cr-Cr bonds in 3 should be stronger than that in 2. Nevertheless, the $|2J|$ values for 3 are smaller and the antiferromagnetic couplings between the chromium atoms are weaker than those in 2. This suggests that the selenido bridges are the better mediators of exchange couplings than the sulfido bridges.

Anderson has proposed the "AXB centrosymmetrical model," which explains the influence of the difference of bridging ligands on the magnitudes of interaction through them in dinuclear complexes.⁹⁰ This model postulates a compound comprising metal centers A and B which are bridged by a ligand X (Figure 22a). Each metal center has only one unpaired electron (accommodated on d_A or d_B atomic orbital) and a bridging atom X has one electron pair (entering ϕ_X atomic orbital). d_A and d_B correspond to d orbitals forming bonding interaction with bridging ligands, while ϕ_X orbital is assignable to the highest occupied atomic orbital of bridging ligand. The linear combination of d_A , d_B , and ϕ_X gives the following three molecular orbitals:

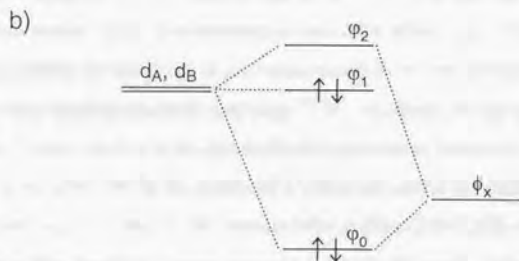
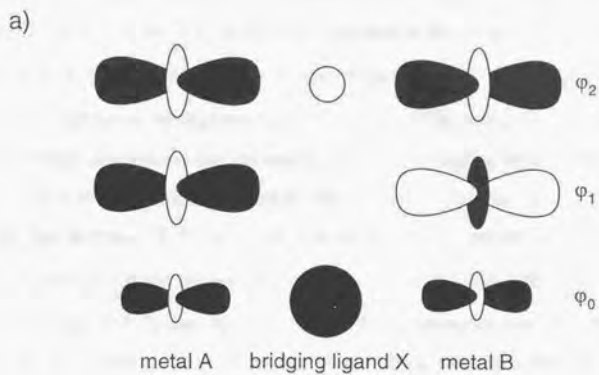


Figure 22. The ABX model system: (a) Schematic representation of the molecular orbitals; (b) Energy diagram of the $S = 0$ ground state.

$$\varphi_0 \approx \phi_s + \varepsilon (d_A + d_B) \quad (\varepsilon \ll 1)$$

$$\varphi_1 \approx d_A - d_B$$

$$\varphi_2 \approx (d_A + d_B) - \varepsilon' \phi_s \quad (\varepsilon' \ll 1)$$

When A and B are antiferromagnetically coupled, the $S = 0$ ground state electron configuration is $\varphi_0^2 \varphi_1^2$ (Figure 22b), while the configuration for the first $S = 1$ excited state is represented as $\varphi_0^2 \varphi_1 \varphi_2$. The energy gap between these two states corresponds to the strength of the magnetic interaction through the bridging ligand. If the energy level of ϕ_s becomes higher, φ_2 are more destabilized and the antiferromagnetic coupling between the two metal increases. The ABX model may account for the stronger interaction through selenido bridges than that through sulfido ones in the chromium cluster complexes. In these complexes, d_A and d_B orbitals are assigned to $3d_{x^2-y^2}$ of Cr, while ϕ_s orbital corresponds to Se 4p (for selenides) or S 3p (for sulfides). Since Se 4p has higher energy level than that for S 3p, the selenido ligands are more effective in transmitting interaction than the sulfido ones.

In complex **2**, the sharp decrease of the μ_{eff} values at lower temperatures cannot be explained by using the HDVV Hamiltonian alone. For obtaining satisfactory fits for the whole experimental curve, it is necessary to take other effect into consideration. Many complexes exhibit similar drops of μ_{eff} values which have been interpreted by using the intermolecular antiferromagnetic couplings.^{91,92} However, the sharp decrease of the μ_{eff} values for **2** cannot be due to the intermolecular interaction, because (i) the similar magnetic anomaly is not observed for the isotypical **3** which has almost the same intermolecular distances as those of **2**, and (ii) the unusual large g value (2.847(10)) cannot be explained. It is more plausible that the μ_{eff} curve anomaly should be the result of the spin-orbital coupling at each chromium center, since it is known that this coupling effect also causes the abnormal g values for some dinuclear complexes.⁹¹⁻⁹³ When an octahedral coordination environment around a metal atom is tetragonally or trigonally distorted, the energy levels of metal d orbitals split, which leads to coupling of the d orbitals through the resulting small energy gap, namely spin-orbital coupling. The spin-orbital coupling effect increases as the participating energy gap is smaller. In chromium complexes **1-3**, the metal centers have a square pyramidal coordination environment (C_{4v} symmetry), and 3d orbital levels split into four

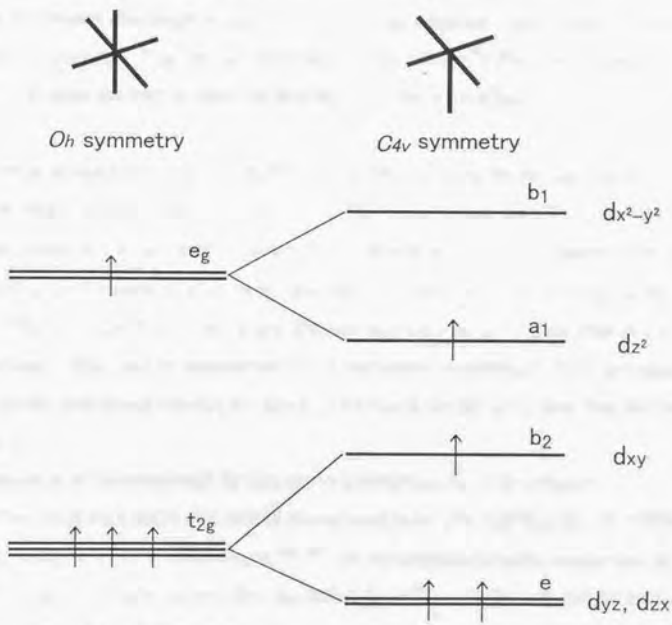


Figure 23. Energy level diagram for d^4 configuration in an octahedral (O_h) and a square pyramidal (C_{4v}) field.

(Figure 23). These energy levels are affected by the presence or absence of interstitial hydride and the difference of chalcogen atoms. It seems conceivable that the energy levels of some 3d orbitals at one or more chromium centers in **2** lie very closer as compared with **1** and **3**, and the resulting large spin-orbital coupling of **2** causes the abnormal g value and the sharper decrease of μ_{eff} curve at lower temperatures. In high temperature region, however, kT values overwhelm the energy gaps between d orbitals and the antiferromagnetic interaction between chromium atoms contributes to the magnetic curve much more than the spin-orbital coupling. Thus the $2J$ values for **2** ($-748(14) \text{ cm}^{-1}$) obtained by using the data above 100 K must not vary so much even if the spin-orbital coupling effect is included in the analysis.

A telluride analogue of **1** [$\text{Cr}_6\text{Te}_8(\text{PEt}_3)_6$] has been reported by Steigerwald *et al.*⁷ The magnetic behavior obeys the Curie law from 100 K to 300 K, and the effective magnetic moment is close to $2.8 \mu_B$ corresponding to two unpaired spins. The apparent decrease in μ_{eff} values at low temperatures has been observed. It is noteworthy that the telluride cluster is very different magnetically from **1** and does not approach the $S = 0$ state even at low temperatures. This may be because the Cr-Cr interatomic distances (2.95 \AA (average)) are longer and the interaction through the direct Cr-Cr bonds should be weaker than that in the selenide **1**.

Bencini *et al.* have reported the theoretical interpretations of the magnetic susceptibilities of octahedral iron sulfide cluster complexes [$\text{Fe}_6\text{S}_8(\text{PEt}_3)_6$] X_2 ($\text{X} = \text{BPh}_4^-$, PF_6^-) by using the HDVV Hamiltonian.^{94, 95} In the analyses of these complexes, no distinction has been made between the interaction for *cis*-iron atoms and that for *trans*-iron centers. The $\chi_M T$ vs. T plots for the iron complexes suggest a spin transition below 80 K, and they are reproduced by two curves.^{94, 95} In the low-temperature region, the low-spin $S = 1/2$ state has been assigned to six Fe^{III} sites, and the magnetic curves have been explained by the antiferromagnetic interaction between the iron centers ($2J = -0.78(8) \text{ cm}^{-1}$, $\text{X} = \text{BPh}_4^-$; $2J = -0.2(8) \text{ cm}^{-1}$, $\text{X} = \text{PF}_6^-$). In the high-temperature region, however, the iron complexes have been described as a mixed-valence and mixed-spin-state compound in which one intermediate-spin ($S = 3/2$), and five low-spin ($S = 1/2$) Fe^{III} sites are localized. The best fit

parameters indicate that the interaction between the low-spin centers are antiferromagnetic ($2J = -23.1(1) \text{ cm}^{-1}$, $X = \text{BPh}_4^-$; $2J = -21.2(6) \text{ cm}^{-1}$, $X = \text{PF}_6^-$) while that between the low-spin and the intermediate-spin centers are ferromagnetic ($2J = 79.0(4) \text{ cm}^{-1}$, $X = \text{BPh}_4^-$; $2J = 330.7(4) \text{ cm}^{-1}$, $X = \text{PF}_6^-$). These results contrast with the good fittings of the experimental data to single curves for the chromium complexes 1-3.

1-3-8. Conclusion

The reaction of CrCl_2 with NaS_xH and PEt_3 in methanol yielded a hexanuclear chromium-sulfide cluster complex $[\text{Cr}_6\text{S}_8(\text{H})(\text{PEt}_3)_6]$. A similar procedure except for using Na_2Se_x in place of NaS_xH , however, gave a mixture of two selenide clusters $[\text{Cr}_6\text{Se}_8(\text{PEt}_3)_6]$ and $[\text{Cr}_6\text{Se}_8(\text{H})(\text{PEt}_3)_6]$. The author separated these selenides by exploiting the difference of their redox properties. The extra hydrogen atoms in $[\text{Cr}_6\text{Se}_8(\text{H})(\text{PEt}_3)_6]$ and $[\text{Cr}_6\text{S}_8(\text{H})(\text{PEt}_3)_6]$ were characterized by FAB mass spectra. The single-crystal X-ray structure determination, powder neutron diffraction analysis, and reactivity studies suggested that the hydrogen atoms lie at the center of octahedral cluster core. These complexes are the first examples of metal-chalcogenide octahedral cluster complexes with an interstitial hydride.

The temperature-dependent paramagnetic data of $[\text{Cr}_6\text{Se}_8(\text{PEt}_3)_6]$, $[\text{Cr}_6\text{Se}_8(\text{H})(\text{PEt}_3)_6]$, and $[\text{Cr}_6\text{S}_8(\text{H})(\text{PEt}_3)_6]$ were analyzed by the Heisenberg-Dirac-Van Vleck Hamiltonian. The analyses showed that all of these complexes display antiferromagnetic interaction between six chromium atoms. The interaction is mediated by Cr-Cr bonds and Cr-(μ_3 -E)-Cr (E = S, Se) bridges. The comparison of the obtained coupling constants suggested that the shorter Cr-Cr distances cause stronger antiferromagnetic interaction through Cr-Cr bonds, and that the coupling through μ_3 -E bridges increases when chalcogen atoms are changed from sulfur to selenium.

1-4 References

1. Saito, T. In *Early Transition Metal Clusters with π -Donor Ligands*; VCH, New York, 1995, pp 63-164.
2. Saito, T. *Adv. Inorg. Chem.* **1996**, *44*, 45.
3. Perrin, A.; Sergent, M. *New J. Chem.* **1988**, *12*, 337.
4. Lee, S. C.; Holm, R. H. *Angew. Chem. Int. Ed. Engl.* **1990**, *29*, 840.
5. Dance, I.; Fisher, K. *Prog. Inorg. Chem.* **1994**, *41*, 637.
6. Fenske, D.; Grissinger, A.; Loos, M.; Magull, J. Z. *Anorg. Allg. Chem.* **1991**, *598/599*, 121.
7. Hessen, B.; Siegrist, T.; Palstra, T.; Tanzler, S. M.; Steigerwald, M. L. *Inorg. Chem.* **1993**, *32*, 5165.
8. Tsuge, K.; Imoto, H.; Saito, T. *Bull. Chem. Soc. Jpn.* **1996**, *69*, 627.
9. Kamiguchi, S.; Imoto, H.; Saito, T. *Chem. Lett.* **1996**, 555.
10. Saito, T.; Yamamoto, N.; Nagase, T.; Tsuboi, T.; Kobayashi, K.; Yamagata, T.; Imoto, H.; Unoura, K. *Inorg. Chem.* **1990**, *29*, 764.
11. Hilsenbeck, S. J.; Young, V. G.; McCarley, R. E. *Inorg. Chem.* **1994**, *33*, 1822.
12. Hilsenbeck, S. J.; McCarley, R. E. *Chem. Mater.* **1995**, *7*, 499.
13. McCarley, R. E.; Hilsenbeck, S. J.; Xie, X. *J. Solid State Chem.* **1995**, *117*, 269.
14. Amari, S.; Imoto, H.; Saito, T. *Chem. Lett.* **1997**, 967.
15. Mizutani, J.; Amari, S.; Imoto, H.; Saito, T. *J. Chem. Soc. Dalton Trans.* **1998**, 819.
16. Saito, T.; Yoshikawa, A.; Yamagata, T.; Imoto, H.; Unoura, K. *Inorg. Chem.* **1989**, *28*, 3588.
17. Zhang, X.; McCarley, R. E. *Inorg. Chem.* **1995**, *34*, 2678.
18. Ehrlich, G. M.; Warren, C. J.; Vennos, D. A.; Ho, D. M.; Haushalter, R. C.; DiSalvo, F. J. *Inorg. Chem.* **1995**, *34*, 4454.
19. Xie, X.; McCarley, R. E. *Inorg. Chem.* **1995**, *34*, 6124.
20. Xie, X.; McCarley, R. E. *Inorg. Chem.* **1996**, *35*, 2713.
21. Xie, X.; McCarley, R. E. *Inorg. Chem.* **1997**, *36*, 4011.
22. Xie, X.; McCarley, R. E. *Inorg. Chem.* **1997**, *36*, 4665.

23. Uriel, S.; Boubekeur, K.; Batail, P.; Orduna, J.; Canadell, E. *Inorg. Chem.* **1995**, *34*, 5307.
24. Long, J. R.; McCarty, L. S.; Holm, R. H. *J. Am. Chem. Soc.* **1996**, *118*, 4603.
25. Mironov, Y. V.; Pell, M. A.; Ibers, J. A. *Inorg. Chem.* **1996**, *35*, 2709.
26. Mironov, Y. V.; Cody, J. A.; Albrecht-Schmitt, T. E.; Ibers, J. A. *J. Am. Chem. Soc.* **1997**, *119*, 493.
27. Zheng, Z.; Long, J. R.; Holm, R. H. *J. Am. Chem. Soc.* **1997**, *119*, 2163.
28. Fedin, V. P.; Fedorov, V. E.; Imoto, H.; Saito, T. *Polyhedron* **1997**, *16*, 1615.
29. Zheng, Z.; Holm, R. H. *Inorg. Chem.* **1997**, *36*, 5173.
30. Willer, M. W.; Long, J. R.; McLauchlan, C. C.; Holm, R. H. *Inorg. Chem.* **1998**, *37*, 328.
31. Cecconi, F.; Ghilardi, C. A.; Midollini, S. *J. Chem. Soc. Chem. Commun.* **1981**, 640.
32. Agresti, A.; Bacci, M.; Cecconi, F.; Ghilardi, C. A.; Midollini, S. *Inorg. Chem.* **1985**, *24*, 689.
33. Cecconi, F.; Ghilardi, C. A.; Midollini, S.; Orlandini, A.; Zanello, P. *J. Chem. Soc. Dalton Trans.* **1987**, 831.
34. Steigerwald, M. L.; Siegrist, T.; Gyorgy, E. M.; Hessen, B.; Kwon, Y. -U.; Tanzler, S. M. *Inorg. Chem.* **1994**, *33*, 3389.
35. Goddard, C. A.; Long, J. R.; Holm, R. H. *Inorg. Chem.* **1996**, *35*, 4347.
36. Cecconi, F.; Ghilardi, C. A.; Midollini, S.; Orlandini, A. *Inorg. Chim. Acta* **1981**, *64*, L47.
37. Fenske, D.; Hachgenei, J.; Ohmer, J. *Angew. Chem. Int. Ed. Engl.* **1985**, *24*, 706.
38. Fenske, D.; Ohmer, J.; Hachgenei, J. *Angew. Chem. Int. Ed. Engl.* **1985**, *24*, 993.
39. Diana, E.; Gervasio, G.; Rossetti, R.; Valdemarin, F.; Bor, G.; Stanghellini, P. L. *Inorg. Chem.* **1991**, *30*, 294.
40. Steigerwald, M. L.; Siegrist, T.; Stuczynski, S. M. *Inorg. Chem.* **1991**, *30*, 2256.
41. Hong, M.; Huang, Z.; Lei, X.; Wei, G.; Kang, B.; Liu, H. *Polyhedron* **1991**, *10*, 927.
42. Cecconi, F.; Ghilardi, C. A.; Midollini, S.; Orlandini, A. *Inorg. Chim. Acta* **1993**, *214*, 13.
43. Cecconi, F.; Ghilardi, C. A.; Midollini, S.; Orlandini, A.; Zanello, P.; Cinquantini, A.; Bencini, A.; Uytterhoeven, M. G.; Giorgi, G. *J. Chem. Soc. Dalton Trans.* **1995**, 3881.
44. Cecconi, F.; Ghilardi, C. A.; Midollini, S.; Orlandini, A.; Zanello, P. *Polyhedron* **1996**, *5*,

45. Ceccconi, F.; Ghilardi, C. A.; Midollini, S.; Orlandini, A.; Bencini, A. *J. Chem. Soc. Dalton Trans.* **1996**, 3991.
46. Thompson, D. P.; Boudjouk, P. *J. Org. Chem.* **1988**, *53*, 2109.
47. Noller, C. R.; Dinsmore, R. In *Organic Syntheses*; Whitmore, F. C., Badertscher, D. E., Lux, A. R., Eds.; Wiley & Sons: New York, 1943, Vol. 2, pp 358-360.
48. Slater, C. J. In *The calculation of Molecular Orbitals*; John Wiley & Sons, New York, 1979, p 52.
49. Averill, F. W.; Ellis, D. E. *J. Chem. Phys.* **1973**, *59*, 6412.
50. Rosén, A.; Ellis, D. E.; Adachi, H.; Averill, F. W. *J. Chem. Phys.* **1976**, *65*, 3629.
51. Adachi, H.; Tsukuda, M.; Satoko, C. *J. Phys. Soc. Jpn.* **1978**, *45*, 875.
52. Satoko, C.; Tsukuda, M.; Adachi, H. *J. Phys. Soc. Jpn.* **1978**, *45*, 1333.
53. Adachi, H.; Shiokawa, S.; Tsukuda, M.; Satoko, C.; Sugano, S. *J. Phys. Soc. Jpn.* **1979**, *47*, 1528.
54. Löwdin, P. O. *Adv. Quantum. Chem.* **1970**, *5*, 185.
55. Szabo, A.; Ostlund, N. S. In *Modern Quantum Chemistry*, revised 1st ed.; McGraw-Hill, New York, 1989, p 149.
56. Imoto, H.; Saito, T.; Adachi, H. *Inorg. Chem.* **1995**, *34*, 2415.
57. *teXsan: Crystal Structure Analysis Package*; Molecular Structure Corporation, Houston, TX, 1985&1992.
58. Sheldrick, G. M. *SHELXS86, a program for crystal structure determination*; University of Göttingen, Göttingen, Federal Republic of Germany, 1986.
59. Beurskens, P. T.; Admiraal, G.; Beurskens, G.; Bosman, W. P.; de Gelder, R.; Israel, R.; Smits, J. M. *The DIRDIF-94 program system, Technical Report of the Crystallography Laboratory*; University of Nijmegen, Nijmegen, The Netherlands, 1994.
60. Kamiyama, T.; Oikawa, K.; Tsuchiya, N.; Osawa, M.; Asano, H.; Watanabe, N.; Furusaka, M.; Satoh, S.; Fujikawa, I.; Ishigaki, T.; Izumi, F. *Physica B* **1995**, *213-214*, 875.
61. Rietveld, H. M. *J. Appl. Crystallogr.* **1969**, *2*, 65.
62. In *International Tables for Crystallography*; Kluwer Academic Publishers, Dordrecht,

1992, p 383.

63. Nakamoto, K. In *Infrared and Raman Spectra of Inorganic and Coordination Compounds*; John Wiley & Sons, New York, 1998; part B, pp 195-199.
64. Klayman, D. L.; Griffin, T. S. *J. Am. Chem. Soc.* **1973**, *95*, 197.
65. Barber, M.; Bell, D.; Eckersley, M.; Morris, M.; Tetler, L. *Rapid Commun. Mass Spectrom.* **1988**, *2*, 18.
66. Oxtou, I. A.; Kettle, S. F. A.; Jackson, P. F.; Johnson, B. F. G.; Lewis, J. *J. Chem. Soc. Chem. Commun.* **1979**, 687.
67. (a) Petersen, J. L.; Brown, R. K.; Williams, J. M. *Inorg. Chem.* **1981**, *20*, 158; (b) Heintz, R. A.; Koetzle, T. F.; Ostrander, R. L.; Rheingold, A. L.; Theopold, K. H.; Wu, P. *Nature* **1995**, *378*, 359.
68. Simon, V. A. Z. *Anorg. Allg. Chem.* **1967**, *355*, 311.
69. Eady, C. R.; Johnson, B. F. G.; Lewis, J.; Malatesta, M. C. *J. Chem. Soc. Chem. Commun.* **1976**, 945.
70. Hart, D. W.; Teller, R. G.; Wei, C. -Y.; Bau, R.; Longoni, G.; Campanella, S.; Chini, P.; Koetzle, T. F. *Angew. Chem. Int. Ed. Engl.* **1979**, *18*, 80.
71. Eady, C. R.; Jackson, P. F.; Johnson, B. F. G.; Lewis, J.; Malatesta, M. C. *J. Chem. Soc. Dalton Trans.* **1980**, 383.
72. Imoto, H.; Corbett, J. D. *Inorg. Chem.* **1980**, *19*, 1241.
73. Jackson, P. F.; Johnson, B. F. G.; Lewis, J.; Raithby, P. R.; McPartlin, M.; Nelson, W. J. H.; Rouse, K. D.; Allibon, J.; Mason, S. A. *J. Chem. Soc. Chem. Commun.* **1980**, 295.
74. Hart, D. W.; Teller, R. G.; Wei, C. -Y.; Bau, R.; Campanella, S.; Chini, P.; Koetzle, T. F. *J. Am. Chem. Soc.* **1981**, *103*, 1458.
75. Imoto, H.; Simon, A. *Inorg. Chem.* **1982**, *21*, 308.
76. Fitch, A. N.; Barrett, S. A.; Fender, B. E. F. *J. Chem. Soc. Dalton Trans.* **1984**, 501.
77. Simon, A.; Stollmaier, F.; Gregson, D.; Fuess, H. *J. Chem. Soc. Dalton Trans.* **1987**, 431.
78. Chu, P. J.; Ziebarth, R. P.; Corbett, J. D.; Gerstein, B. C. *J. Am. Chem. Soc.* **1988**, *110*, 5324.
79. Meyer, H. -J.; Corbett, J. D. *Inorg. Chem.* **1991**, *30*, 963.
80. Gade, L. H.; Johnson, B. F. G.; Lewis, J. *Croat. Chem. Acta* **1995**, *68*, 693.

81. Pauling, L. In *The Nature of the Chemical Bond*, Cornell University Press, Ithaca, New York, 1960, p 224.
82. Holden, N. E. In *Handbook of Chemistry and Physics*; Lide, D. R., Ed. ; CRC Press: Boca Raton, 1997, Chap. 11, p 151 (79th ed.).
83. Simon, A.; Botcher, F.; Cockcroft, J. K. *Angew. Chem. Int. Ed. Engl.* **1991**, *30*, 101.
84. Stevens, R. C.; McLean, M. R.; Bau, R. *J. Am. Chem. Soc.* **1989**, *111*, 3472.
85. Beringhelli, T.; D'Alfonso, G.; Ciani, G.; Sironi, A.; Molinari, H. *J. Chem. Soc. Dalton Trans.* **1990**, 1901.
86. Kambe, K. *J. Phys. Soc. Jpn.* **1950**, *5*, 48.
87. Larkworthy, L. F.; Nolan, K. B. In *Comprehensive Coordination Chemistry*; Wilkinson, G., Gillard, R. D., McCleverty, J. A., Eds.; Pergamon: Oxford, 1987; Vol. 4, pp. 701-772.
88. Tsukerblat, B. S.; Belinskii, M.; Fainzil'berg, V. E. *Sov. Chem. Rev.* **1987**, *9*, 339.
89. Blondin, G.; Girerd, J. -J. *Chem. Rev.* **1990**, *90*, 1359.
90. Anderson, P. W. In *Magnetism*; Academic Press, New York, 1963.
91. Kahn, O. In *Molecular Magnetism*; VCH, New York, 1993, pp 9-29.
92. Kahn, O. In *Molecular Magnetism*; VCH, New York, 1993, pp 103-134.
93. Kahn, O. In *Molecular Magnetism*; VCH, New York, 1993, pp 31-52.
94. Bencini, A.; Uytterhoeven, M. G.; Zanchini, C. *Int. J. Quantum. Chem.* **1994**, *52*, 903.
95. Bencini, A.; Ghilardi, C. A.; Midollini, S.; Orlandini, A.; Russo, U.; Uytterhoeven, M. G.; Zanchini, C. *J. Chem. Soc. Dalton Trans.* **1995**, 963.

Chapter 2

Chemistry of Chromium Sulfido Dodecanuclear Cluster Complexes

2-1 Introduction

In the previous chapter, the study on the hexanuclear chromium cluster complexes with one Cr_6E_8 (E = S, Se) cluster core were described. When this octahedral core is condensed, the resulting cluster oligomers may exhibit the properties due to intercluster interaction, which are never observed in the monomer hexanuclear cluster complexes. Intercluster interaction has been a hot issue in other few systems. For example, the studies on oligomers of Ru_3O trinuclear clusters have dealt with intercluster electronic interaction (Figure 1).¹⁻³ The cyclic voltammometry has suggested that each Ru_3O cluster unit is oxidized and reduced at different potentials, indicative of the electronic interaction between Ru_3O cluster units. The magnitude of intercluster electronic interaction has been related to the intercluster distance,⁴ which is dependent on the difference of the cluster-cluster bridging ligands.² In the field of metal-chalcogenido clusters, however, there have been few reports on intercluster electronic interaction.^{5, 6} Furthermore, the study on intercluster magnetic interaction has been extremely rare even in the whole cluster chemistry.

The study on cluster condensation of a Cr_6E_8 cluster core may also be related to the molybdenum superconducting Chevrel phases $\text{M}_x\text{Mo}_6\text{E}_8$ (M = Cu, Sn, Pb, La, etc.; $x = 0 - 4$; E = S, Se, Te).⁷ In Chevrel phases, the Mo_6E_8 octahedral cluster units are linked by Mo-(μ_4 -E) and Mo-Mo bonds, forming a three-dimensional cluster network (Figure 3 in General Introduction). The interaction between the cluster units through the intercluster bondings is considered to be responsible for the characteristic band structure and superconductivity.⁸

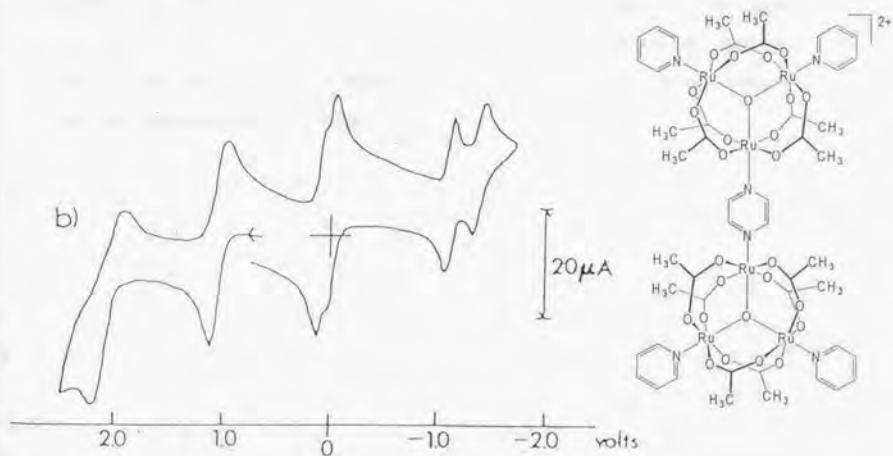
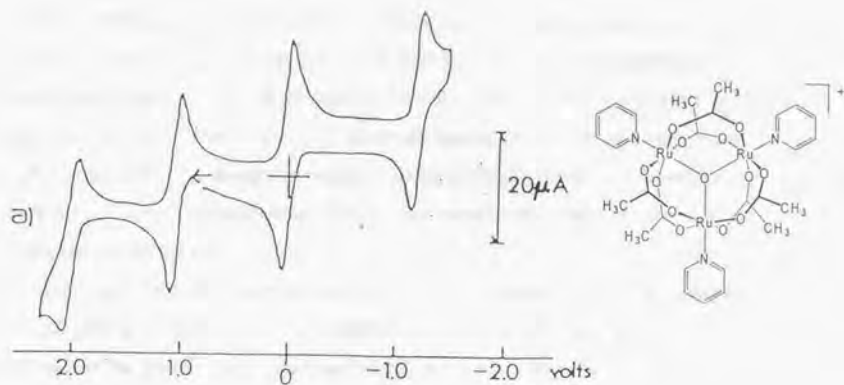


Figure 1. Cyclic voltammograms of a monomeric complex $[\text{Ru}_3\text{O}(\text{CH}_3\text{CO}_2)_6(\text{py})_2(\text{pyr})]^+$ and a dimeric complex $[(\text{py})_2\text{Ru}_3\text{O}(\text{CH}_3\text{CO}_2)_6(\text{pyr})\text{Ru}_3\text{O}(\text{CH}_3\text{CO}_2)_6(\text{py})_2]^{2+}$ (py = pyridine; pyr = pyrazine). (From ref. 2.)

These compounds are usually prepared by high temperature solid state reactions from the elements. Thus similar synthetic techniques have been applied to the preparation of chromium analogue. However, no "chromium Chevrel phases" has been synthesized. The alternative approach to the synthesis of chromium derivatives may be the condensation of Cr_6E_8 cluster cores. Although the oligomerization of $[\text{Cr}_6\text{Te}_8(\text{PEt}_3)_6]$ has failed,⁹ a molybdenum Chevrel phase SnMo_6S_8 has been prepared by the condensation of discrete octahedral cluster units.¹⁰

Previously the author reported the preparation of a dodecanuclear cluster complex " $[\text{Cr}_{12}\text{S}_{16}(\text{PEt}_3)_{10}]$ " by dimerization of hexanuclear complex " $[\text{Cr}_6\text{S}_8(\text{PEt}_3)_6]$."¹¹ The synthesis of the dimeric cluster has been the first step for the preparation of "chromium Chevrels." However, it was clarified that the starting complex " $[\text{Cr}_6\text{S}_8(\text{PEt}_3)_6]$ " was actually $[\text{Cr}_6\text{S}_8(\text{H})(\text{PEt}_3)_6]$ containing an interstitial hydride (*see* Chapter 1), suggesting that the dodecanuclear dimer cluster complexes also have extra hydrogen atoms. This chapter describes the synthesis, FAB mass spectrum, structure, electrochemistry, and magnetic property of the dodecanuclear chromium complex. In addition, the relation between the structure and magnetism is discussed.

2-2. Experimental Section

2-2-1. Synthesis of $[\text{Cr}_{12}\text{S}_{16}(\text{H})_2(\text{PEt}_3)_{10}] \cdot 1.1\text{CH}_2\text{Cl}_2$ ($6 \cdot 1.1\text{CH}_2\text{Cl}_2$)

All of the manipulations were carried out under nitrogen or argon using conventional Schlenk techniques. Solvents were dried and distilled under argon from appropriate drying agents (sodium metal wire for toluene, calcium hydride for hexane and dichloromethane, and calcium sulfate for acetone). All the other reagents (Aldrich) were used as received.

Elemental sulfur (0.0817% w/w toluene; 12 cm^3 , 0.28 mmol) was added to a solution of $3 \cdot 2\text{C}_6\text{H}_6$ (0.40 g, 0.28 mmol) in toluene (80 cm^3), and the mixture was refluxed for 24 h. Toluene was removed *in vacuo*, the residue was extracted with hexane (230 cm^3), and hexane was removed under reduced pressure. The resulting residue was washed with acetone ($3 \times 20 \text{ cm}^3$) for the removal of triethylphosphine sulfide, dried *in vacuo*, and extracted with dichloromethane (17 cm^3). The solution was allowed to stand at $-20 \text{ }^\circ\text{C}$ for 4 d to form black crystals of $6 \cdot 2\text{CH}_2\text{Cl}_2$ (0.044 g, 39%). The crystal solvent molecules were easily lost even at ambient pressure. $6 \cdot 1.1\text{CH}_2\text{Cl}_2$: Found: C, 30.19; H, 6.30; S, 21.07; Cl, 3.12%. Calcd for $\text{C}_{61.1}\text{H}_{154.2}\text{Cr}_{12}\text{P}_{10}\text{S}_{16}\text{Cl}_{2.2}$: C, 30.43; H, 6.36; S, 21.27; Cl, 3.23%.

2-2-2. FAB Mass Spectrum

FAB (fast-atom-bombardment) mass spectrum was obtained with a JEOL JMS-HX 110A double-focusing mass spectrometer equipped with a XMS data system. A fast atom xenon beam was generated from Xe^+ ions, which were accelerated to 1 kV with a FAB gun emission current of 1 mA. The sample ($\sim 1 \text{ } \mu\text{g}$) was placed on the stainless-steel tip of the probe, mixed with *m*-nitrobenzyl alcohol (Aldrich) as a matrix, and exposed to the xenon beam for the desorption.

2-2-3. X-ray Structure Determination

A single crystal of $6 \cdot 2\text{CH}_2\text{Cl}_2$ suitable for the X-ray study was obtained by standing a dichloromethane solution at $5 \text{ }^\circ\text{C}$. It was sealed in a glass capillary for the X-ray measurement. The X-ray measurement of the crystal was performed on a Rigaku AFC-7R

diffractometer with graphite monochromated Mo K α radiation at 207 K. Intensity data were collected with 2θ - ω scans in the range $6^\circ < 2\theta < 55^\circ$. Three standard reflections were monitored every 150 reflections. The crystal showed decay over the period of data collections, and correction was performed by multiplying the decay of standard reflections. The data were additionally corrected for the Lp factor and empirically for the absorption using the ψ -scan method. The positions of the chromium atoms were determined by the direct method using the SHELXS86¹² program, and the other non-hydrogen atoms were located using Fourier techniques with the SHELXS76¹³ and ANYBLK¹² programs. The chromium, chlorine, sulfur, and phosphorous atoms were refined anisotropically, and the carbon atoms were refined isotropically. The hydrogen atoms were not included in the refinements. The final cycle of full-matrix least-squares refinement was based on 7833 observed reflections ($|F_o| > 3\sigma(F_o)$). The crystallographic data are given in Table 1. The final atomic parameters are listed in Table 2.

2-2-4. Cyclic voltammetry

CV (Cyclic voltammetry) was performed on a BAS CV-50W cyclic voltammograph. Three electrodes consisting of a platinum working electrode, a platinum wire counter electrode, and a Ag/Ag⁺ (AgNO₃ (0.01 N) in CH₃CN) reference electrode were used for the measurements. The compounds were dissolved in THF together with 0.1 M tetrabutylammonium perchlorate as a supporting electrolyte and scanning rate was 100 mV/s.

2-2-5. Magnetic Measurement

Magnetic susceptibility was measured in the temperature range 4.5 - 330 K with a Quantum Design MPMS SQUID. The absence of ferromagnetic impurities was checked by the magnetization measurements at 300 K. The magnetic field of the measurements was 5 kG in the temperature range 4.5 - 30 K and 10 kG in the range 30 - 330 K, where the magnetization versus magnetic field curves were linear. The crystalline sample of 6·1.1CH₂Cl₂ (ca. 30 mg) was filled in a cellophane sample holder under nitrogen atmosphere. The magnetic susceptibility of the holder was determined separately. Diamagnetic correction was estimated from Pascal's constants.

Table 1. Crystal Parameters and X-ray Diffraction Data for 6·2CH₂Cl₂

Formula	C ₆₂ H ₁₅₆ Cl ₄ Cr ₁₂ P ₁₀ S ₁₆
Fw	2490.4
Crystal size, mm	0.6 × 0.3 × 0.1
Space group	<i>P</i> $\bar{1}$ (No.2)
<i>a</i> , Å	14.697(6)
<i>b</i> , Å	14.733(5)
<i>c</i> , Å	14.238(5)
α , deg.	96.60(3)
β , deg.	109.77(3)
γ , deg.	65.69(3)
<i>V</i> , Å ³	2643(2)
λ , Å	0.7107
<i>T</i> , K	207
<i>Z</i>	1
μ , cm ⁻¹	17.82
$\rho_{\text{calcd.}}$, g/cm ³	1.565
R^a , R_w^b	0.073, 0.057

$$^a R = \Sigma ||F_o| - |F_c|| / \Sigma |F_o|, \quad ^b R_w = \{ \Sigma [w(|F_o| - |F_c|)^2] / \Sigma [w|F_o|^2] \}^{1/2}, \quad w = 1/\sigma^2(F_o).$$

Table 2. Atomic Coordinates and Temperature Factors for $[\text{Cr}_{12}\text{S}_{16}(\text{H})_2(\text{PEt}_3)_{10}]\cdot 2\text{CH}_2\text{Cl}_2$
(6·2CH₂Cl₂)

atom	<i>x/a</i>	<i>y/b</i>	<i>z/c</i>	<i>U</i> _{iso} ^a
Cr1	0.27464(14)	0.18218(11)	0.18781(13)	0.0190(12)
Cr2	0.10240(14)	0.25479(11)	0.03262(13)	0.0186(12)
Cr3	0.08809(14)	0.28779(12)	0.21195(13)	0.0198(12)
Cr4	0.22672(14)	0.36444(11)	0.26010(13)	0.0192(12)
Cr5	0.24295(14)	0.33663(11)	0.08198(13)	0.0177(12)
Cr6	0.04549(14)	0.45208(11)	0.10007(13)	0.0189(12)
S1	0.1358(2)	0.1298(2)	0.1414(2)	0.023(2)
S2	0.2741(2)	0.1752(2)	0.0228(2)	0.021(2)
S3	0.2493(2)	0.2240(2)	0.3427(2)	0.022(2)
S4	0.3852(2)	0.2678(2)	0.2264(2)	0.021(2)
S5	-0.0527(2)	0.3536(2)	0.0666(2)	0.021(2)
S6	-0.0853(2)	0.6085(2)	0.0492(2)	0.019(2)
S7	0.0557(2)	0.4488(2)	0.2690(2)	0.022(2)
S8	0.1944(2)	0.4910(2)	0.1541(2)	0.020(2)
P1	0.4125(2)	0.0188(2)	0.2389(2)	0.023(2)
P2	0.0369(3)	0.1688(2)	-0.1097(2)	0.029(2)
P3	-0.0057(3)	0.2467(2)	0.2962(2)	0.029(2)
P4	0.3070(3)	0.4309(2)	0.4111(2)	0.028(2)
P5	0.3430(2)	0.3721(2)	0.0009(2)	0.023(2)
C1	0.5105(8)	0.0142(7)	0.3612(8)	0.026(3)
C2	0.6032(10)	-0.0895(8)	0.3950(9)	0.041(3)
C3	0.4878(8)	-0.0398(7)	0.1534(7)	0.025(3)
C4	0.5584(9)	0.0120(7)	0.1441(8)	0.033(3)
C5	0.3707(9)	-0.0800(7)	0.2509(8)	0.032(3)
C6	0.3195(9)	-0.0607(8)	0.3361(9)	0.037(3)
C7	0.0700(11)	0.1907(9)	-0.2158(11)	0.063(4)
C8	0.0448(13)	0.1259(11)	-0.3097(12)	0.090(6)
C9	0.0774(10)	0.0364(8)	-0.1001(9)	0.044(3)
C10	0.1993(10)	-0.0256(8)	-0.0723(9)	0.042(3)
C11	-0.1103(11)	0.2137(9)	-0.1624(11)	0.063(4)
C12	-0.1560(11)	0.1851(9)	-0.0940(10)	0.058(4)
C13	-0.1224(10)	0.2264(8)	0.2147(9)	0.045(3)
C14	-0.2227(10)	0.3233(8)	0.1722(9)	0.045(3)
C15	0.0670(9)	0.1252(8)	0.3630(9)	0.041(3)
C16	0.0100(11)	0.0982(9)	0.4220(10)	0.055(4)
C17	-0.0532(10)	0.3372(8)	0.3888(10)	0.050(4)
C18	0.0389(10)	0.3417(8)	0.4806(9)	0.048(4)
C19	0.4505(9)	0.3794(8)	0.4579(8)	0.037(3)

C20	0.5016(9)	0.2706(8)	0.4963(8)	0.038(3)
C21	0.2683(9)	0.4178(8)	0.5183(9)	0.035(3)
C22	0.3249(10)	0.4508(8)	0.6203(9)	0.048(4)
C23	0.2912(11)	0.5646(9)	0.4021(10)	0.053(4)
C24	0.1795(14)	0.6237(11)	0.3895(12)	0.097(6)
C25	0.3767(9)	0.4816(7)	0.0453(8)	0.029(3)
C26	0.4541(9)	0.4664(8)	0.1570(9)	0.038(3)
C27	0.4713(9)	0.2689(7)	0.0062(8)	0.032(3)
C28	0.5337(9)	0.2890(8)	-0.0505(9)	0.039(3)
C29	0.2718(8)	0.4093(7)	-0.1318(8)	0.028(3)
C30	0.2534(9)	0.3238(7)	-0.2000(8)	0.033(3)
Cl1	0.6912(4)	0.2805(3)	0.3707(3)	0.090(4)
Cl2	0.7455(4)	0.0749(3)	0.4016(5)	0.139(5)
C01	0.6722(11)	0.1727(10)	0.3145(10)	0.065(4)

$${}^a U_{\text{iso}} = (1/3) \sum_i \sum_j U_{ij} a_i^* a_j^* \mathbf{a}_i \cdot \mathbf{a}_j$$

$(U_{ij}) (\times 100)$

atom	U_{11}	U_{22}	U_{33}	U_{12}	U_{13}	U_{23}
Cr1	2.09(11)	1.65(8)	1.77(10)	-0.52(8)	0.61(9)	0.19(7)
Cr2	2.08(11)	1.67(9)	1.57(10)	-0.63(8)	0.33(9)	0.18(7)
Cr3	1.93(11)	1.90(9)	1.86(11)	-0.56(8)	0.46(9)	0.29(8)
Cr4	2.12(11)	1.76(9)	1.61(10)	-0.52(8)	0.54(9)	0.06(7)
Cr5	1.97(11)	1.67(9)	1.52(10)	-0.54(8)	0.57(9)	0.11(7)
Cr6	2.17(11)	1.71(8)	1.54(10)	-0.50(8)	0.59(9)	0.19(7)
S1	2.7(2)	1.97(13)	2.1(2)	-0.97(13)	0.52(14)	0.31(11)
S2	2.2(2)	1.91(13)	1.9(2)	-0.41(12)	0.72(13)	0.10(11)
S3	2.5(2)	2.17(14)	1.6(2)	-0.71(13)	0.44(14)	0.46(11)
S4	1.8(2)	2.33(14)	1.9(2)	-0.65(12)	0.43(13)	0.04(12)
S5	1.7(2)	2.07(14)	2.0(2)	-0.58(12)	0.29(13)	0.37(11)
S6	2.3(2)	1.61(13)	1.3(2)	-0.29(12)	0.50(13)	0.27(11)
S7	2.4(2)	2.07(14)	1.8(2)	-0.43(13)	0.80(14)	-0.16(12)
S8	2.3(2)	1.77(13)	2.0(2)	-0.74(12)	0.73(13)	-0.14(11)
P1	2.5(2)	1.90(14)	2.1(2)	-0.55(13)	0.60(15)	0.22(12)
P2	3.6(2)	3.0(2)	1.9(2)	-1.5(2)	0.3(2)	0.05(13)
P3	2.7(2)	3.4(2)	2.7(2)	-0.9(2)	1.1(2)	0.77(14)
P4	3.9(2)	2.5(2)	1.7(2)	-1.42(15)	0.5(2)	-0.09(12)
P5	2.7(2)	2.09(14)	2.0(2)	-0.84(13)	0.86(15)	0.04(12)
Cl1	10.3(4)	8.8(3)	11.9(4)	-6.5(3)	6.2(3)	-3.9(3)
Cl2	5.7(3)	9.7(4)	23.3(7)	-2.6(3)	-0.3(4)	5.9(4)

2-2-6. Other Physical Measurements

The IR spectrum of 6·1.1CH₂Cl₂ (Figure 2) was measured (4000 - 250 cm⁻¹) with a HITACHI I-3000 spectrometer using KBr disk. The electronic spectrum of hexane solution of 6·1.1CH₂Cl₂ (Figure 3) was measured (210 - 1680 nm) with a HITACHI U-3500 spectrometer. The ¹H NMR (500 MHz) spectrum was measured in CD₂Cl₂ with a JEOL A500 spectrometer using CH₂Cl₂ as the internal standard.

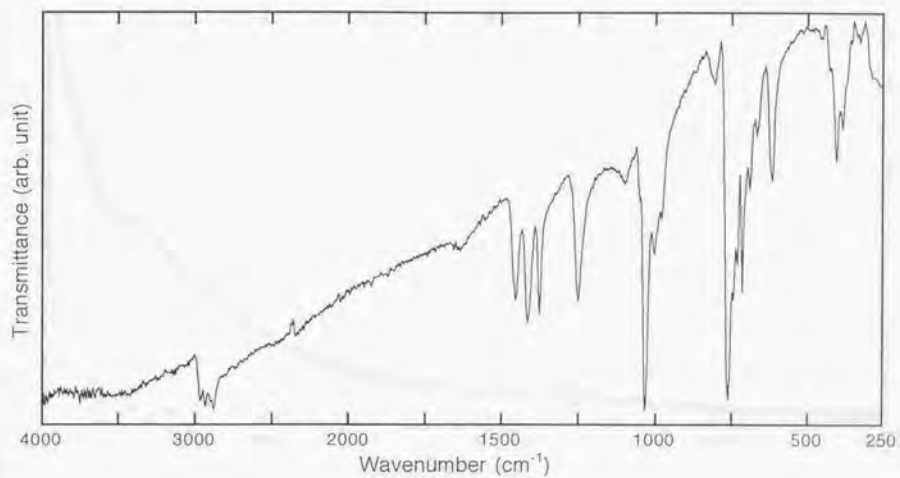


Figure 2. IR spectrum of $[\text{Cr}_{12}\text{S}_{16}(\text{H})_2(\text{PEt}_3)_{10}] \cdot 1.1\text{CH}_2\text{Cl}_2$ ($6 \cdot 1.1\text{CH}_2\text{Cl}_2$). All the peaks are due to triethylphosphine ligands.¹⁴

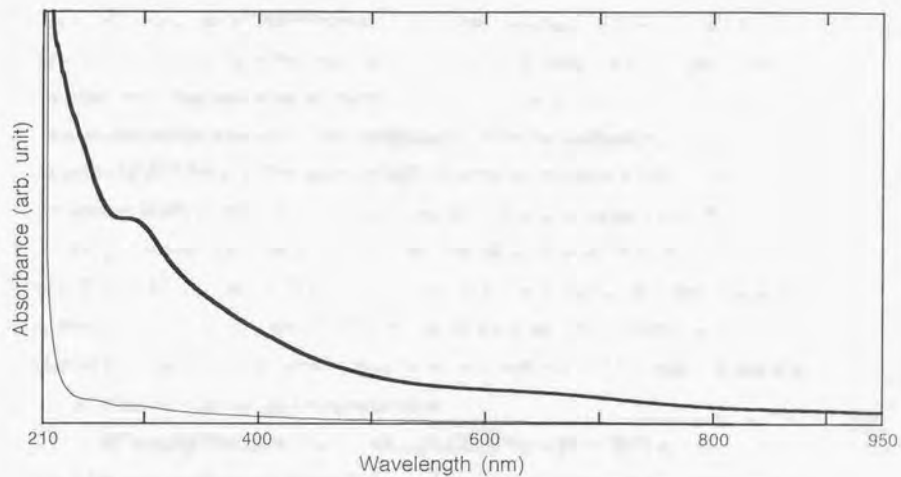
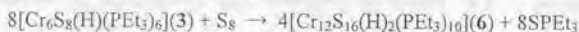


Figure 3. Electronic spectrum of $[\text{Cr}_{12}\text{S}_{16}(\text{H})_2(\text{PEt}_3)_{10}] \cdot 1.1\text{CH}_2\text{Cl}_2$ ($6 \cdot 1.1\text{CH}_2\text{Cl}_2$) in hexane. No absorption peak was observed between 950 and 1680 nm.

2-3 Results and Discussion

2-3-1. Synthesis of Dodecanuclear Cluster Complex $[\text{Cr}_{12}\text{S}_{16}(\text{H})_2(\text{PEt}_3)_{10}]$

The target compound in this work was a dodecanuclear cluster complex in which two Cr_6S_8 cluster units are linked by two Cr-(μ_4 -S) and one Cr-Cr bond. In order to prepare the desired dimeric clusters from the hexanuclear cluster complex $[\text{Cr}_6\text{S}_8(\text{H})(\text{PEt}_3)_6]$ (**3**), it was necessary to remove one of the coordinated PEt_3 ligands by reagents with higher affinity to the phosphines than the chromium atoms. Morris *et al.* have reported the reaction of a mononuclear molybdenum complex coordinated by PMePh_2 (methylidiphenylphosphine) ligands with $[\text{9-BBN}]_2$ (9,9'-bi-borabicyclo[3.3.1]nonane), in which a PMePh_2 ligand are removed as $\text{MePh}_2\text{P-BH}(\text{C}_8\text{H}_{14})$.¹⁵ The treatment of the hexanuclear cluster **3** with $[\text{9-BBN}]_2$, however, gave very low yield of the desired dodecanuclear cluster $[\text{Cr}_{12}\text{S}_{16}(\text{H})_2(\text{PEt}_3)_{10}]$ (**6**) (ca. 7%). After examining other reagents, the author found that elemental sulfur is the best agent. The reaction of the monomer complex **3** with 1 eq of elemental sulfur in refluxing toluene gave the dimer cluster **6** in a 39% yield. A probable overall chemical equation can be represented as



The FAB mass spectrum has shown that complex **6** has two extra hydrogen atoms associated with the Cr_6S_8 cluster units (*vide infra*). Thus the cluster complex " $[\text{Cr}_{12}\text{S}_{16}(\text{PEt}_3)_{10}]$ " reported previously has been reformulated as a hydride **6**. Whereas several dodecanuclear metal-chalcogenide cluster complexes are known,^{5, 6, 16, 17} those with hydride ligands have not been reported so far.

A few other dimers of octahedral clusters have been prepared in various methods. Before the present work, $[\text{Co}_{12}\text{S}_{16}(\text{PEt}_3)_{10}](\text{TCNQ})_2$ (TCNQ = tetracyanoquinodimethane) was obtained as a byproduct in the synthesis of $[\text{Co}_6\text{S}_8(\text{PEt}_3)_6](\text{TCNQ})$.¹⁶ After the establishment of the synthesis of chromium dimer cluster **6**, $[\text{Re}_{12}\text{Se}_{16}(\text{PEt}_3)_{10-2n}(\text{CH}_3\text{CN})_{2n}]^{4+}$ ($n = 0, 1$) have been reported by the thermal removal of the acetonitrile ligand on $[\text{Re}_6\text{Se}_8(\text{PEt}_3)_{5-n}(\text{CH}_3\text{CN})_n]^{2+}$,^{6, 17} and $[\text{Mo}_{12}\text{E}_{16}(\text{PEt}_3)_{10}]$ (E = S, Se) have been prepared by the elimination of a triethylphosphine ligand of $[\text{Mo}_6\text{E}_8(\text{PEt}_3)_6]$ using sulfur or Cp_2TiSe_3 .⁵

On the other hand, oligomers with more than two octahedral clusters have not been reported so far. Holm *et al.* have suggested that a tetramer of Re_6 units is likely to form by the dimerization of the *cis*- $[\text{Re}_{12}\text{Se}_{16}(\text{PEt}_3)_{10}(\text{CH}_3\text{CN})_2]^{4+}$.⁶ Since the opportunity of the removal of any triethylphosphine is equally open after the dimerization in **6**, oligomers or even polymers such as the "chromium Chevrel phases" may be obtained by the condensation reactions of the dodecanuclear and hexanuclear octahedral clusters.

2-3-2. FAB Mass Spectrum

The starting hexanuclear complex **3** contains an extra hydrogen atom associated with the Cr_6S_8 cluster unit, as indicated by a FAB mass spectrum (mentioned in Chapter 1). Since the dodecanuclear complex **6** was also considered to have extra hydrides, the positive-ion FAB mass spectrum of **6** was measured with NBA (*m*-nitrobenzyl alcohol) as a matrix. The comparison of the isotope pattern of the molecular ion peak with that calculated is shown in Figure 4. The chromium cluster complexes $[\text{Cr}_6\text{Se}_8(\text{PEt}_3)_6]$ (**1**), $[\text{Cr}_6\text{Se}_8(\text{H})(\text{PEt}_3)_6]$ (**2**), and **3** exhibit the molecular ion peaks corresponding to $[\text{M}]^+$ rather than protonated $[\text{M-H}]^+$ in the positive-ion FAB mass spectra measured with NBA. The molecular ion peak for **6** is assignable to $[\text{Cr}_{12}\text{S}_{16}(\text{H})_2(\text{PEt}_3)_{10}]^+$, indicating that complex **6** is $[\text{Cr}_{12}\text{S}_{16}(\text{H})_2(\text{PEt}_3)_{10}]$.

2-3-3. X-ray Structure Analysis

The structure of the dodecanuclear cluster complex **6** was determined with the single-crystal X-ray structure analysis. Molecular structural drawing of **6** is shown in Figure 5. The selected interatomic distances and angles are listed in Table 3. There is a crystallographic inversion center at the middle point of Cr6-Cr6', and the molecule has C_i point group symmetry. Two Cr_6S_8 cluster cores are contained in one molecule. Each core comprises a Cr_6 octahedron and eight face-capping sulfur atoms. Five chromium atoms (Cr1-Cr5) are coordinated by triethylphosphine ligands, while the other chromium site (Cr6) is bound to one of the sulfur atoms in the adjacent Cr_6S_8 unit. Thus the two Cr_6S_8 cores are linked by two Cr-S bonds. This intercluster bonding mode is similar to those in the superconducting Chevrel phases. Therefore, the $\text{Cr}_{12}\text{S}_{16}$ cluster framework in **6** represents two neighboring cluster units in the "chromium Chevrel phases."

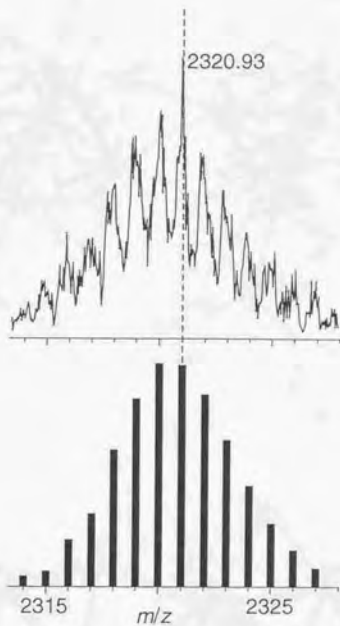


Figure 4. Measured and calculated isotope patterns for the molecular ion of $[\text{Cr}_{12}\text{S}_{16}(\text{H})_2(\text{PEt}_3)_{10}]$ (6).

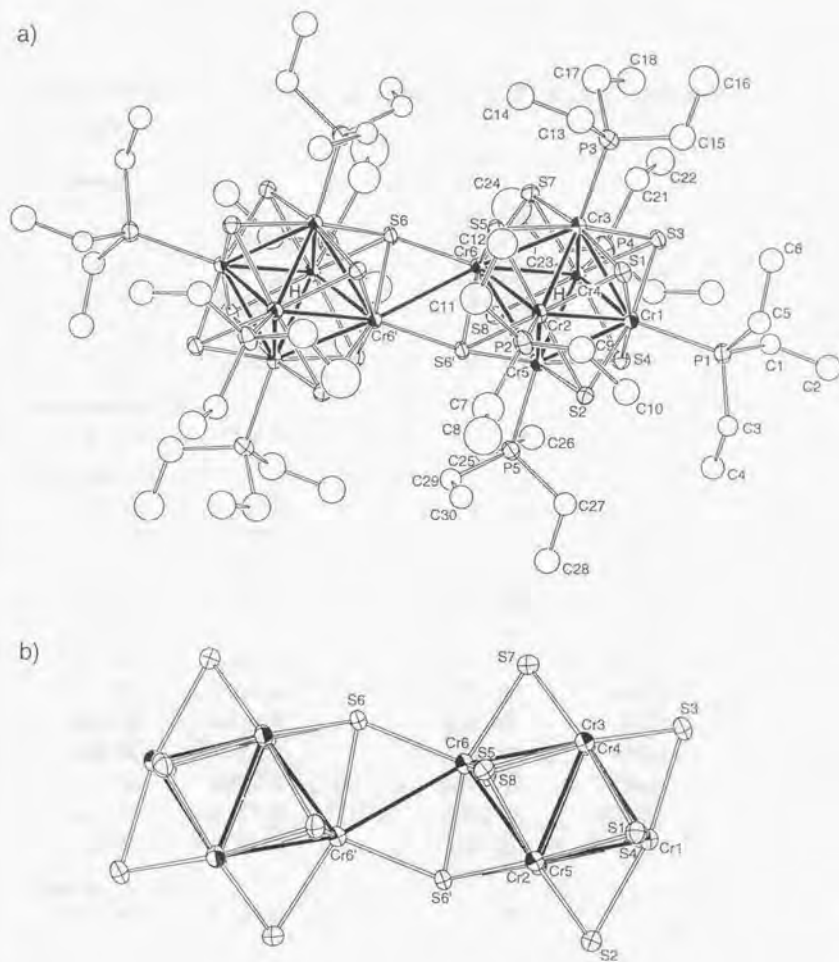


Figure 5. (a) ORTEP drawing of $[\text{Cr}_{12}\text{S}_{16}(\text{H})_2(\text{PEt}_3)_{10}]$ (**6**). H denotes the proposed positions of the interstitial hydrides. The other hydrogen atoms are omitted for clarity. (b) ORTEP drawing of the $\text{Cr}_{12}\text{S}_{16}$ cluster framework in **6** viewed in the direction perpendicular to the intercluster Cr_2S_2 rhomboid. It is shown that Cr6 projects from the square of the surrounding sulfur atoms (S5, S6', S7, S8). The thermal ellipsoids are drawn at the 50% level in both (a) and (b).

Table 3. Bond Distances (Å) and Angles (deg) for $[\text{Cr}_{12}\text{S}_{16}(\text{H})_2(\text{PEt}_3)_{10}] \cdot 2\text{CH}_2\text{Cl}_2$
(6·2CH₂Cl₂)

intracluster Cr-Cr

Cr1 - Cr2	2.639(3)	Cr2 - Cr6	2.823(2)
Cr1 - Cr3	2.657(3)	Cr3 - Cr4	2.582(3)
Cr1 - Cr4	2.658(2)	Cr3 - Cr6	2.784(2)
Cr1 - Cr5	2.666(2)	Cr4 - Cr5	2.597(3)
Cr2 - Cr3	2.607(3)	Cr4 - Cr6	2.773(2)
Cr2 - Cr5	2.662(3)	Cr5 - Cr6	2.779(2)

intercluster Cr-Cr

Cr6 - Cr6'	2.948(3)
------------	----------

intracluster Cr-S

Cr1 - S1	2.337(4)	Cr4 - S3	2.347(3)
Cr1 - S2	2.337(3)	Cr4 - S4	2.356(3)
Cr1 - S3	2.332(3)	Cr4 - S7	2.341(3)
Cr1 - S4	2.336(3)	Cr4 - S8	2.326(3)
Cr2 - S1	2.330(3)	Cr5 - S2	2.341(3)
Cr2 - S2	2.351(3)	Cr5 - S4	2.335(3)
Cr2 - S5	2.324(3)	Cr5 - S6'	2.321(3)
Cr2 - S6'	2.324(3)	Cr5 - S8	2.314(3)
Cr3 - S1	2.348(3)	Cr6 - S5	2.347(3)
Cr3 - S3	2.355(3)	Cr6 - S6'	2.373(3)
Cr3 - S5	2.327(3)	Cr6 - S7	2.363(3)
Cr3 - S7	2.325(3)	Cr6 - S8	2.345(3)

intercluster Cr-S

Cr6 - S6	2.307(3)
----------	----------

Cr-P

Cr1 - P1	2.412(3)	Cr4 - P4	2.393(3)
Cr2 - P2	2.394(3)	Cr5 - P5	2.385(4)
Cr3 - P3	2.383(4)		

intracluster Cr-Cr-Cr within triangular faces

Cr2 - Cr1 - Cr3	58.97(6)	Cr1 - Cr2 - Cr3	60.85(6)
Cr2 - Cr1 - Cr5	60.25(6)	Cr1 - Cr2 - Cr5	60.37(6)
Cr3 - Cr1 - Cr4	58.14(6)	Cr3 - Cr2 - Cr6	61.54(6)
Cr4 - Cr1 - Cr5	58.41(6)	Cr5 - Cr2 - Cr6	60.79(6)

Cr1 - Cr3 - Cr2	60.17(6)	Cr1 - Cr5 - Cr2	59.38(6)
Cr1 - Cr3 - Cr4	60.95(6)	Cr1 - Cr5 - Cr4	60.65(6)
Cr2 - Cr3 - Cr6	63.06(6)	Cr2 - Cr5 - Cr6	62.47(6)
Cr4 - Cr3 - Cr6	62.10(6)	Cr4 - Cr5 - Cr6	62.00(6)
Cr1 - Cr4 - Cr3	60.90(6)	Cr2 - Cr6 - Cr3	55.40(5)
Cr1 - Cr4 - Cr5	60.94(6)	Cr2 - Cr6 - Cr5	56.75(6)
Cr3 - Cr4 - Cr6	62.52(6)	Cr3 - Cr6 - Cr4	55.38(6)
Cr5 - Cr4 - Cr6	62.21(6)	Cr4 - Cr6 - Cr5	55.79(6)
intracluster Cr-Cr-Cr within equatorial squares			
Cr2 - Cr1 - Cr4	88.51(7)	Cr1 - Cr4 - Cr6	94.77(7)
Cr3 - Cr1 - Cr5	87.83(7)	Cr3 - Cr4 - Cr5	90.90(8)
Cr1 - Cr2 - Cr6	94.03(7)	Cr1 - Cr5 - Cr6	94.47(8)
Cr3 - Cr2 - Cr5	88.94(7)	Cr2 - Cr5 - Cr4	89.29(8)
Cr1 - Cr3 - Cr6	94.55(8)	Cr2 - Cr6 - Cr4	82.67(6)
Cr2 - Cr3 - Cr4	90.86(8)	Cr3 - Cr6 - Cr5	83.15(6)
Cr-Cr-Cr between intracluster Cr-Cr and intercluster Cr-Cr			
Cr2 - Cr6 - Cr6'	95.67(8)	Cr4 - Cr6 - Cr6'	146.42(11)
Cr3 - Cr6 - Cr6'	146.23(11)	Cr5 - Cr6 - Cr6'	95.31(8)
intracluster Cr-S-Cr			
Cr1 - S1 - Cr2	68.86(10)	Cr2 - S5 - Cr3	68.17(10)
Cr1 - S1 - Cr3	69.09(10)	Cr2 - S5 - Cr6	74.37(10)
Cr2 - S1 - Cr3	67.73(9)	Cr3 - S5 - Cr6	73.11(10)
Cr1 - S2 - Cr2	68.51(10)	Cr2' - S6 - Cr5'	69.95(9)
Cr1 - S2 - Cr5	69.47(10)	Cr2' - S6 - Cr6'	73.89(10)
Cr2 - S2 - Cr5	69.15(9)	Cr5' - S6 - Cr6'	72.59(10)
Cr1 - S3 - Cr3	69.05(10)	Cr3 - S7 - Cr4	67.20(9)
Cr1 - S3 - Cr4	69.22(10)	Cr3 - S7 - Cr6	72.86(10)
Cr3 - S3 - Cr4	66.62(9)	Cr4 - S7 - Cr6	72.24(10)
Cr1 - S4 - Cr4	69.01(10)	Cr4 - S8 - Cr5	68.07(9)
Cr1 - S4 - Cr5	69.60(10)	Cr4 - S8 - Cr6	72.83(10)
Cr4 - S4 - Cr5	67.25(10)	Cr5 - S8 - Cr6	73.21(10)
Cr-S-Cr between intracluster Cr-S and intercluster Cr-S			
Cr2' - S6 - Cr6	135.02(15)	Cr6 - S6 - Cr6'	78.08(10)
Cr5' - S6 - Cr6	132.39(14)		

Cr-S-Cr between intracluster Cr-S and intercluster Cr-S

Cr2' - S6 - Cr6	135.02(15)	Cr6 - S6 - Cr6'	78.08(10)
Cr5' - S6 - Cr6	132.39(14)		

intracluster S-Cr-S between *cis*-sulfides

S1 - Cr1 - S2	91.10(12)	S3 - Cr4 - S4	88.13(11)
S1 - Cr1 - S3	88.82(12)	S3 - Cr4 - S7	91.03(12)
S2 - Cr1 - S4	88.58(12)	S4 - Cr4 - S8	90.03(12)
S3 - Cr1 - S4	88.96(12)	S7 - Cr4 - S8	89.21(11)
S1 - Cr2 - S2	90.95(11)	S2 - Cr5 - S4	88.54(11)
S1 - Cr2 - S5	90.74(12)	S2 - Cr5 - S6'	87.79(11)
S2 - Cr2 - S6'	87.48(12)	S4 - Cr5 - S8	90.85(11)
S5 - Cr2 - S6'	88.65(11)	S6' - Cr5 - S8	90.92(11)
S1 - Cr3 - S3	88.02(11)	S5 - Cr6 - S7	87.52(12)
S1 - Cr3 - S5	90.22(12)	S6' - Cr6 - S5	86.93(11)
S3 - Cr3 - S7	91.23(12)	S6' - Cr6 - S8	88.89(12)
S5 - Cr3 - S7	88.91(11)	S7 - Cr6 - S8	88.23(12)

intracluster S-Cr-S between *trans*-sulfides

S1 - Cr1 - S4	168.00(12)	S3 - Cr4 - S8	170.50(13)
S2 - Cr1 - S3	167.76(12)	S4 - Cr4 - S7	170.22(13)
S1 - Cr2 - S6'	169.21(13)	S2 - Cr5 - S8	169.91(14)
S2 - Cr2 - S5	168.07(13)	S4 - Cr5 - S6'	168.83(14)
S1 - Cr3 - S7	171.18(14)	S5 - Cr6 - S8	158.25(11)
S3 - Cr3 - S5	169.48(14)	S6' - Cr6 - S7	157.48(11)

S-Cr-S between intracluster Cr-S and intercluster Cr-S

S5 - Cr6 - S6	101.75(12)	S6 - Cr6 - S7	100.58(11)
S6 - Cr6 - S6'	101.92(10)	S6 - Cr6 - S8	100.00(11)

intracluster S-Cr-P

S1 - Cr1 - P1	95.54(11)	S5 - Cr3 - P3	96.81(13)
S2 - Cr1 - P1	95.96(11)	S7 - Cr3 - P3	97.62(12)
S3 - Cr1 - P1	96.23(11)	S3 - Cr4 - P4	93.15(12)
S4 - Cr1 - P1	96.42(12)	S4 - Cr4 - P4	95.37(13)
S1 - Cr2 - P2	91.72(12)	S7 - Cr4 - P4	94.40(12)
S2 - Cr2 - P2	91.24(12)	S8 - Cr4 - P4	96.30(11)
S5 - Cr2 - P2	100.51(13)	S2 - Cr5 - P5	96.20(12)
S6' - Cr2 - P2	98.99(12)	S4 - Cr5 - P5	94.72(12)
S1 - Cr3 - P3	91.19(12)	S6' - Cr5 - P5	96.16(12)
S3 - Cr3 - P3	93.59(12)	S8 - Cr5 - P5	93.89(11)

Complex **6** has two extra hydrogen atoms as indicated by FAB mass spectrum (*vide supra*). In the study on the monomeric cluster **3**, the location of the extra hydride was attempted, and its interstitial position was supported by its inertness toward Lewis bases such as ethanol, acetone, THF, or $^t\text{BuNH}_2$. The extra hydrides in **6** are also stable toward these reagents, suggesting that the hydrides are inside the Cr_6 octahedra.

The monomer **3** has the nearly regular Cr_6 octahedron, and all of the Cr-Cr distances are almost equal (mean 2.59 Å). However, the Cr_6 cores in the dimer **6** are considerably distorted, where the four intracluster Cr-Cr distances between Cr6 and other four chromium atoms (Cr2-Cr5) (mean 2.79 Å) are longer by 0.16 Å than the other eight intracluster Cr-Cr distances. The mean value of 24 intracluster Cr-Cr bond distances of **6** (2.69 Å) is 0.10 Å longer than that in the monomer **3** (Table 4). The cobalt dimer $[\text{Co}_{12}\text{S}_{16}(\text{PEt}_3)_{10}]^{2+16}$ also has more distorted Co_6 octahedra and the longer intracluster Co-Co distances (mean 2.84 Å) than those in the monomer $[\text{Co}_6\text{S}_8(\text{PEt}_3)_6]^+$ (mean 2.79 Å).¹⁹ On the other hand, the intracluster M-M distances in the molybdenum⁵ and rhenium dimers^{6, 17} are not much different from those in the corresponding monomers,^{6, 17, 20} and the distortion of each unit is minimal as compared with that in the chromium and cobalt congeners.

The distortion of octahedral cluster core depends on two factors. One is the weakness of intracluster metal-metal bonds, which is characteristic of 3d-metal cluster complexes, and the other is the magnetism of the octahedral cluster units. If the M_6 cluster units have unpaired electrons, the antiferromagnetic coupling arises between the linking metal atoms, and the intercluster metal-metal distances become shorter, which leads to the projection of the linking M sites from the square of the surrounding chalcogen atoms (Figure 5b).²¹ In the chromium and cobalt dimer clusters, the metal-metal bonds are weak and each octahedral cluster unit has the unpaired spin,^{22, 23} which is a cause of the shorter intercluster metal-metal distances and the elongation of the intracluster metal-metal bonds (Table 4). Therefore, it is conceivable that the octahedral cluster cores are more distorted as compared with the molybdenum and rhenium dimers. The intercluster antiferromagnetic coupling in chromium dimer **6** was also revealed by the magnetic measurement (*vide infra*).

Table 4. Relationship of Interatomic Distances (Å)

	intracluster M-M		intercluster	intercluster	ref
	mean	deviation	M-M	M-(μ-E)	
[Cr ₆ S ₈ (H)(PEt ₃) ₆]	2.59	0.004			This work
[Co ₆ S ₈ (PEt ₃) ₆] ⁺	2.79	0.037			19
[Mo ₆ S ₈ (PEt ₃) ₆]	2.66	0.002			20
[Mo ₆ Se ₈ (PEt ₃) ₆]	2.70	0.011			20
[Re ₆ Se ₈ (PEt ₃) ₅ (CH ₃ CN)] ²⁺	2.64	0.028			17
[Re ₆ Se ₈ (PEt ₃) ₄ (CH ₃ CN) ₂] ²⁺	2.63	0.039			17
[Cr ₁₂ S ₁₆ (H) ₂ (PEt ₃) ₁₀]	2.69	0.241	2.95	2.31	This work
[Co ₁₂ S ₁₆ (PEt ₃) ₁₀] ²⁺	2.84	0.125	2.64	2.15	16
[Mo ₁₂ S ₁₆ (PEt ₃) ₁₀]	2.65	0.052	3.42	2.55	5
[Mo ₁₂ Se ₁₆ (PEt ₃) ₁₀]	2.70	0.048	3.55	2.71	5
[Re ₁₂ Se ₁₆ (PEt ₃) ₁₀] ⁴⁺	2.64	0.057	3.42	2.64	17
[Re ₁₂ Se ₁₆ (PEt ₃) ₈ (CH ₃ CN) ₂] ⁴⁺	2.63	0.049	3.39	2.61	6

2-3-4. Electrochemistry

The redox potentials referenced to the $\text{Cp}_2\text{Fe}^+ / \text{Cp}_2\text{Fe}$ couple in the CV (cyclic voltammograms) of **3** and **6** are listed in Table 5. The hexanuclear cluster complex **3** exhibits one oxidation step and one reduction step (Figure 6a), while two oxidation steps and two reduction steps were observed in the CV of the dodecanuclear cluster complex **6** (Figure 6b). All the waves are assumed to correspond to one electron redox processes of a Cr_6S_8 octahedral cluster unit. The two oxidation steps of **6** are assigned to the formation of $[\text{Cr}_6\text{S}_8^+ - \text{Cr}_6\text{S}_8]$ and $[\text{Cr}_6\text{S}_8^{2+} - \text{Cr}_6\text{S}_8^+]$ species, and the reduction steps to that of $[\text{Cr}_6\text{S}_8^- - \text{Cr}_6\text{S}_8]$ and $[\text{Cr}_6\text{S}_8^{2-} - \text{Cr}_6\text{S}_8^-]$ ones. Thus the two octahedral units are oxidized and reduced at different potentials. The potential differences for oxidation and reduction (0.33 V vs. 0.55 V) are as large as those for the molybdenum analogue $[\text{Mo}_{12}\text{E}_{16}(\text{PEt}_3)_{10}]$ (0.41 V vs. 0.49 V, E = S; 0.38 V vs. 0.47 V, E = Se)⁵ and larger than that for the rhenium selenide derivative $[\text{Re}_{12}\text{Se}_{16}(\text{PEt}_3)_{10}]^{4+}$ (0.22 V) in the successive two oxidation steps.⁶ The separation of the redox processes is indicative of the electronic effects of the charge in an octahedral unit on the adjacent cluster.⁴ The magnitudes of the separation of the potentials suggest that the intermediate mixed valence states of clusters are rather stable, and the electronic delocalization between the cluster units is extensive. In the chromium complex **6** and the molybdenum analogues, the potential differences for reduction are larger than those for oxidation, indicating that the electronic interaction between the cluster units becomes stronger as the clusters are more reduced. It is interesting that such electrochemical trend is common among almost all the cluster oligomers which exhibit mixed valence states of clusters in the CV.¹⁻³

Table 5. Redox Potentials^a in the Cyclic Voltammetry of **3** and **6**

	+2 / +1	+1 / 0	0 / -1	-1 / -2
$[\text{Cr}_6\text{S}_8(\text{H})(\text{PEt}_3)_6](\mathbf{3})$		-0.81	-1.51	
$[\text{Cr}_{12}\text{S}_{16}(\text{H})_2(\text{PEt}_3)_{10}](\mathbf{6})$	-0.51	-0.84	-1.54	-2.09

^a Potentials / V are referenced to $\text{F}_e / \text{F}_e^+$ ($\text{F}_e = \text{Cp}_2\text{Fe}$) couple

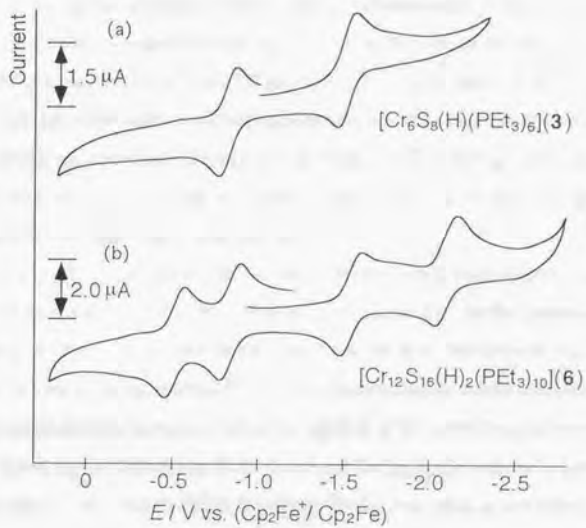


Figure 6. Cyclic voltammograms of (a) $[\text{Cr}_6\text{S}_8(\text{H})(\text{PEt}_3)_6] \cdot 2\text{C}_6\text{H}_6$ ($\mathbf{3} \cdot 2\text{C}_6\text{H}_6$) and (b) $[\text{Cr}_{12}\text{S}_{16}(\text{H})_2(\text{PEt}_3)_{10}] \cdot 1.1\text{CH}_2\text{Cl}_2$ ($\mathbf{6} \cdot 1.1\text{CH}_2\text{Cl}_2$).

2-3-5. Magnetic Property

The measured temperature dependence of the μ_{eff} and $\chi_{\text{M}}T$ values of **3** and **6** are shown in Figures 7 and 8. The dimer **6** is paramagnetic over the whole temperature range measured. The oxidation states of the chromium metals in **6** are the same as those in the monomer **3**. The $\chi_{\text{M}}T$ value ($1.48 \text{ cm}^3 \text{ mol}^{-1} \text{ K}$) is a little smaller than twice that of **3** ($0.82 \text{ cm}^3 \text{ mol}^{-1} \text{ K}$) at 330 K, reflecting the existence of two octahedral cluster units in the dimer **6** with some intercluster antiferromagnetic coupling. However, the values decrease more rapidly to *ca.* 1/4 at 4.5 K ($\chi_{\text{M}}T = 0.10 \text{ cm}^3 \text{ mol}^{-1} \text{ K}$ for **6**; $\chi_{\text{M}}T = 0.36 \text{ cm}^3 \text{ mol}^{-1} \text{ K}$ for **3**), indicative of much stronger intercluster antiferromagnetic interaction at lower temperatures between two Cr_6S_8 cluster units probably through Cr-(μ -S) and Cr-Cr bonding interaction. The existence of intercluster antiferromagnetic coupling was supported by the distortion of the octahedral cluster cores in **6** (*vide supra*).

In the study on the hexanuclear cluster complexes **1-3**, their magnetic data were analyzed by using the HDVV Hamiltonian (*see* Chapter 1). In the analyses, calculations of the energy levels E did not take much time, since the spin Hamiltonian could be simplified with the vector coupling method.²⁴ For the dodecanuclear cluster complex **6**, however, similar simplification technique cannot be applied, if the interaction between the chromium atoms linked by the intercluster Cr-Cr bond and Cr-(μ -S)-Cr bridges is taken into consideration. In order to obtain the energy levels, it is necessary to solve the secular determinant of very high order ($= 5^6 \times 4^6$) without any diagonalization, and the calculation will take extremely long time. The analyses of the magnetic behavior of **6** have not been performed yet for this reason.

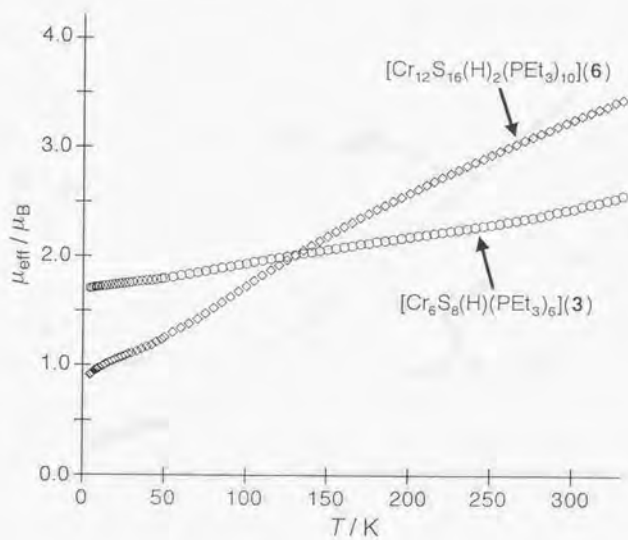


Figure 7. Thermal dependence of the magnetic susceptibilities of $[\text{Cr}_{12}\text{S}_{16}(\text{H})_2(\text{PEt}_3)_{10}]$ (6) in the form of μ_{eff} vs. T .

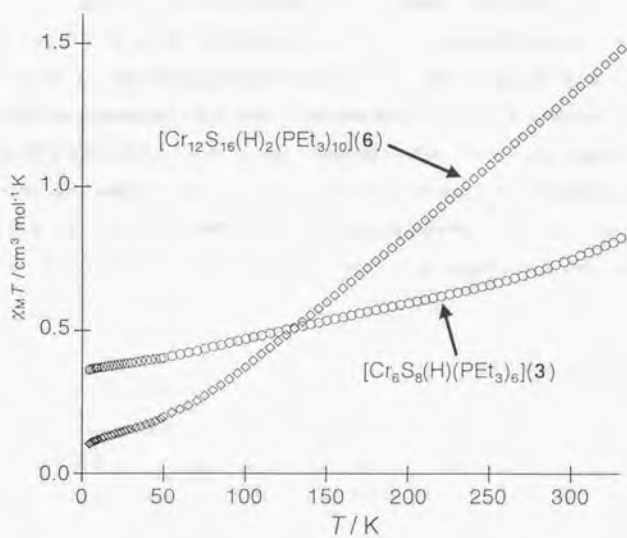


Figure 8. Thermal dependence of the magnetic susceptibilities of $[\text{Cr}_{12}\text{S}_{16}(\text{H})_2(\text{PEt}_3)_{10}](\mathbf{6})$ in the form of $\chi_M T$ vs. T .

2-3-6. Conclusion

A dodecanuclear chromium-sulfide cluster complex $[\text{Cr}_{12}\text{S}_{16}(\text{H})_2(\text{PEt}_3)_{10}]$ was prepared by the dimerization of a hexanuclear cluster complex $[\text{Cr}_6\text{S}_8(\text{H})(\text{PEt}_3)_6]$ with elemental sulfur, and characterized by the single-crystal X-ray analysis and FAB mass spectrum. This dodecanuclear complex has two Cr_6S_8 cluster cores with an interstitial hydrogen atom, and the cores are linked by two Cr-S and one Cr-Cr bond. The intercluster bonding mode is similar to those in the molybdenum superconducting Chevrel phases. Whereas the Cr_6 octahedron in the starting hexanuclear complex is almost regular, those in the dodecanuclear dimer are considerably distorted. The distortion was related to the weak intracluster metal-metal bonds and antiferromagnetic interaction between two Cr_6S_8 cluster units. The intercluster antiferromagnetic coupling was also revealed by the magnetic measurement. Electrochemical measurements indicated the intercluster electronic interaction between the two Cr_6S_8 cluster units and the stable mixed-valence states of octahedral clusters.

2-4 References

1. Wilson, S. T.; Bondurant, R. F.; Meyer, T. J.; Salmon, D. J. *J. Am. Chem. Soc.* **1975**, *97*, 2285.
2. Baumann, J. A.; Salmon, D. J.; Wilson, S. T.; Meyer, T. J. *Inorg. Chem.* **1979**, *18*, 2472.
3. Baumann, J. A.; Wilson, S. T.; Salmon, D. J.; Hood, P. L.; Meyer, T. J. *J. Am. Chem. Soc.* **1979**, *101*, 2916.
4. Richardson, D. E.; Taube, H. *Inorg. Chem.* **1981**, *20*, 1278.
5. Amari, S.; Imoto, H.; Saito, T. *J. Chin. Chem. Soc.* **1998**, *45*, 445.
6. Zheng, Z.; Holm, R. H. *Inorg. Chem.* **1997**, *36*, 5173.
7. Chevrel, R.; Sergent, M. In *Superconductivity in Ternary Compounds I*; Springer, Berlin, 1982, pp 25-86.
8. Nohl, H.; Klose, W.; Anderson, O. K. In *Superconductivity in Ternary Compounds I*; Springer, Berlin, 1982, pp 165-221.
9. Hessen, B.; Siegrist, T.; Palstra, T.; Tanzler, S. M.; Steigerwald, M. L. *Inorg. Chem.* **1993**, *32*, 5165.
10. McCarley, R. E.; Hilsenbeck, S. J.; Xie, X. *J. Solid State Chem.* **1995**, *117*, 269.
11. Kamiguchi, S.; Imoto, H.; Saito, T. *Chem. Lett.* **1996**, 555.
12. Sheldrick, G. M. *SHELXS86, a program for crystal structure determination*; University of Göttingen, Göttingen, Federal Republic of Germany, 1986.
13. Sheldrick, G. M. *SHELXS76, a Program for Crystal Structure Determination*. University of Cambridge, Cambridge, U.K, 1976.
14. Nakamoto, K. In *Infrared and Raman Spectra of Inorganic and Coordination Compounds*; John Wiley & Sons, New York, 1998; part B, pp 195-199.
15. Luck, R.; Morris, R. H. *Inorg. Chem.* **1984**, *23*, 1489.
16. Cecconi, F.; Ghilardi, C. A.; Midollini, S.; Orlandini, A. *Inorg. Chim. Acta* **1993**, *214*, 13.
17. Zheng, Z.; Long, J. R.; Holm, R. H. *J. Am. Chem. Soc.* **1997**, *119*, 2163.
18. Oxtou, I. A.; Kettle, S. F. A.; Jackson, P. F.; Johnson, B. F. G.; Lewis, J. *J. Chem. Soc. Chem. Commun.* **1979**, 687.
19. Cecconi, F.; Ghilardi, C. A.; Midollini, S.; Orlandini, A.; Zanello, P. *Polyhedron* **1996**, *5*, 2021.

20. Saito, T.; Yamamoto, N.; Nagase, T.; Tsuboi, T.; Kobayashi, K.; Yamagata, T.; Imoto, H.; Unoura, K. *Inorg. Chem.* **1990**, *29*, 764.
21. Mealli, C.; Orlandini, A. *Gazz. Chim. Ital.* **1995**, *125*, 271.
22. Bencini, A.; Ghilardi, C. A.; Orlandini, A.; Midollini, S.; Zanchini, C. *J. Am. Chem. Soc.* **1992**, *114*, 9898.
23. Bencini, A.; Midollini, S.; Zanchini, C. *Inorg. Chem.* **1992**, *31*, 2132.
24. Kambe, K. *J. Phys. Soc. Jpn.* **1950**, *5*, 48.

General Conclusion

The present thesis is concerned with the chromium chalcogenide hexanuclear and dodecanuclear cluster complexes with the Cr_6E_8 (E = S, Se) cluster core. The main results are summarized below.

- 1) The establishment of new synthetic techniques of cluster complexes.
- 2) The preparation of metal-chalcogenido cluster complexes with hydride ligands.
- 3) The elucidation of the magneto-structural correlation in the Cr_6E_8 cluster.
- 4) The clarification of intercluster interaction in dodecanuclear cluster complex.

The establishment of new synthetic techniques of cluster complexes.

Most of the cluster complexes were discovered by serendipity, and the methodology for the syntheses of designed cluster compounds has yet to be established. The synthetic methods of cluster complexes are classified into four (Scheme 1).

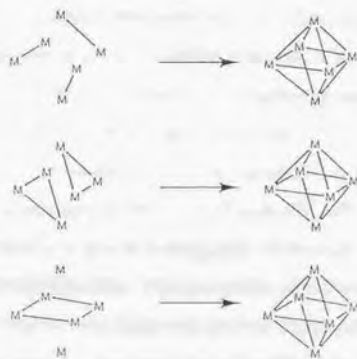
- a) *Self-assembly*: the spontaneous formation of cluster cores from mononuclear complexes or non-molecular compounds which do not contain cluster units. This method has generated most various types of cluster frameworks. However, self-assembly has two disadvantages, namely, (i) no structural predictability of the product of the reaction and (ii) the formation of the mixture of cluster complexes.
- b) *Fragment Condensation*: the linking of the smaller cluster cores to give higher cluster frameworks. Although this approach has not been well-developed, it is expected as a useful synthetic method for the selective formation of cluster complexes.
- c) *Excision reaction*: cutting out a molecular cluster core from a non-molecular clusters. Since the structures of cluster frameworks in non-molecular cluster compounds are limited, discovery of non-molecular cluster phases with novel cluster frameworks may be necessary for the syntheses of various molecular clusters.

- d) *Ligand exchange*: the exchange reaction of terminal or bridging ligands on cluster units.

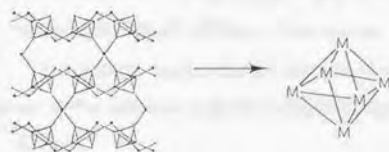
Self-assembly



Fragment Condensation



Excision



Scheme 1 (From ref. 1.)

The improvements of these synthetic methods will facilitate the selective formation of designed cluster complexes, which may lead to systematic studies of the properties of cluster complexes.

Several preparative techniques used in the present study may contribute to the development of synthetic methodology for cluster complexes. In Chapter 1, the preparations of the hexanuclear cluster complexes $[\text{Cr}_6\text{Se}_8(\text{PEt}_3)_6]$ (**1**), $[\text{Cr}_6\text{Se}_8(\text{H})(\text{PEt}_3)_6]$ (**2**), and $[\text{Cr}_6\text{S}_8(\text{H})(\text{PEt}_3)_6]$ (**3**) are described. These complexes were obtained by a self-assembly method. Whereas the reaction of CrCl_2 with NaS_xH and PEt_3 yielded the hydride cluster **3** predominantly, a similar procedure except for using Na_2Se_x in place of NaS_xH afforded a mixture of the non-hydride **1** and the hydride **2**. Accordingly, the author separated them by exploiting the difference of their redox properties. In other systems of cluster complexes, self-assembly reactions have sometimes yielded a mixture of cluster complexes, which are difficult to separate.² The separation method established in the present study may be a new approach for isolating cluster complexes from a mixture.

Chapter 2 describes the condensation of hexanuclear cluster complex **3**. The target compound in this synthesis was a dimer cluster $[\text{Cr}_{12}\text{S}_{16}(\text{H})_2(\text{PEt}_3)_{10}]$ (**6**), in which two Cr_6S_8 cluster units are connected in a similar linking mode to those of the Chevrel phases. Whereas there were several precedent examples of the cluster dimerization methods before the present study,³⁻¹⁰ none of them were available for yielding the target dimer cluster complex from the monomer **3**. However, the author found that the reaction of elemental sulfur with **3** gave the desired dimer cluster **6**. Later, similar synthetic technique afforded the molybdenum dodecanuclear analogue $[\text{Mo}_{12}\text{S}_{16}(\text{PEt}_3)_{10}]$ from the hexanuclear monomer cluster $[\text{Mo}_6\text{S}_8(\text{PEt}_3)_6]$.^{11, 12} These studies suggest that the dimerization of cluster cores with elemental sulfur may be one of the selective preparative methods for cluster condensation.

The preparation of metal-chalcogenido cluster complexes with hydride ligands.

When the author started the present study, there were only two precedent examples of metal-chalcogenido cluster complexes with the hydrido-coordinated M_6E_8 octahedral unit ($[\text{Re}_6\text{S}_7(\text{SH})\text{Br}_6]^{3-}$ and $[\text{Re}_6\text{Se}_7(\text{SeH})\text{I}_6]^{3-}$).¹³ The chromium-chalcogenido dodecanuclear

complex **6** and the hexanuclear compounds **2** and **3** are very rare instances of octahedral metal-chalcogenide cluster complexes with hydrido ligands.

The conventional methods of structure determinations of cluster complexes were mostly dependent on X-ray crystallography. However, the analysis is not always useful for detecting hydrogen atoms.¹⁴ In the present study, FAB mass spectra revealed the existence of the extra hydrides in **2**, **3**, and **6**. There have been no precedent examples of the $[M_6E_8L_6]$ type cluster complexes that have been characterized by FAB mass spectra. The characterization of hydrogen atoms is indispensable for the studies on the magnetism of the cluster complexes. As mentioned in Chapter 1, the coordination of extra hydride to a cluster core causes the increase of the number of metal cluster electrons (MCE) by one, which leads to significant effects on the magnetic behavior of the cluster complex.

The location of hydrogen atoms associated with cluster cores has been a very difficult problem. In the studies on the rhenium cluster complexes $[Re_6S_7(SH)Br_6]^{3-}$ and $[Re_6Se_7(SeH)I_6]^{3-}$, it has been proposed that the extra hydrogen atoms are bonded to one of eight chalcogen atoms.¹³ But no physical measurements have confirmed their positions. In the present study, the author attempted to determine the position of the extra hydrides in **2**, **3**, and **6**. The single-crystal X-ray structure determination and reactivity studies of **2** and **3**, and powder neutron diffraction analysis of the deuterated derivative of **3** suggested that the extra hydrogen atoms of **2** and **3** lie at the center of the Cr_6 octahedron. It is conceivable that further conclusive evidence for their interstitial positions may be afforded by single-crystal neutron diffraction analysis. The interstitial positions of the extra hydrides in **6** were also suggested by their reactivity.

The elucidation of the magneto-structural correlation in the Cr_6E_8 cluster.

It is known that some 3d-metal chalcogenido cluster complexes exhibit thermal variation of the number of unpaired electrons. However, the relations between structures and magnetic properties have remained unclear. To elucidate the structural-magnetism correlation in 3d-metal chalcogenide cluster complexes, the author analyzed the temperature-dependent paramagnetic behaviors of chromium cluster complexes **1-3** by using the Heisenberg-Dirac-Van Vleck (HDVV) Hamiltonian. The calculated coupling constants $[2J]$ decrease in the

order $2 > 3 > 1$. This indicates that the shorter Cr-Cr distances cause stronger antiferromagnetic interaction through Cr-Cr bonds, and that the couplings mediated by chalcogen bridges increase by the substitution of sulfido ligands for selenido ones. The present study suggests that the analyses of the magnetic behaviors with the HDVV Hamiltonian are useful to investigate the structural-magnetism correlation in cluster complexes.

Bencini *et al.* have reported the theoretical interpretations of the temperature-dependent paramagnetism of octahedral iron sulfide cluster complexes $[\text{Fe}_6\text{S}_8(\text{PEt}_3)_6]\text{X}_2$ ($\text{X} = \text{BPh}_4^-, \text{PF}_6^-$).^{15, 16} In the analyses of these complexes, it has been assumed that no distinction has been made between the interaction for *trans*-metal atoms and that for *cis*-metal atoms in the Fe_6S_8 cluster core. Actually, the *trans*-interaction is much weaker than the *cis*-interaction, because the former is mediated by no atoms nor direct bonds while the latter should be more effectively transmitted through metal-metal bonds and metal-(μ_2 -chalcogen)-metal bridges. In the chromium cluster complexes **1-3**, only the *cis*-interaction was taken into consideration. Presumably this model reflects the actual structural features more exactly than those used in the analyses of the iron cluster complexes.

The relation between the structure and magnetism in the Cr_6E_8 core suggested in the present thesis is based on the properties of three compounds. To investigate the relation more quantitatively, it seems necessary to prepare several analogous chromium octahedral cluster complexes. The preparations of $[\text{Cr}_6\text{S}_8(\text{PEt}_3)_6]$ and $[\text{Cr}_6\text{Te}_8(\text{H})(\text{PEt}_3)_6]$ give the complete series of non-hydrides $[\text{Cr}_6\text{E}_8(\text{PEt}_3)_6]$ and hydrides $[\text{Cr}_6\text{E}_8(\text{H})(\text{PEt}_3)_6]$ ($\text{E} = \text{S}, \text{Se}, \text{Te}$), respectively. The comparison of the magnetic properties of the compounds in each series will make the relation between the difference of chalcogen atoms and the magnitude of the magnetic interaction through them clearer. The relation between the strength of magnetic coupling through Cr-Cr bonds and their distances may be elucidated by the syntheses of derivatives with different Cr-Cr bond distances. In cubane-type chromium sulfide cluster complexes $[\text{Cr}_4\text{S}_4\text{L}_4]$ ($\text{L} = \text{Cp}^*$ (methylcyclopentadienyl), Cp (cyclopentadienyl)), the change of terminal ligands L from Cp^* to Cp elongates Cr-Cr bond lengths (2.82 Å vs. 2.82-2.89 Å).^{17, 18} The Cr-Cr distances in the octahedral cluster complexes **1-3** may be varied by the substitution of the terminal triethylphosphine ligands.

In addition, the oxidation and reduction of $[\text{Cr}_6\text{E}_8(\text{PEt}_3)_6]$ and $[\text{Cr}_6\text{E}_8(\text{H})(\text{PEt}_3)_6]$ may also yield the Cr_6E_8 cluster cores with different Cr-Cr bond lengths from those in the starting neutral clusters.

The clarification of intercluster interaction in dodecanuclear cluster complex.

When cluster cores are condensed, the resulting cluster oligomers exhibit the properties due to intercluster interaction, which are never observed in the monomer cluster complexes. In the field of metal-chalcogenido clusters, however, there have been few reports on the interaction between cluster units.^{12, 19} The present study deals with intercluster interaction in dodecanuclear chromium sulfide cluster complex **6**. Electrochemical and magnetic measurements showed the electronic and antiferromagnetic interaction between the two Cr_6S_8 cluster units. The intercluster antiferromagnetic interaction is responsible for the distortion of the Cr_6 octahedra in the dimer cluster **6**. Since each Cr_6S_8 cluster unit is paramagnetic, the antiferromagnetic coupling arises between the linking chromium atoms and the intercluster Cr-Cr bond becomes shorter, which leads to the projection of the linking Cr sites from the square of the surrounding sulfur atoms and the distortion of Cr_6 octahedra.

In the studies on the oligomers of Ru_3O trinuclear clusters, the magnitude of intercluster electronic interaction has been related to the intercluster distance, which is dependent on the difference of the cluster-cluster bridging ligand.²⁰ On the other hand, the precedent reports on metal-chalcogenide cluster oligomers have rarely dealt with the relation of intercluster distance to interaction between cluster cores. In the dodecanuclear chromium cluster complex **6**, the two Cr_6S_8 cluster cores are linked by two Cr-S bonds, whose lengths are considered to determine the intercluster distance. Since selenium and tellurium atoms have larger covalent radii (1.17 Å for Se; 1.37 Å for Te) than that for sulfur atom (1.04 Å),²¹ the selenido- and tellurido-analogues of **6** may give longer intercluster chromium-chalcogen bonds, which make two octahedral cluster units more separated as compared with the sulfide complex **6**. It is conceivable that the comparison of the electronic and magnetic properties of the selenido- and tellurido-dimers with those in the sulfido-dimer **6** will clarify the relation of intercluster distance to the electronic and magnetic interaction between the octahedral cluster units.

The chemistry of cluster complexes may be still in the early stage of development. The author hopes that the present thesis will contribute to the progress of the chemistry of this field.

References

1. Saito, T. In *Early Transition Metal Clusters with IT-Donor Ligands*; VCH, New York, 1995, pp 63-164.
2. Cecconi, F.; Ghilardi, C. A.; Midollini, S.; Orlandini, A.; Zanello, P.; Cinquantini, A.; Bencini, A.; Uytterhoeven, M. G.; Giorgi, G. *J. Chem. Soc. Dalton Trans.* **1995**, 3881.
3. Palermo, R. E.; Singh, R.; Bashkin, J. K.; Holm, R. H. *J. Am. Chem. Soc.* **1984**, *106*, 2600.
4. Shibahara, T.; Yamamoto, T.; Kanadani, H.; Kuroya, H. *J. Am. Chem. Soc.* **1987**, *109*, 3495.
5. Shibahara, T.; Akashi, H.; Kuroya, H. *J. Am. Chem. Soc.* **1988**, *110*, 3314.
6. Shibahara, T.; Akashi, H. *Inorg. Chem.* **1989**, *28*, 2906.
7. Saito, T.; Yamamoto, N.; Nagase, T.; Tsuboi, T.; Kobayashi, K.; Yamagata, T.; Imoto, H.; Unoura, K. *Inorg. Chem.* **1990**, *29*, 764.
8. Shibahara, T.; Akashi, H.; Yamasaki, M.; Hashimoto, K. *Chem. Lett.* **1991**, 689.
9. Murata, T.; Gao, H.; Mizobe, Y.; Nakano, F.; Motomura, S.; Hidai, M. *J. Am. Chem. Soc.* **1992**, *114*, 8287.
10. Mizutani, J.; Yamada, S.; Imoto, H.; Saito, T. *Inorg. Chem.* **1996**, *35*, 244.
11. Amari, S.; Imoto, H.; Saito, T. *Chem. Lett.* **1997**, 967.
12. Amari, S.; Imoto, H.; Saito, T. *J. Chin. Chem. Soc.* **1998**, *45*, 445.
13. Long, J. R.; McCarty, L. S.; Holm, R. H. *J. Am. Chem. Soc.* **1996**, *118*, 4603.
14. Gade, L. H.; Johnson, F. G.; Lewis, J. *Croat. Chem. Acta* **1995**, *68*, 693.
15. Bencini, A.; Uytterhoeven, M. G.; Zanchini, C. *Int. J. Quantum. Chem.* **1994**, *52*, 903.
16. Bencini, A.; Ghilardi, C. A.; Midollini, S.; Orlandini, A.; Russo, U.; Uytterhoeven, M.

- G.; Zanchini, C. *J. Chem. Soc. Dalton Trans.* **1995**, 963.
17. Pasynskii, A. A.; Eremenko, I. L.; Rakitin, Y. V.; Novotortsev, V. M.; Ellert, O. G.; Kalinnikov, V. T.; Shklover, V. E.; Struchkov, Y. T.; Lindeman, S. V.; Kurbanov, T. K.; Gasanov, G. S. *J. Organomet. Chem.* **1983**, *248*, 309.
18. Wei, C.; Goh, L. -Y.; Bryan, R. F.; Sinn, E. *Acta Crystallogr. C.* **1986**, *42*, 796.
19. Zheng, Z.; Holm, R. H. *Inorg. Chem.* **1997**, *36*, 5173.
20. Baumann, J. A.; Salmon, D. J.; Wilson, S. T.; Meyer, T. J. *Inorg. Chem.* **1979**, *18*, 2472.
21. Pauling, L. In *The Nature of the Chemical Bond*; Cornell University Press, Ithaca, New York, 1960, p 224.

Acknowledgement

The present work has been conducted under the guidance of Professor Dr. Taro Saito, and has been completed under the supervision of Professor Dr. Atsushi Koma. The author would like to express his sincere gratitude for their appropriate directions, discussions, suggestions, and encouragement.

The author gratefully acknowledges Associate Professor Dr. Akiko Kobayashi for valuable discussions, encouragement, and assists in X-ray structure analyses. Sincere acknowledgement is also due to Associate Professor Dr. Hideo Imoto for assists in powder neutron diffraction measurement and enlightening suggestion about syntheses, X-ray crystallography, and molecular orbital calculations.

The author is grateful to Professor Dr. Renji Okazaki (Japan Women's University) and Dr. Mitsuhiro Ito for their sincere help in NMR spectra measurements. Grateful acknowledgement is also made to Professor Dr. Takayuki Kawashima (School of Science, the University of Tokyo) for his helpful discussion about the synthesis of the deuterated cluster.

The author gratefully acknowledges Dr. Yasuo Wakatsuki, Dr. Teiji Chihara, and Mr. Yasuaki Esumi (all at The Institute of Physical and Chemical Research, RIKEN) for their sincere help and valuable discussions about FAB mass spectra.

The author would like to acknowledge Associate Professor Dr. Reizo Kato (The Institute for Solid State Physics, The University of Tokyo) and Dr. Yuko Hosokoshi (The Institute of Molecular Science) for their sincere collaboration in measuring magnetic susceptibilities. The author is also grateful to Professor Dr. Wasuke Mori (Kanagawa University) for many valuable discussions and encouragement about magnetic fitting calculations. Many thanks are given to Mr. Hikaru Tsuchiya (Cryogenic Center in Tokyo University) for operating the SQUID magnetometer.

The author would like to thank Professor Fujio Izumi (National Institute for Research in Inorganic Materials), Associate Professor Dr. Takashi Kamiyama, and Mr. Takashi Ikeda (both at the University of Tsukuba) for their sincere help in powder neutron diffraction measurement and analysis.

Many thanks are given to those who were and are the members of laboratories of Professor Taro Saito. The author is debted to Ms. Toshiko Seki and Ms. Kimiyo Saeki for sincere taking elemental analyses. All the officers and the technicians in the department are acknowledged for their provision of comfortable environments for the study.



